CADMIUM SULFIDE - COPPER SULFIDE HETEROJUNCTION CELL RESEARCH

Final Report

September 1, 1978 - August 31, 1979

XR-9-8063-1

December 1979

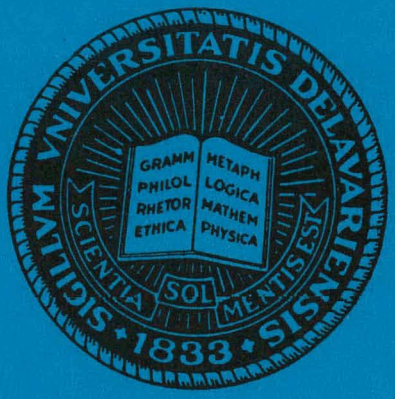

INSTITUTE OF ENERGY CONVERSION

UNIVERSITY OF DELAWARE

NEWARK, DELAWARE 19711

Supported by the Solar Energy Research Institute, Report XR-9-8063-1-FR

DISCLAIMER

NOTICE

1. Abstract

The thrust of the research on the planar CdS/Cu_2S cell has been to increase the short circuit currents to the levels achieved with the 9.15% textured cell. It was established early in the contract that light trapping is essential for high currents and a front surface texturing process has been developed to achieve this. As a result, short circuit currents have been raised to over 21.0 mA/cm^2. The highest efficiency achieved with the planar junction cell during the contract was 7.81%. Cells heat treated to their highest short circuit currents have shown fill factors below the design requirement of about 74% thus putting a limit on achievable efficiency. Further improvement of fill factor and a small additional increment of current will produce cells with efficiencies of over 10%. Progress has been made on improving the performance of the $(CdZn)S/Cu_2S$ again with the major emphasis being on improved short circuit currents. Modifying the CdZn/S deposition procedure as directed by material studies has resulted in considerably improved short circuit currents during the course of this contract. The highest short circuit currents have now raised to over 21 mA/Cm^2 and a cell efficiency of 8.19% has been recorded. Fundamental studies have focused on the influence of substrate composition and heat treatment on junction field and collection efficiency. These studies have been conducted in parallel with experiments on photoluminescence in an attempt to relate deposition conditions to optimum substrate parameters. Quantitative analysis has been carried out of the optimal material parameters required to maximize energy conversion efficiency. It has been shown that a relatively narrow range of properties in the CdS and Cu_2S is necessary to achieve the highest efficiencies. The encapsulation task has focused on trial depositions of glass applied by electron beam evaporation. A limited number of cells have been encapsulated behind sheet glass and exposed to sunlight for a number of months.

2. Table of Contents

LIST OF ILLUSTRATIONS

3. Introduction

The development of a low cost thin-film solar cell based on the CdS/Cu_2S heterojunction has been continued under the same four tasks established under DOE contract number EG-77-C-03-1576. During that program it became clear that the conversion efficiency of the conventional textured CdS/Cu_2S cell was limited to between 9 and 10%. The primary limiting factor is the open circuit voltage and it was concluded that it would be unlikely to exceed 0.52 V because of the voltage penalty caused by a large junction area. Further advances in conversion efficiency were concluded to be possible if the junction could be made more planar with an area more nearly equal to the projected area of the cell. Work during this year has focused on the planar CdS/Cu_2S cell and substantial improvements in conversion efficiency from the initial values have been realized. The goal efficiency of 10% has not been reached mainly because short circuit currents have not yet been raised to levels achieved with the textured cell. It is concluded that this will require further technology development and does not represent an ultimate limitation on the behavior of the cell. Junction formation by a solid state reaction process has been developed and substantial gains made in photon economy with a modified front surface texturing procedure.

Development of $(CdZn)S/Cu_2S$ cells has been guided by the previous experience with CdS/Cu_2S cells. Structural studies revealed that the mixed sulfides being deposited had substantially different grain morphological structures to those of the CdS which gave high efficiency cells. Modifications to the deposition procedures have now succeeded in producing mixed sulfides with properties much more closely akin to the CdS material. Considerable improvements in short circuit current and fill factor have been achieved with the mixed sulfide cell, and conversion efficiencies over 8.1% have now been realized.

All cell development efforts in the CdS programs at the Institute of Energy Conversion have been directed by the output of the various analytical studies carried out. During this year a detailed quantitative study has been made of optimum cell performance and the acceptable ranges of component material properties defined. It is found that these are relatively narrow in order to achieve the highest possible efficiency in the CdS/Cu_2S cell. In addition, photocapacity, spectral response and photoluminescence measurements have been made in an attempt to identify the trap population essential for high efficiency energy conversion and to relate the trap population to the original CdS deposition conditions. Some progress has been made in this research but considerably more work is necessary before the full picture is available. A major difficulty with batch type cell production is maintaining consistent material properties from run to run. Although considerable progress has been made in identifying and maintaining optimum deposition conditions, it was still found that there was an unacceptable degree of variability between substrate and substrate. In addition to a sequence of parameter measurements to assist in selecting substrates capable of producing high efficiency cells a further selection procedure was found to be necessary. This procedure is to make a trial set of four cells using the conventional solution reaction process. Following a minimum number of heat treatments an accept-reject decision is made on the basis of the achieved light generated current and the diode pre-exponential factor. This "substrate evaluation procedure" (SEP) has been very successful in preventing cell production efforts on material which is intrinsically unlikely to reach the highest efficiencies. It should be noted however that the selection criteria is aimed towards achieving the highest possible efficiencies. All the CdS material produced would be capable of reaching efficiencies in the 7 to 8% range.

A limited level of effort has been maintained aimed at developing an integral encapsulation to protect the Cu_2S layer from the atmosphere. Some success has been achieved with electron beam deposited glass with thicknesses up to 5 μm. A few cells have been protected from the atmosphere behind sheet glass, exposed to sunlight and their degradation behavior monitored. Cells in a reduced efficiency state were restored to pre-exposure performance levels by appropriate reducing heat treatments.

4.1 Task 1 Development of CdS/Cu_2S Solar Cells

The primary goal of this phase of the research has been to develop a cell with conversion efficiency of over 10%. Previous efficiency goals were met by increasing the fill factor and short circuit current of a textured cell that was limited in open circuit voltage to ~ 0.5 V. The potential for improving either the fill factor or current levels achieved in the 9.15% cell was judged to be limited and accordingly a major cell design change was made to a planar junction cell. In this design the Cu_2S is formed by a solid state reaction between CdS and Cu_2Cl_2 which very largely eliminates the deep grain boundary intrusions of Cu_2S formed by the more traditional solution "barriering" process. Cells made early in this contract period were formed on as deposited CdS but optical measurements established that this resulted in very poor photon economy. Subsequently it was established that some surface texturing of the CdS was possible without significant loss of open circuit voltage.

During the course of the contract the short circuit currents for high open circuit voltage cells have been raised from ~ 18 mA/cm^2 to over 21 mA/cm^2 while maintaining V_{oc} at > 0.54 V. The best cell efficiency achieved under 94 mW/cm^2 ELH simulation is 7.81% with V_{oc} = 0.54 V, FF = 74.2%, J_{sc} = 18.1 mA/cm^2 (19.2 mA/cm^2 at 100 mW/cm^2). Overall accuracy is estimated to be ± 2%.

4.1.1 Phase 1 Planar Junction with Good Open Circuit Voltage and Fill Factor

The achievable open circuit voltage is reduced by the area of the actual heterojunction, A_J, according to the following relation,

$$\Delta V_{oc} = kT/q \ \ell n \ A_j/A_1$$

where (A_1) is the projected area of the cell. At least two factors influence the junction area, namely the morphology of the front surface of the CdS and the production of Cu_2S down the CdS grain boundaries. The morphology of the CdS on a gross scale reflects the surface of the metallic substrate and on a fine scale it is affected by the hydrochloric acid etch normally used to texture the surface before reaction to Cu_2S. The gross morphology of the CdS surface can therefore be influenced by selecting either the matte or smooth side of the copper substrate. Initially cells with V_{oc} in the range of 560-570 mV were produced on the smooth side of the substrate. However, reflectance measurements coupled with theoretical analysis showed that increased photon losses would eventually offset any V_{oc} gain achieved in this way as long as no provisions for improved light trapping were made. This coupled to a decreased cell yield due to CdS adhesion problems, resulted in the abandonment of this cell design.

The fine morphology of the CdS was found to be key to improved photon efficiency, as shown in Task III, Phase 7, and a light HCl etch (LE) was developed so as not to affect V_{oc} while also achieving the desired light trapping (see Phase 3). It was found that as long as grain boundary penetration was avoided by using the solid-state formation technique for Cu_2S, V_{oc} was not affected. Table I shows typical V_{oc} values achieved with the various CdS and Cu_2S growth processes. Since the photon economy and light-generated current J_L depended on the Cu_2S morphology V_{oc} values have been adjusted to constant J_L = 21 mA/cm^2 to permit comparison.

Table I

Maximum V_{oc} as recorded[+] and normalized to J_L=21 mA/cm^2, for various cell types

Cell	Substrate	Cu_2S Formation	CdS etch	V_{oc}(mV)	Comments
686.A24	Smooth	Solid State	None	561[+]	
20939.121	Rough	Solid State	12 sec.	562[+]	Best Value Using Light etch
20949.212	Rough	Solution	10 sec.	513[+]	Processed Together
20949.221	Rough	Solid State	10 sec.	540[+]	
20948.211	Rough	Solution	None	504[+]	
20948.221	Rough	Solid State	None	535[+]	

*Etch - 20% HCl at 60°C for stated times

Fill factor values are strongly affected by series resistance, which is largely determined by lateral current flow in the Cu_2S layer, which in turn depends critically on the Cu_2S morphology. While FF > 0.72 were achieved using the unetched CdS/solid state Cu_2S cell design, cells made using the solid state reaction process showed unusually large variations in series resistance upon H_2 heat treatment leading to maximum J_{sc}. The maximum conversion efficiency was achieved at values of J_{sc} below maximum as illustrated in Table II. This is interpreted as due to thin Cu_2S regions caused by the lack of uniformity of the evaporated CuCl layer on the CdS surface, leading to high R_s when the Cu_2S stoichiometry is high. This obstacle to integral cell optimization is further analyzed in Phase 5.

Table II

Cell Parameters at Maximum J_{sc} and Efficiency for #939 Series

Cell	State	V_{oc} [mV]	J_{sc} [mA/cm^2]	FF [%]	η [%]	R_s [Ωcm^2]
20939.122	Maximum efficiency	555	17.4	72.2	7.51	2.56
	Maximum current	540	18.5	64.1	6.89	4.42

A study of the influence of heat treatment temperature on fill factor revealed that at 200°C a non-recoverable loss of fill took place. Figure 1 shows that substantial heat treatment at 150°C can be carried out with only a small decline in fill factor.

4.1.2 Phase 2 Achievement of Low Photon Losses

The low photon loss in the traditional textured cell is in part due to the anti-reflection effects of the textured surfaces. The high index of refraction of Cu_2S will produce major first surface reflection losses with a smooth surface and it has been clear for some time that the planar cell will require development of a good anti-reflection technology. A single layer anti-reflection coating can in principal achieve zero reflection at one specific wavelength but in the absence of texturing it would not be expected to achieve the low photon losses required for high efficiency cells. By using two layers it is possible in principal to achieve zero reflectance at two wavelengths. By appropriately positioning these in the active photon range of the solar cell one can anticipate having a low overall front surface reflectance of less than 5%. Measurements with an integrating sphere showed that for cells with Cu_2S thickness, d, less than about half the electron diffusion distance (≈1500 Å) as required for high carrier collection efficiency, photon losses due to reemitted light were limiting J_L even in double layer A-R planar cells.[1,2] Experimental[3] and analytical work,[2] showed that modification of the substrate texture to increase light trapping was a low benefit option. Of the other two options, texturing the front Cu_2S surface or texturing the front surface of an anti-reflection cover applied to a smooth Cu_2S layer, the first proved fruitful. Based on the analysis (Task III, phase 7) the front surface of the Cu_2S could be expected to be amenable to texture with minimum V_{oc} loss.

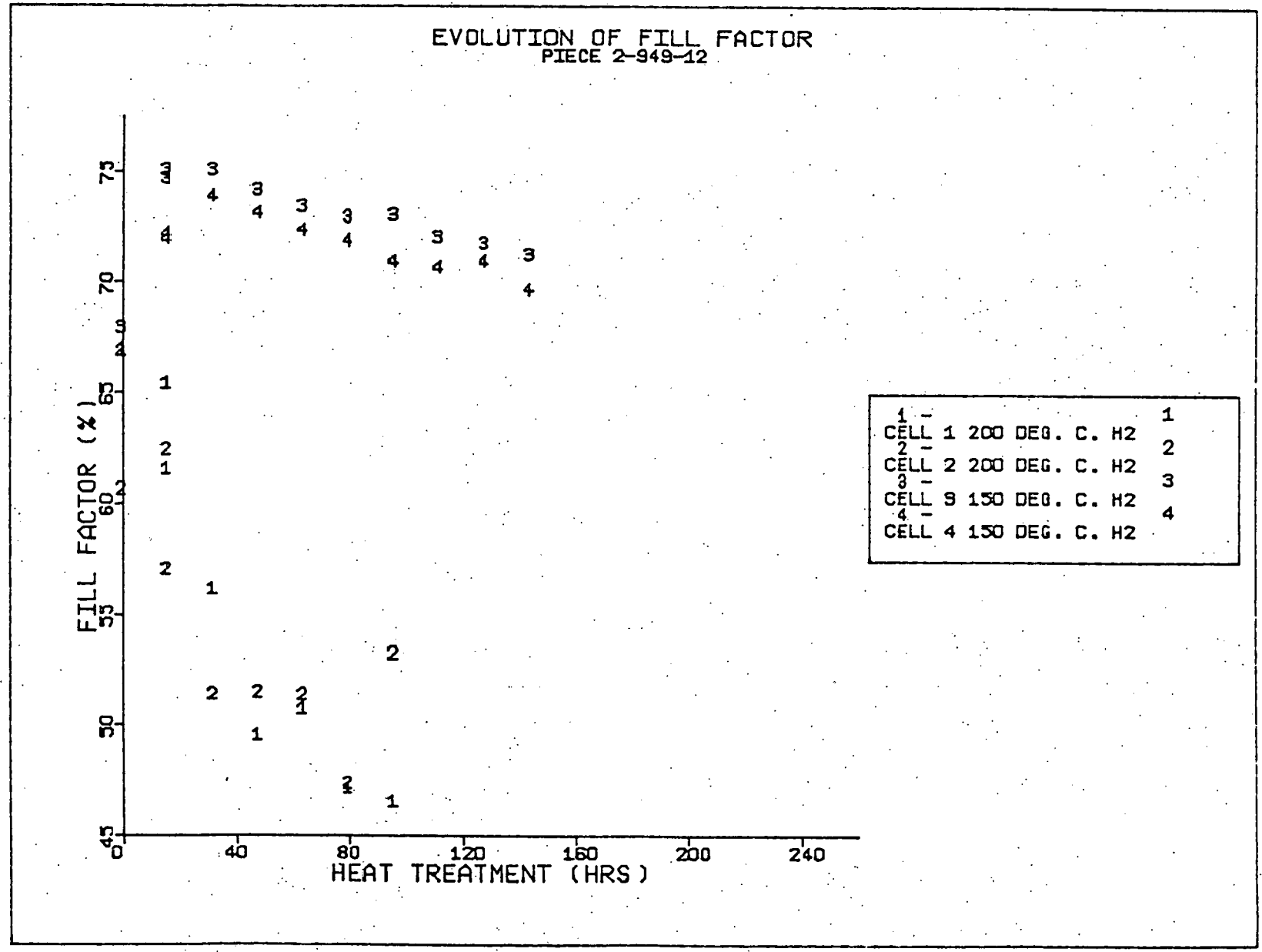

Figure 1 Influence of Heat Treatment on Fill Factor

A light etch (20-25% HCl, 60°C, 10-40 seconds) was developed, that achieved a decrease in reflectance with no significant decrease in V_{oc} and a substantial gain in J_L. The best current achieved in an untextured (unetched) CdS/Cu_2S cell was 19.8 mA/cm^2 (100 mW/cm^2). As shown by the results in the following section the light etch gave light generated currents up to 21.8 mA/cm^2 while maintaining $V_{oc} \geq 0.54$ V.

4.1.3 Phase 3 Combine Technologies to Give $J_{sc} \geq 27$ mA/cm^2

The most significant improvement in short circuit current was achieved with the introduction of the light texturing HCl etch. A sequence of three experiments were carried out to determine the optimum combination of etching time and Cu_2S thickness. The experimental conditions for these experiments were as follows.

Experiment #2 Substrate #20939 Resistivity 1.2 Ω-cm
Etch times 12, 25, 40 seconds. Cu_2S thickness 1500, 1000, 1900 Å

Experiment #3 Substrate #20960 Resistivity 2.0 Ω-cm
Etch time 25 seconds (20% HCl, 60°C). Cu_2S thickness 930, 1800, 3000 Å

Experiment #4 Substrate #20952 Resistivity 3.0 Ω-cm
Etch time 25 seconds (20% HCl, 60°C). Cu_2S thickness 1200, 1700, 2300 Å

Figures 2 through 7 illustrate the various cell parameters as a function of the process variables. Figures 8 through 10 reveal some of the interdependence between the operating parameters.

From these data the following conclusions can be drawn.

The optimum Cu_2S thickness under the present cell production conditions is between 1500 and 1700 Å.

The short circuit current (or J_L) is relatively insensitive to etch times between 10 and 60 seconds.

The open circuit voltage trends slowly down with the etching time

The efficiency probably maximizes at ∿ 25 second etch time.

The short circuit current (or J_L) dominates the achievable efficiency under the conditions of these experiments.

Further development work is planned to improve the short circuit current. A further increase of about 13% is necessary to achieve 10% conversion efficiency at 0.54 V.

4.1.4 Transfer Integral Encapsulant from Task 4

Progress on the integral encapsulant is described in section 4.4. The technology has not advanced to an appropriate stage to introduce into the cell development efforts of Task 1.

4.1.5 Statistical Sample of High Efficiency Cells

A total of 36 cells were made as part of experiments 2,3 and 4 described in section 4.1.3. The distribution of J_L, V_{oc} and efficiency is given in Figures 11 through 13. It should be noted that the cell production conditions cover a broad range of both etching time and Cu_2S thickness. The results for cells made using the apparent optimum values for these variables (25 seconds, 1800 Å) are identified on the figures.

Of the 36 cells, 5 (14%) were shorted. Twenty-six cells (72%) exceeded 5% efficiency. All the live cells (86%) exceeded 0.54 V open circuit voltage.

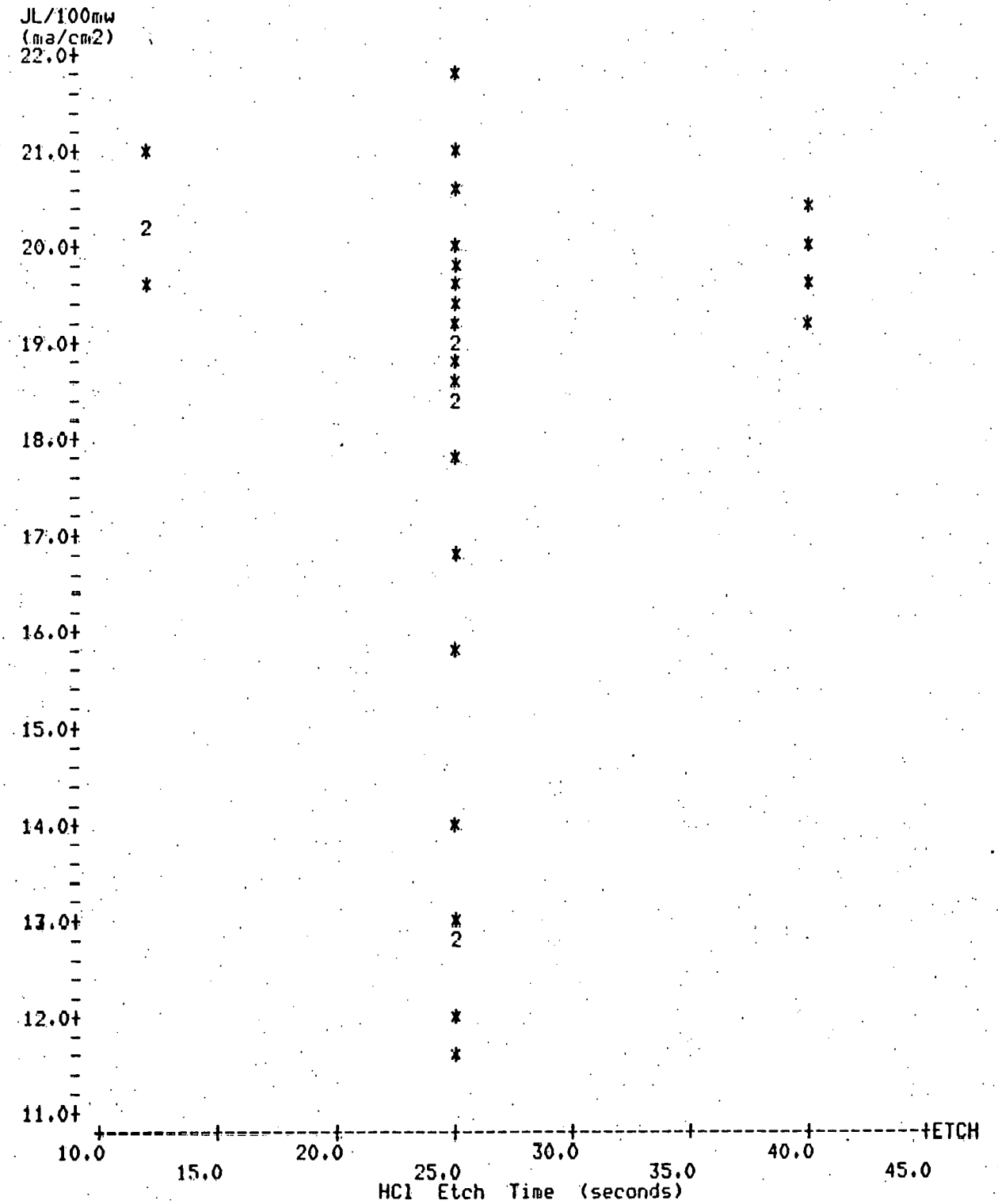

Figure 2 MAXIMUM JL/100mw AS A FUNCTION OF HCl ETCH TIME
For EXPERIMENTS 2-4

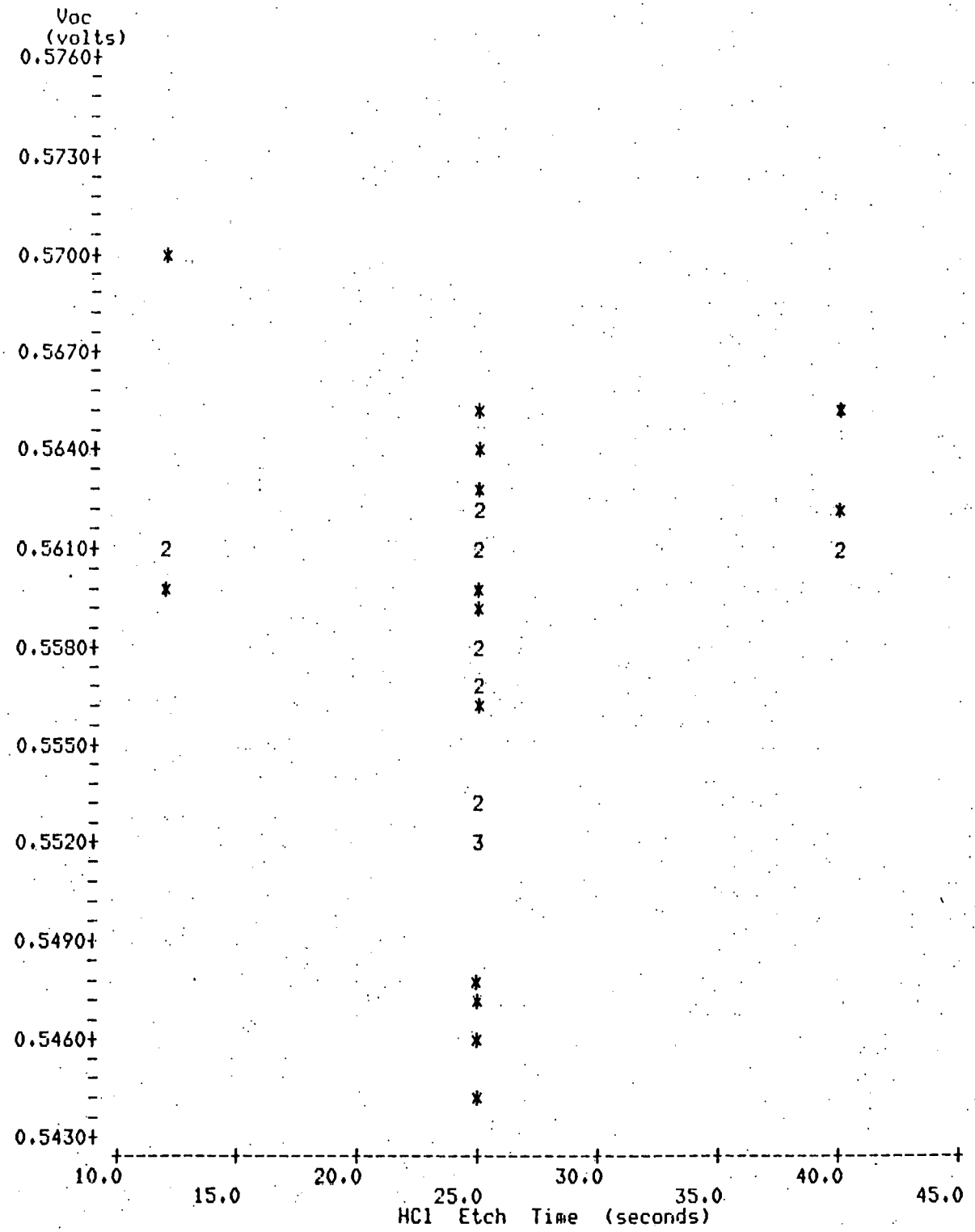

Figure 3 MAXIMUM VOC(norm. to 21ma/cm2) AS A FUNCTION OF HCl ETCH TIME For EXPERIMENTS 2-4

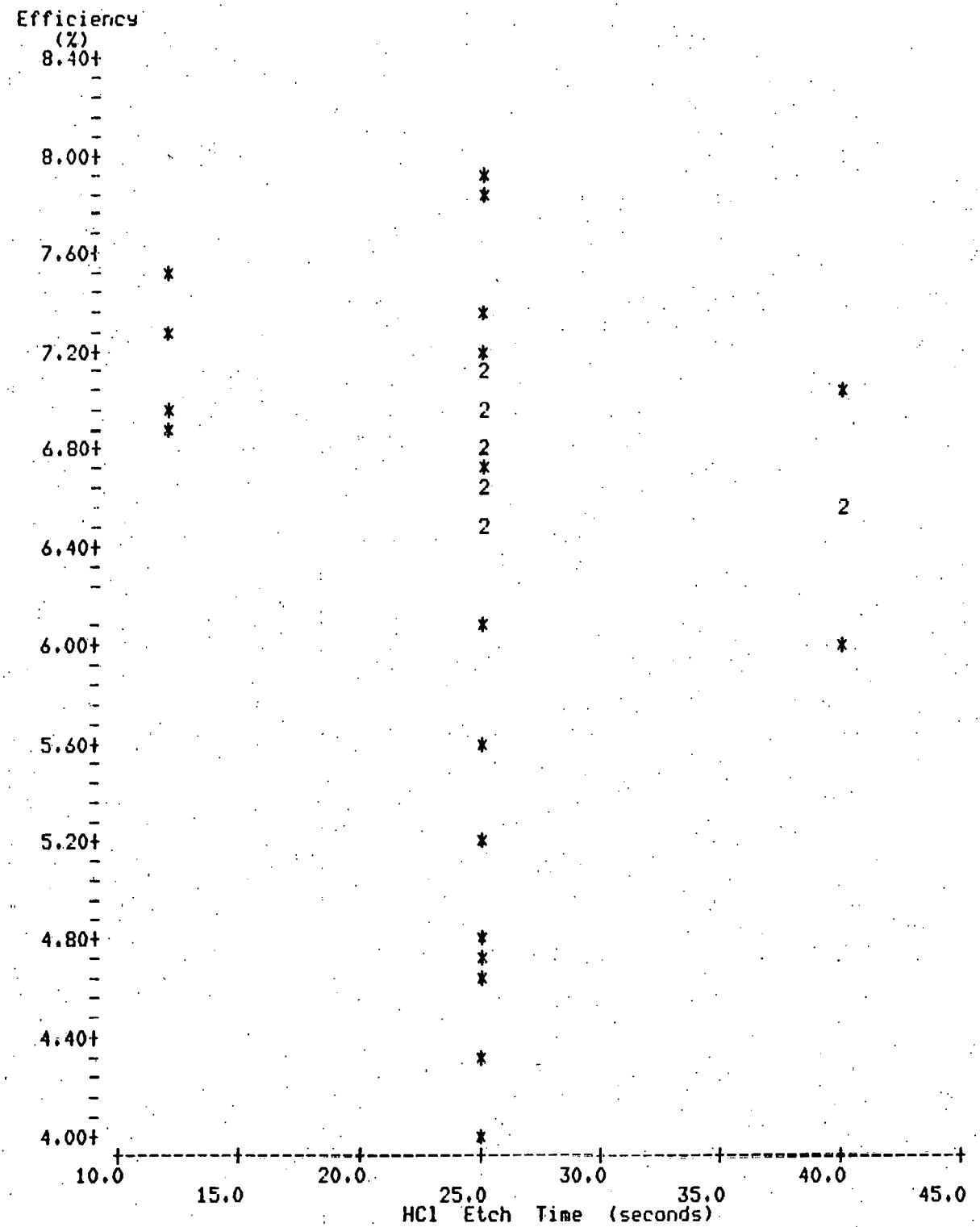

Figure 4 MAXIMUM EFFICIENCY AS A FUNCTION OF HCl ETCH TIME
For EXPERIMENTS 2-4

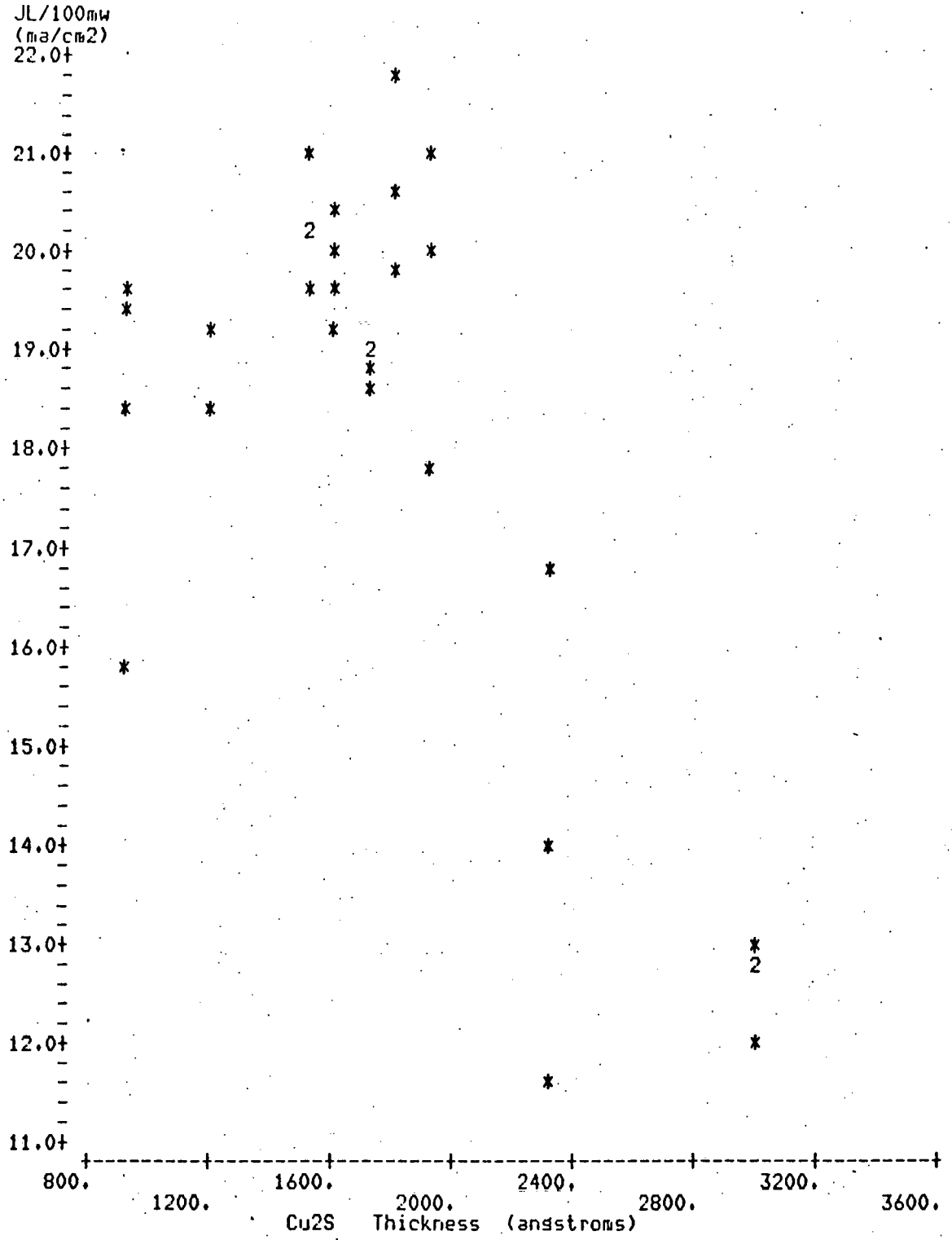

Figure 5 MAXIMUM JL/100mw AS A FUNCTION OF Cu2S THICKNESS
For EXPERIMENTS 2-4

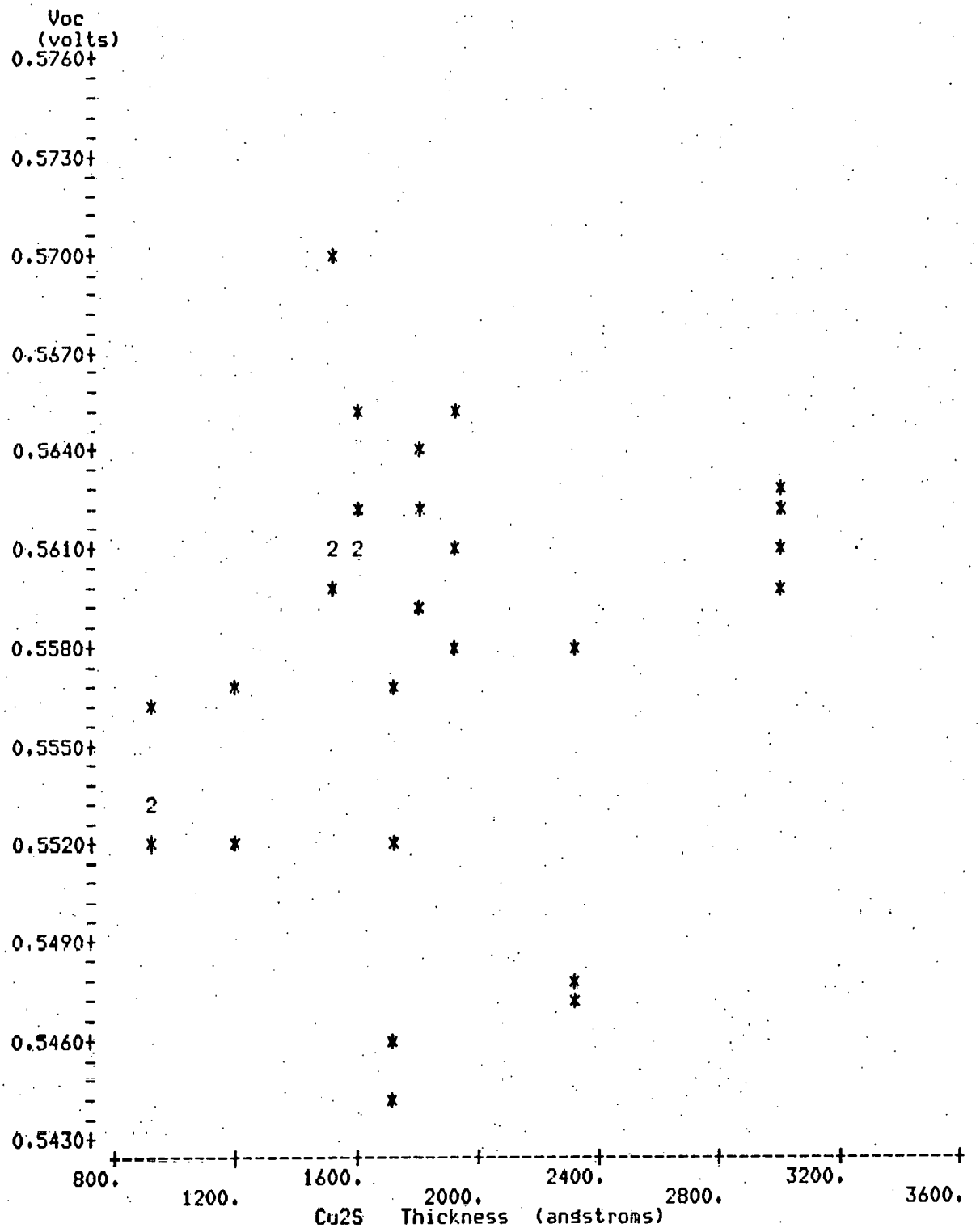

Figure 6 MAXIMUM VOC(norm. to 21ma/cm2) AS A FUNCTION OF Cu2S THICKNESS For EXPERIMENTS 2-4

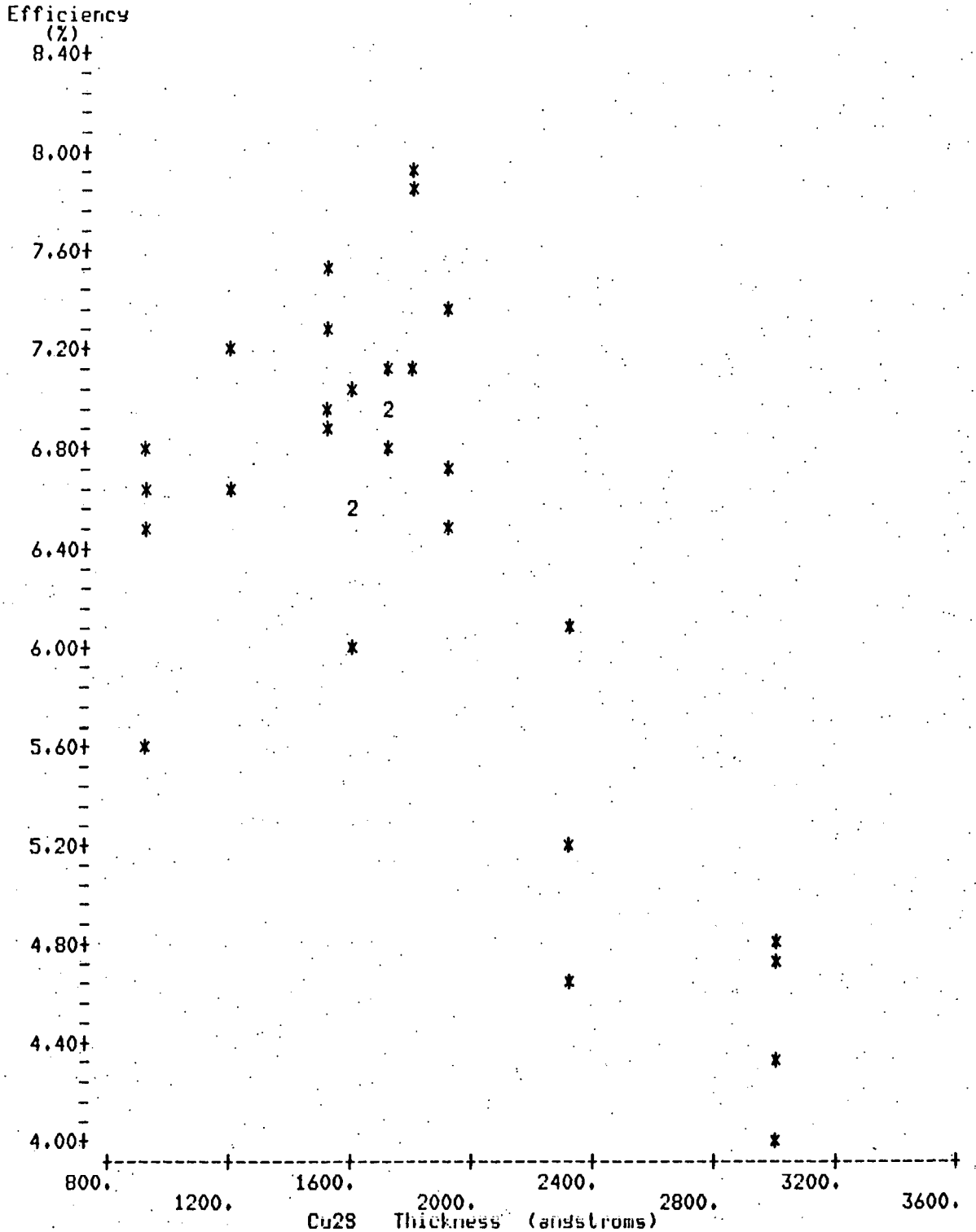

Figure 7 MAXIMUM EFFICIENCY AS A FUNCTION OF Cu2S THICKNESS For EXPERIMENTS 2-4

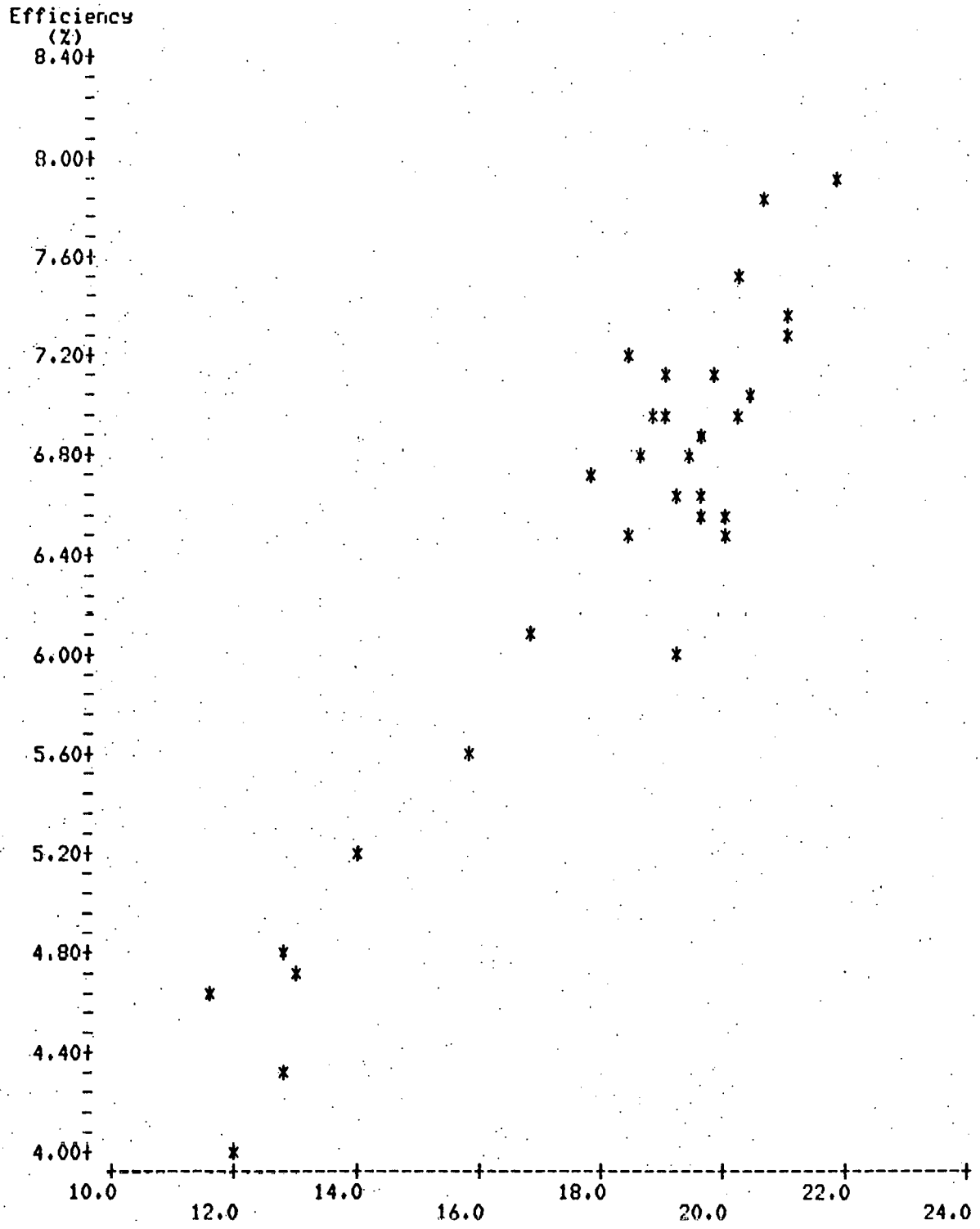

Figure 8 MAXIMUM EFFICIENCY AS A FUNCTION OF MAXIMUM JL
For EXPERIMENTS 2-4

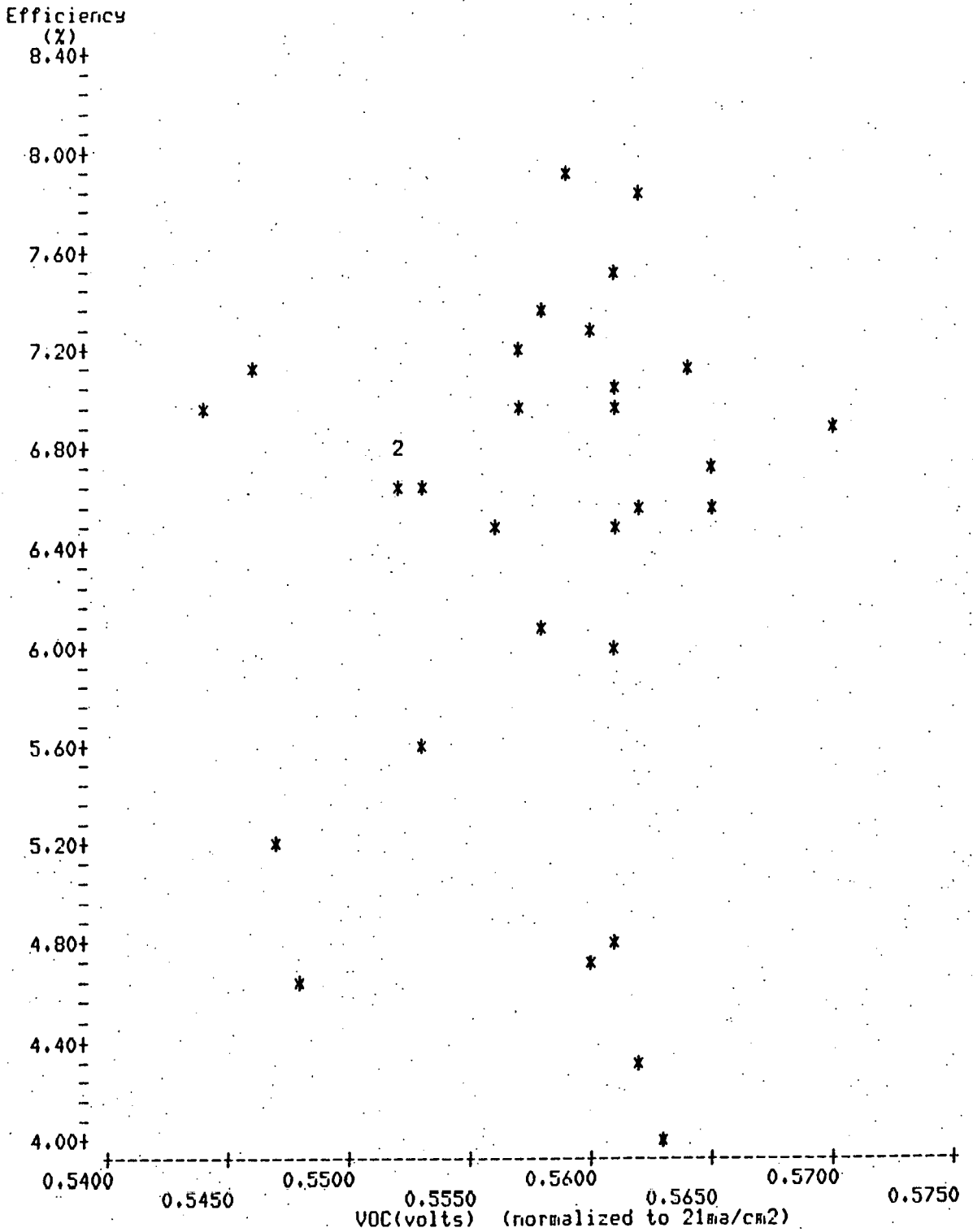

Figure 9 MAXIMUM EFFICIENCY AS A FUNCTION OF MAXIMUM VOC
For EXPERIMENTS 2-4

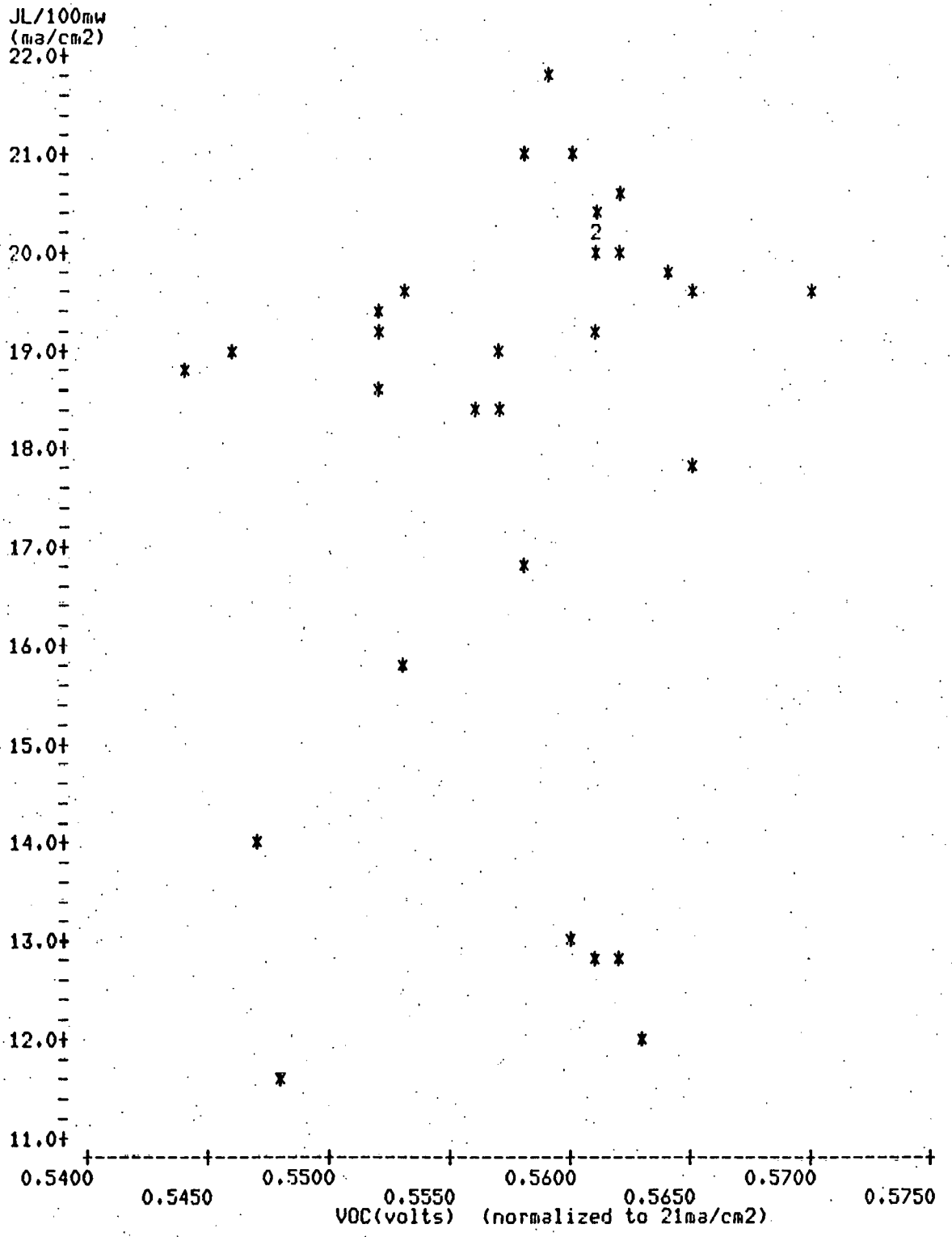

Figure 10 MAXIMUM JL at 100mw/cm2 AS A FUNCTION OF MAXIMUM VOC
For EXPERIMENTS 2-4

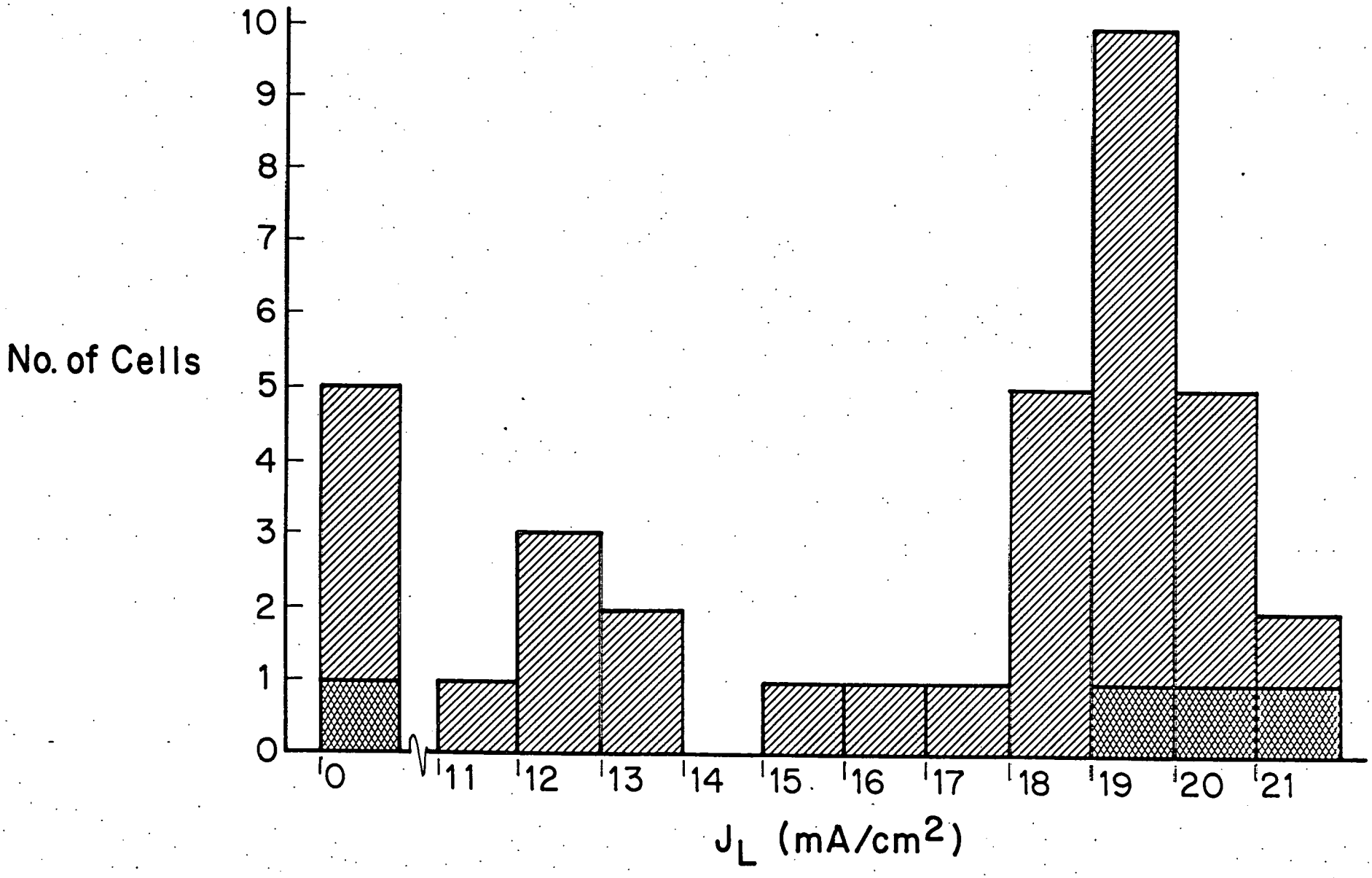

Figure 11 Distribution of Light Generated Current for a Sample of 36 cells. Cross hatching indicates cells from substrate #20960, 25 sec. HCl etch. 1800 Å Cu_2S.

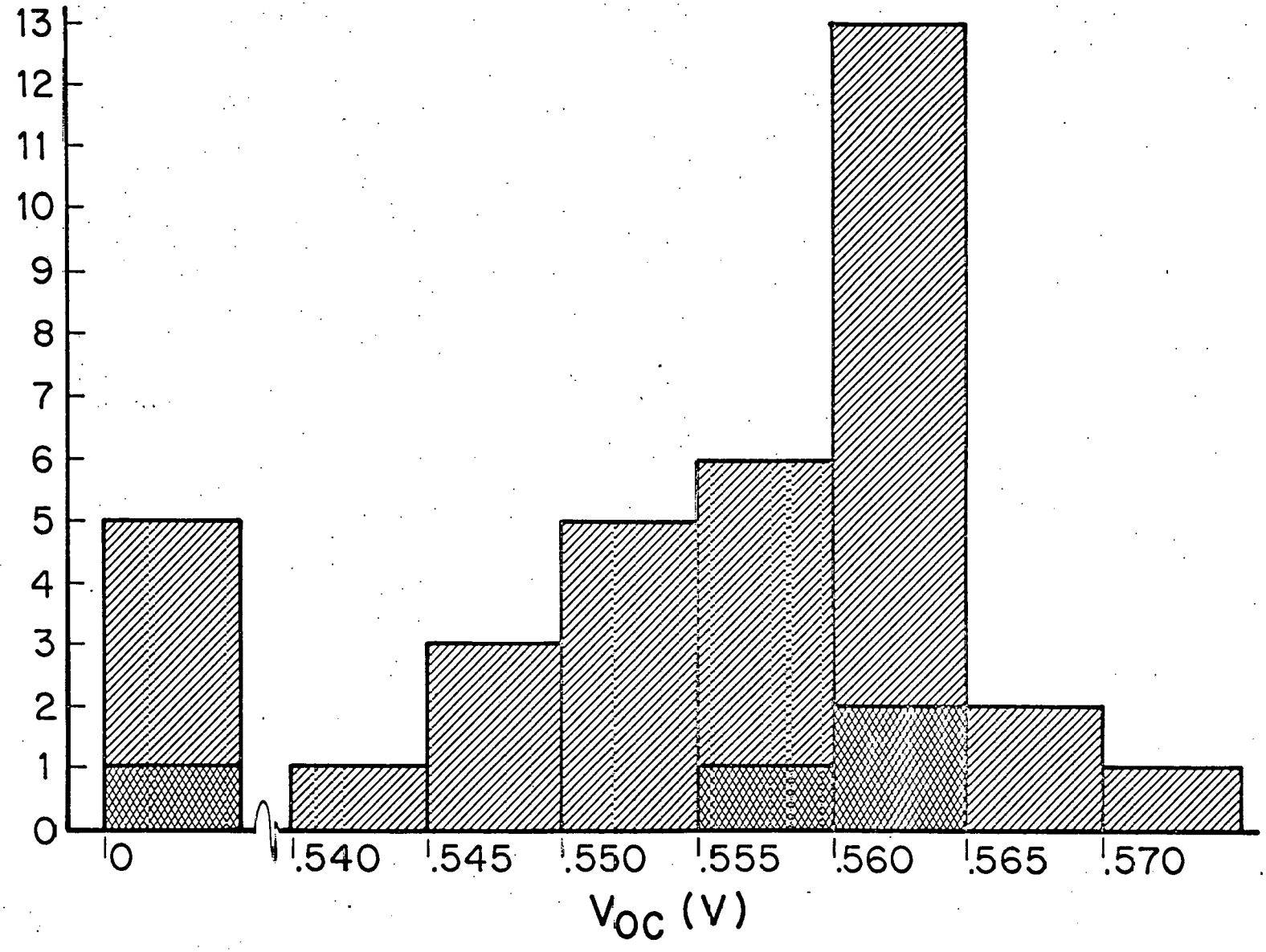

Figure 12 Distribution of Open Circuit Voltage for a Sample of 36 Cells

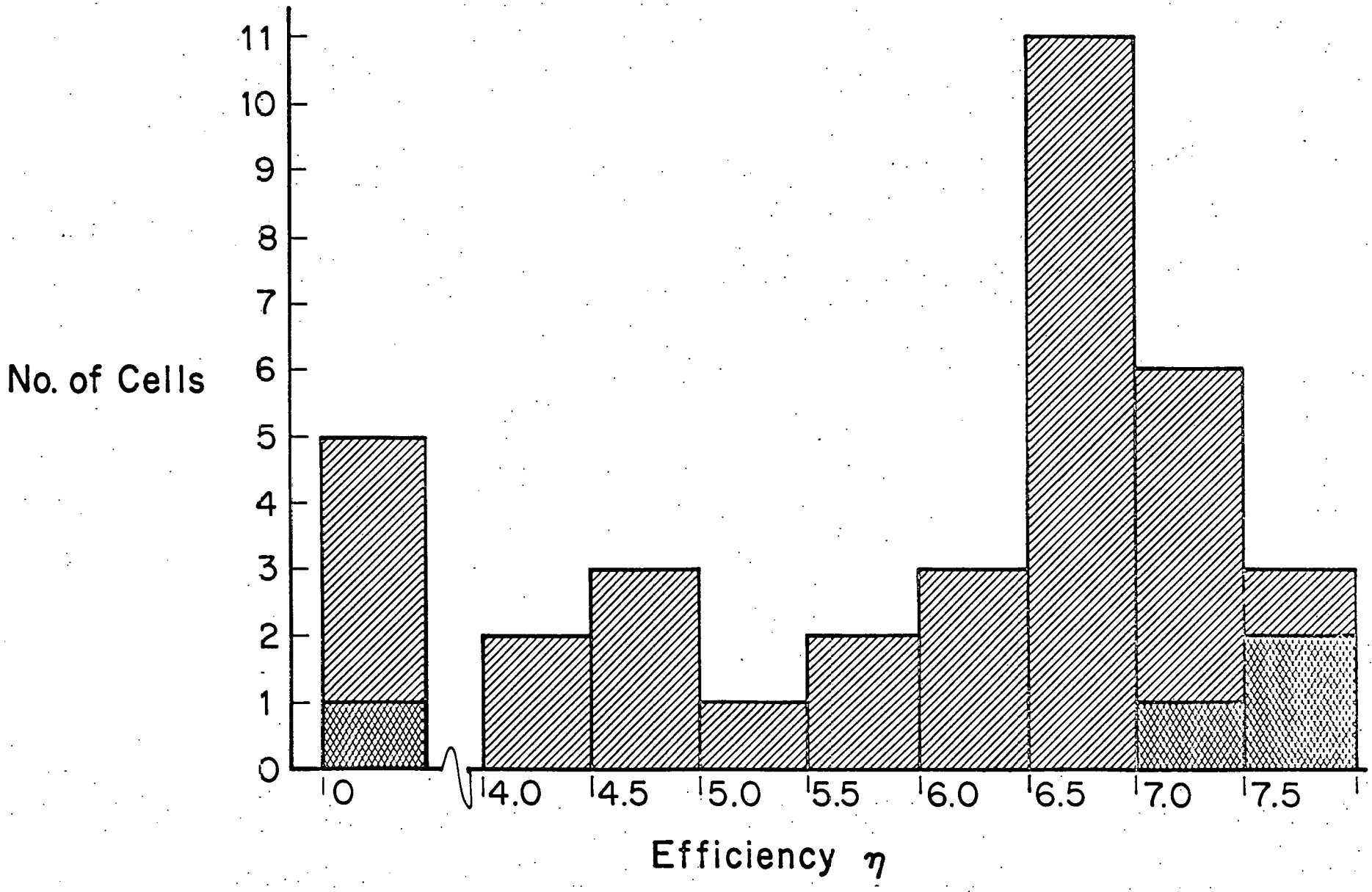

Figure 13 Distribution of Efficiency for 30 Cells. Cross-hatching indicates cells from substrate #20960.

4.2 Task 2 Development of (CdZn)S/Cu_2S Solar Cells

There has been no difficulty historically with achieving high open circuit voltages with (CdZn)S/Cu_2S junctions. The analysis that the improved electron affinity match results in a higher barrier to forward electron flow appears to be well founded and supported by the available evidence. The main focus of the research effort has therefore been directed to increasing short circuit currents with the goal being set by the achievements with the CdS/Cu_2S cell.

In addition to setting an "achievable" current level the CdS/Cu_2S experience has also provided detailed guidance for cell production modifications. Specifically the desired (CdZn)S morphology, grain structure resistivity and photoluminescence and the junction morphology have been judged from the CdS/Cu_2S experience.

4.2.1 Phase 1 Optimum (CdZn)S Films

Film Growth

The preparation of 20-30 μm thick (CdZn)S films having zinc compositions in the range of 10-20% with resistivity values less than 20 ohm-cm is now routine. Films exhibiting these properties, and which are compositionally homogeneous over an eight centimeter square substrate, are achieved using a concentric evaporation source. During the first part of this past year, a companion CdS film to each (CdZn)S film was grown using identical conditions of source temperature, substrate temperature and orifice geometry and size within the source. Solar cells were simultaneously fabricated on the companion films thus allowing for the relative comparison of V_{oc}, j_{sc} and FF.

Table 3 shows (CdZn)S and CdS cell data for the best cells (no A-R) fabricated using companion substrates. For comparable fill factors the short

Table 3

Cell Performance for (CdZn)S and CdS Cells made in Parallel

ELH simulation at 87 mW/cm^2

				Before Heat Treatment				After 16 hrs. in CO @ 170°C			
Cell #	Zinc	ρ(ohm-cm)	R(m/min)	V_{oc}(V)	J_{sc}(mA/cm^2)	FF(%)	η(%)	V_{oc}(V)	J_{sc}(mA/cm^2)	FF(%)	η(%)
1-214-111	.14	15	2.8	.590	14.36	73.2	7.1	.579	15.56	71.9	7.4
1-215-112	0	2	2.7	.493	14.96	73.9	6.3	.476	17.06	64.2	6.0
1-216-111	.16	11	4.0	.575	15.82	68.7	7.2				
1-217-114	0	1	3.4	.447	16.52	64.1	5.4				

circuit currents in the (CdZn)S devices are typically only 4-6% less than in the companion CdS devices. The difference in V_{oc} between companion pieces remains approximately the same with heat treatment. Although the two substrate sets show that the V_{oc} value is less in the (CdZn)S film with greater zinc content, the V_{oc} difference for the two sets of companion pieces increase with zinc concentration. This companion substrate approach indicated that the concentric source design could produce good cell performance grade CdS, but that the required growth parameters for optimal (CdZn)S was different than for optimal CdS. Therefore, this companion substrate approach was discontinued.

Presently, the modified concentric source bottle shown in Figure 14 is employed for the growth of (CdZn)S films. This design has eliminated the difficulties associated with the condensation of material in the bottle threads, which prevents cap removal. The tantalum heater used is constructed to assure that the temperature in the mixing chamber exceeds the temperature in the charge chambers.

Film Characterization

Three techniques are used to characterize as grown (CdZn)S films: electrical resistivity, scanning electron microscopy, and photoluminescence. The through-the-film electrical resistivity is determined using an Indium dot as one contact and the copper substrate as the other; a resistivity value is calculated only for those samples which exhibit linear I-V characteristics. When the resistivity is greater than 20 ohm-cm, it may be reduced by heat treatment in a flowing hydrogen ambient at temperatures above 200°C for several hours. Figure 15 shows two representative plots of the quantity ρ/ρ_o, which is the ratio of the reduced resistivity to the as-grown resistivity, versus hydrogen heat treatment time at 250°C. These preliminary data indicate that

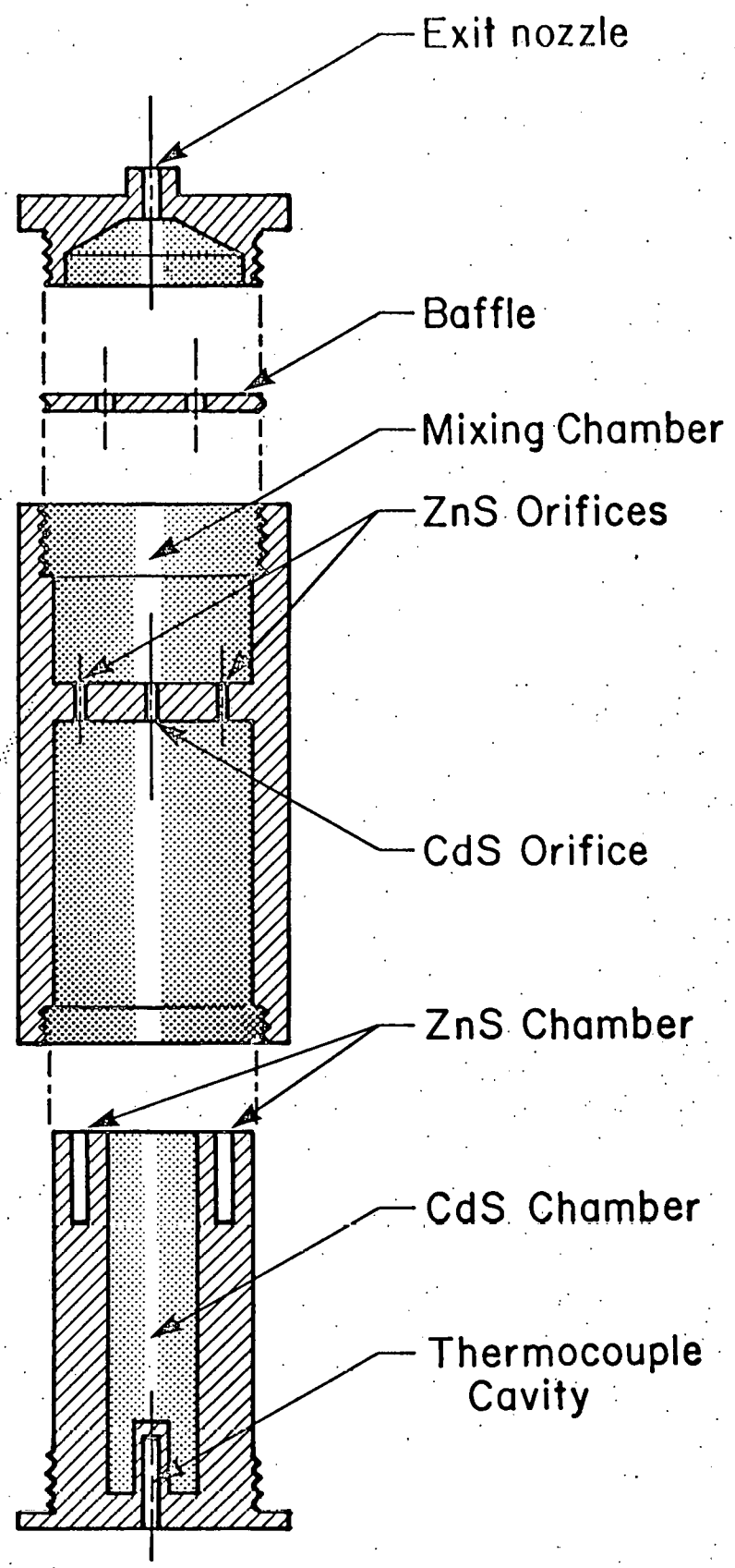

Figure 14 Concentric Source for Deposition of (CdZn)S Films.

(CdZn)S resistivity can be reduced to approximately one-third for as-grown values in the 20-100 ohm-cm range.

Figure 16 shows the scanning electron micrograph of the top surface of a (CdZn)S film which has had the grain boundaries decorated by Cu_2S. This boundary decoration is accomplished by first forming Cu_2S from the surface of the (CdZn)S film by the solution process, then stripping the Cu_2S with KCN; the removal of Cu_2S that has formed down the grains reveals the boundaries. A technique has been developed[4] to analyze the average grain size in the plane of the film using these micrographs. Figure 17 shows a plot of the derived grain size versus the average (CdZn)S film growth rate. The data represent two sets of approximately isocompositional ($\sim$ 15% zinc) (CdZn)S films, one set prepared at substrate temperature of 195°C, the other at 230°C. Since Cu_2S intrusions are most likely to occur down grain boundaries, and to the extent that deep intrusions are deleterious to cell operation, films with the largest average grain size are preferred. Accordingly films are presently prepared at a growth rate of approximately 2.0 μm/min on a 225°C substrate. These initial results of grain boundary analysis have proven valuable, and further application of the technique is intended.

Figure 19 shows a plot of the energetic position of the free exciton peak for (CdZn)S film as a function of zinc concentration. The zinc concentration was inferred from the lattice constant versus zinc composition relationship which had been established for earlier films.[6] Thus, from a measurement of the exciton peak energy a value of the zinc concentration may be inferred. In addition a qualitative evaluation of the (CdZn)S film can be made using the relative peak heights of the three major bands. Specifically, the absence of

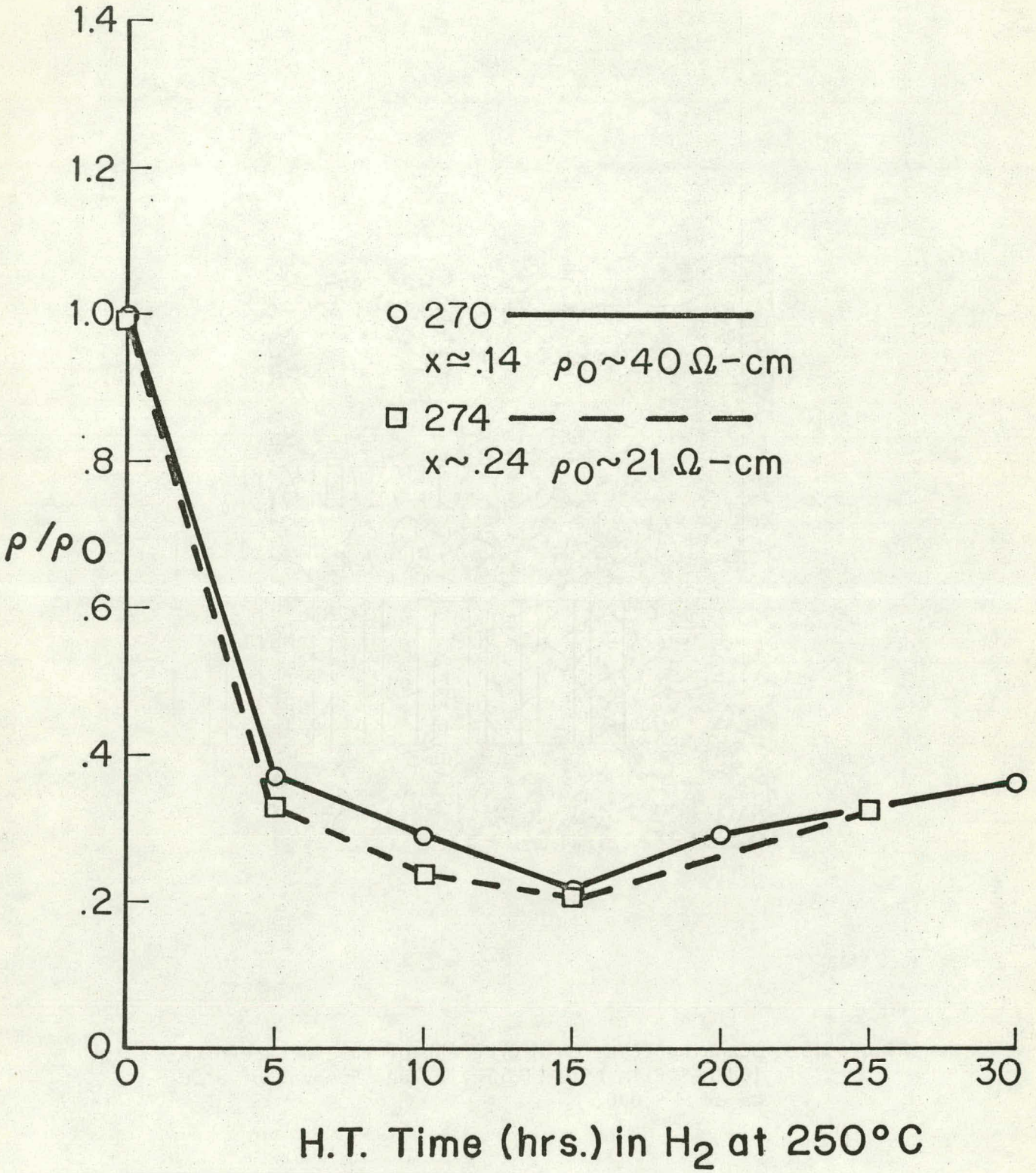

Figure 15 Influence of Heat Treatment on the Resistivity of (CdZn)S Films.

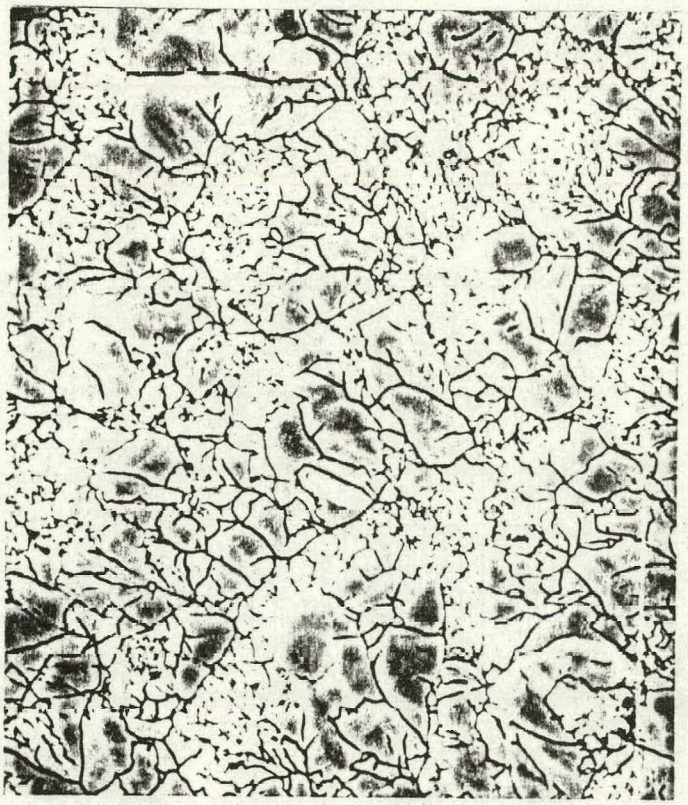

Figure 16 Scanning Electron Micrograph of the Surface of a (CdZn)S Film After Formation and Removal of a Cu_2S Layer x 5,000.

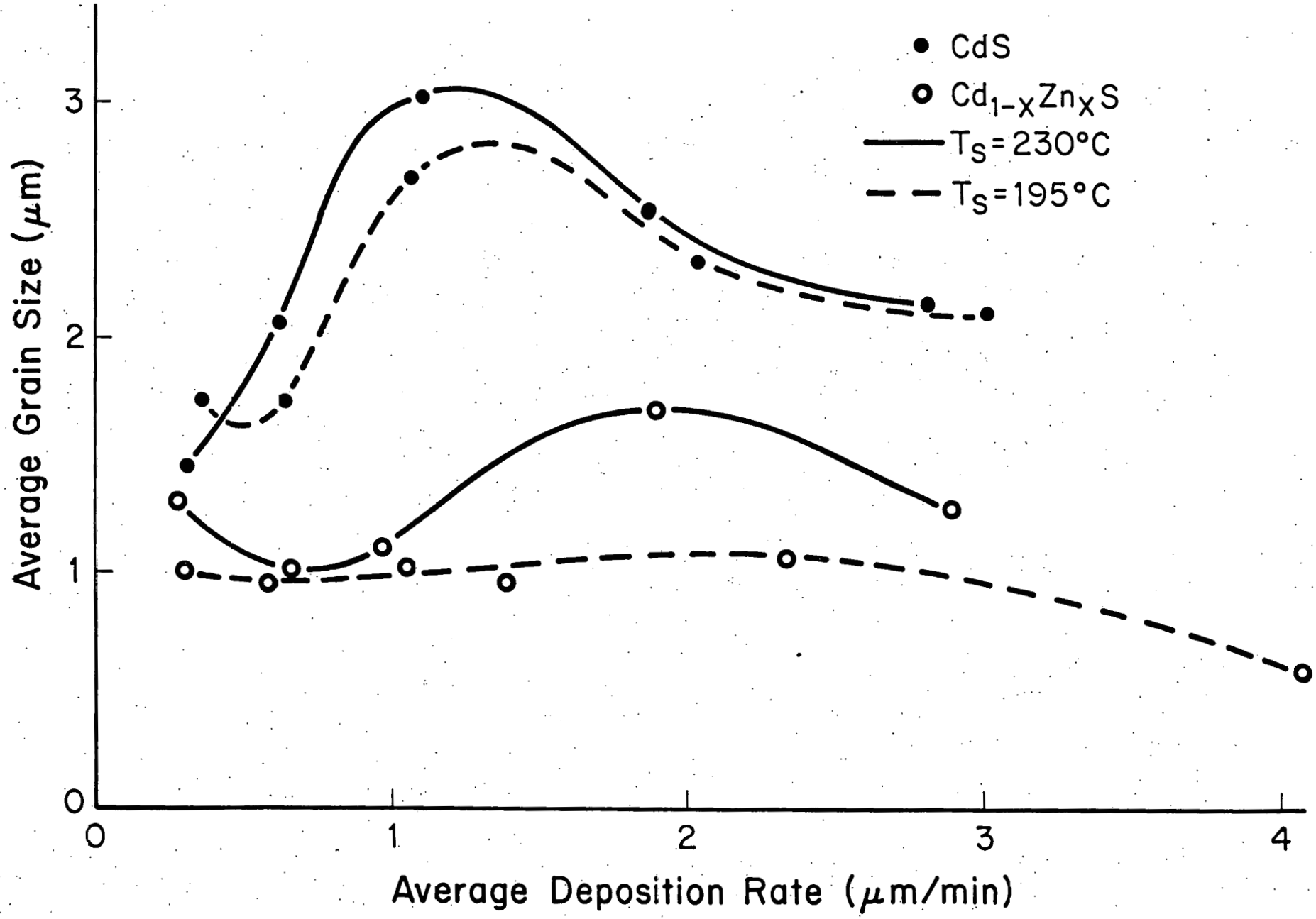

Figure 17 Influence of Deposition Rate on CdS and (CdZn)S Grain Size.

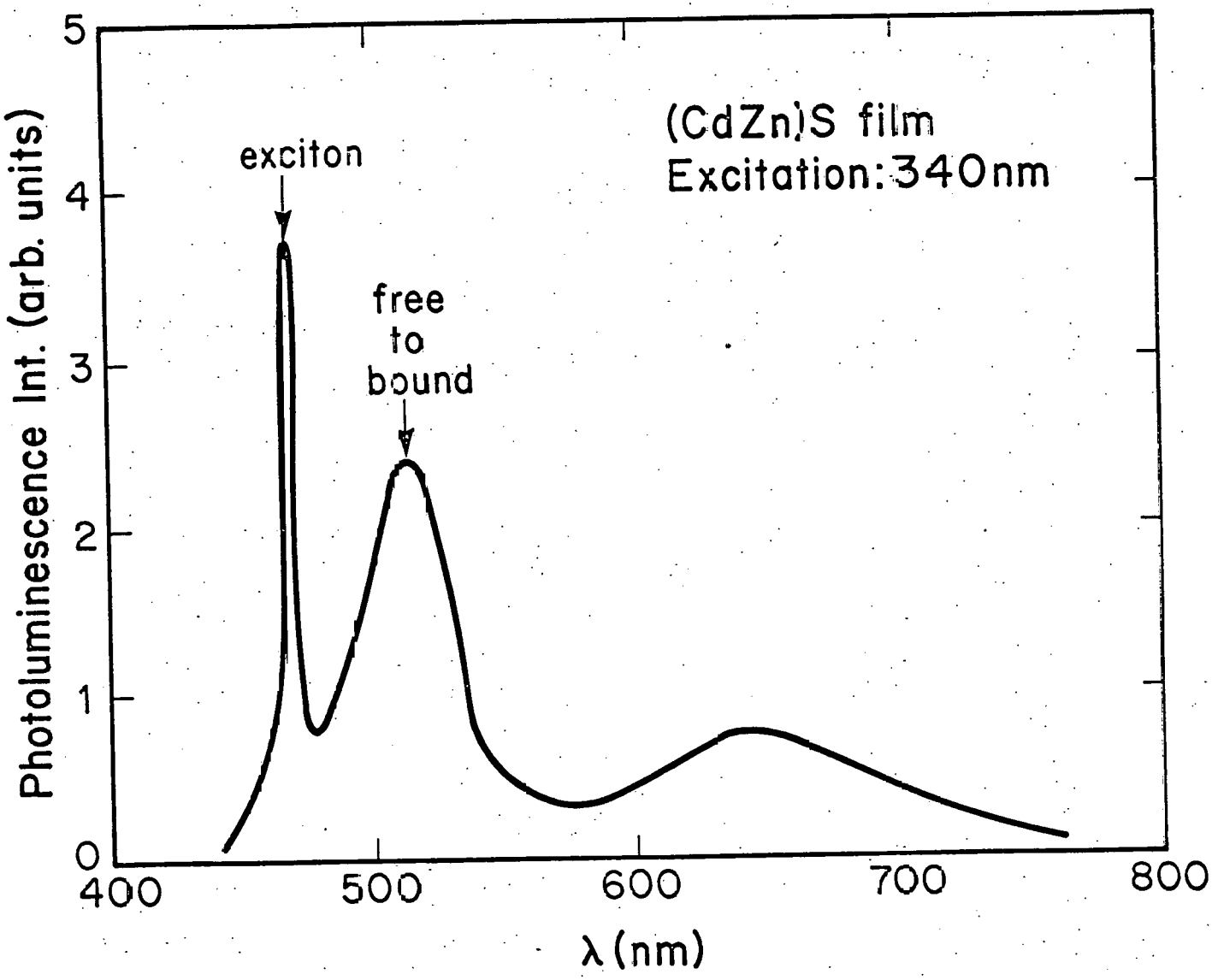

Figure 18 Photoluminescence at 77°K of (CdZn)S Film.

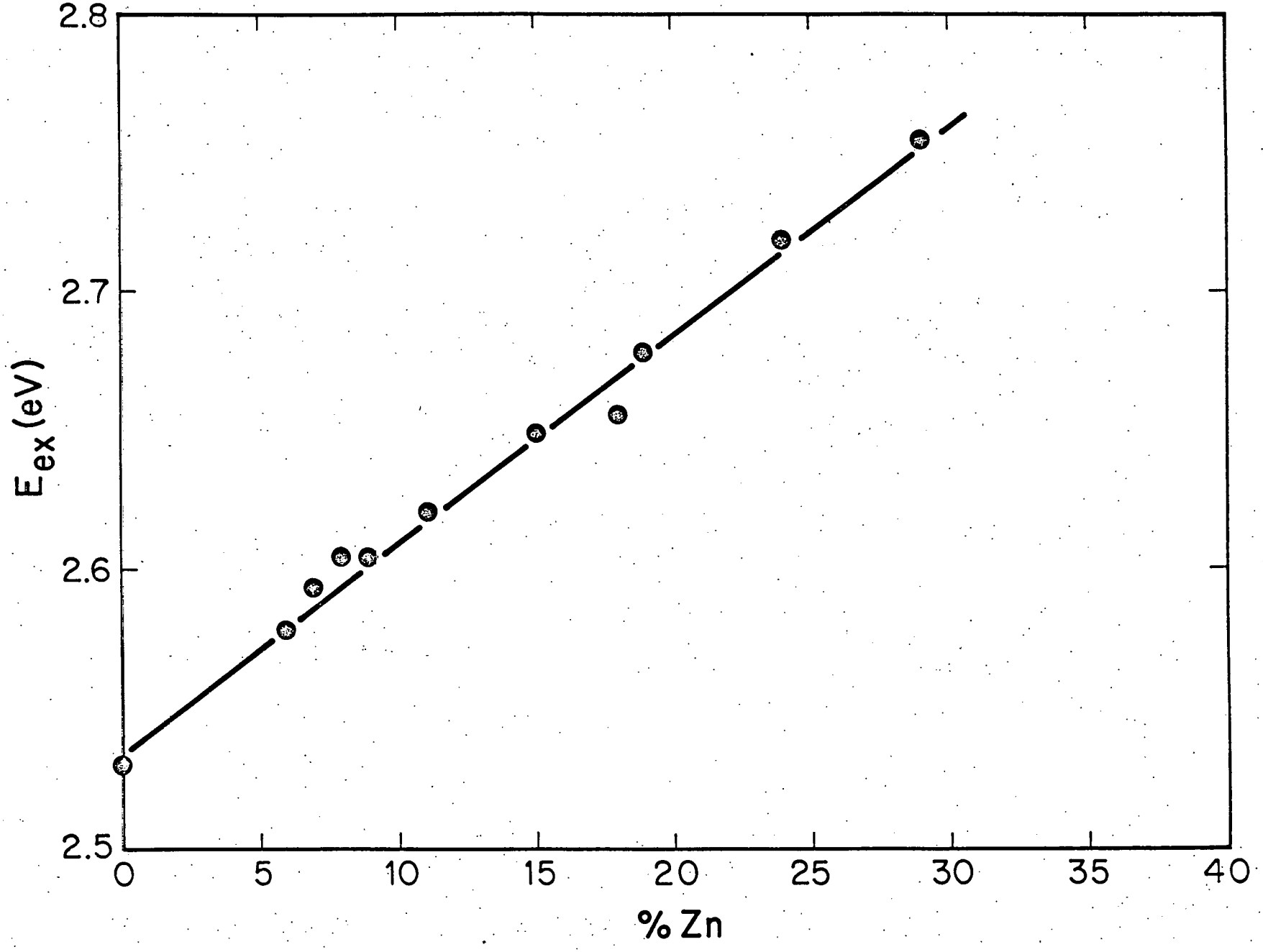

Figure 19 Energy of the Exciton Peak as a Function of Zinc Content for (CdZn)S Films.

the free-to-bound transition results in devices having lower V_{oc} than would be anticipated from a given zinc composition. The long wavelength band is generally observed in all (CdZn)S films; when this band has been observed in CdS, it is found that the light generated current of Cu_2S cells fabricated on it are influenced by a wavelength dependent collector-converter junction field. Work continues toward the identification of the lattice defect responsible for this emission.

4.2.2 Phase 2 Development of Junction Formation

Relationships of Cell Characteristics and Cu_2S Formation

The chemical and morphological details of the formation, and the electrical and optical consequences on the operation of the Cu_2S-(CdZn)S junction, have been investigated during the past year. Table 4 shows relevant component property, cell formation and cell property data for two sets of companion substrate samples. On one set the Cu_2S was prepared by the standard solution process,[7] on the other by the solid state reaction process. The performance of these cells has not been fully optimized nor do they have anti-reflection coatings, which has a particularly strong effect on the currents and hence on measured efficiencies.

The listed parameters indicate significant differences in the junction structure for the (CdZn)S as compared to the CdS. The dark capacitances for the (CdZn)S/Cu_2S cells are approximately twice those for the CdS/Cu_2S having the same treatment sequence. This could be either a major difference in the junction area, or a consequence of slower diffusion of compensating copper into the (CdZn)S. The degree of change of the open circuit voltage in the (CdZn)S is quite dramatic indicating that the morphology of the junction is sensitive to the Cu_2S formation procedure. Although the a-c shunt conductance

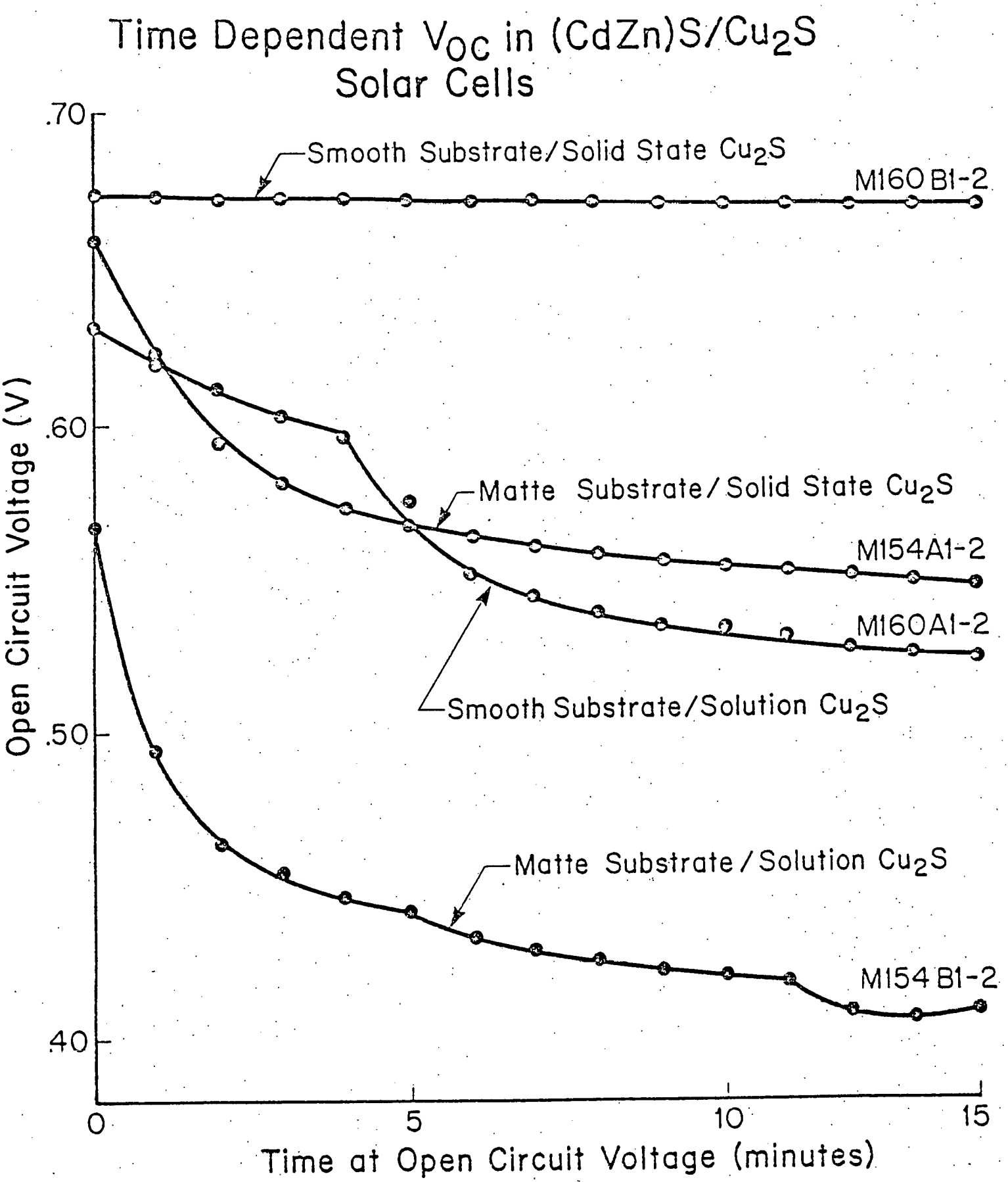

Figure 20 Time Dependent V_{cc} for (CdZn)S/Cu_2S Cells of Various Designs.

Table 4

CdS/Cu_2S and $(CdZn)S/Cu_2S$ Cell Data

Cell Formation				
CdS Surface	Smooth		Textured	
Cu_2S Formation	Solid State		Solution	
Zinc Content	0	19%	0	19%
Substrate Piece Number	1-155-11	1-154-11	1-155-21	1-154-21
Component Properties				
Resistivity(Ω-cm) CdS or (CdZn)S	6	15	6	15
Cu_2S Thickness (Å)	2180	1370	3146	2480
Cell Properties				
V_{oc}(V)	.500	.655	.501	.616
J_{sc}(mA/cm^2)	11.0	9.35	14.5	10.8
FF (%)	69.1	66.0	71.1	66.0
η (%)	3.82	4.05	5.18	4.37
$G_{sh}(\Omega\text{-cm}^2)^{-1}\times10^{-3}$	1.76	2.62	1.98	3.11
C/A Dark(nF/cm^2)	7.?	18.0	16.0	33.0
C/A AM1(nF/cm^2	59	65	74	93

is lower for Cu_2S formed on the (CdZn)S by the solid state process, both conductances are higher than observed in the CdS companion prices. Previous experience with the CdS cell has shown that high shunt conductances are related to defects in the Cu_2S layer, in particular the intrusion into the CdS by the Cu_2S.

As has already been reported[2] (CdZn)S cells often have open circuit voltages which decay with time. Experiments conducted with cells manufactured by the solution and solid state reaction show quite substantial differences in behavior. Figure 20 shows the open circuit voltage decay for a number of cells that have significantly different junction morphology, owing to the manner of Cu_2S preparation. It is seen that the more stable cells are those expected to have the most planar junction suggesting the temporal instability is related to the morphology of the junction.

Cu_2S Morphology

Optical cross sections were employed to illustrate differences in Cu_2S morphology accompanying different formation processes. Data were gathered for a range of (CdZn)S compositions for which the junction with Cu_2S was formed by the solution process. These data indicated that the linear density of intrusions and their average penetration depth increased with increasing zinc composition. This optical technique did not reveal evidence of Cu_2S intrusions for (CdZn)S/Cu_2S junctions formed by the solid state process, although the time dependence of V_{oc} decay persisted to some extent.

The Cu_2S morphology is revealed in considerable detail by using an SEM to view free standing Cu_2S from which the CdS film has been dissolved away.[8] The SEM micrographs of the free standing Cu_2S reveal the existence of 6-8 μm long cone-like Cu_2S structures (i.e. "intruding" into the (CdZn)S. Cu_2S

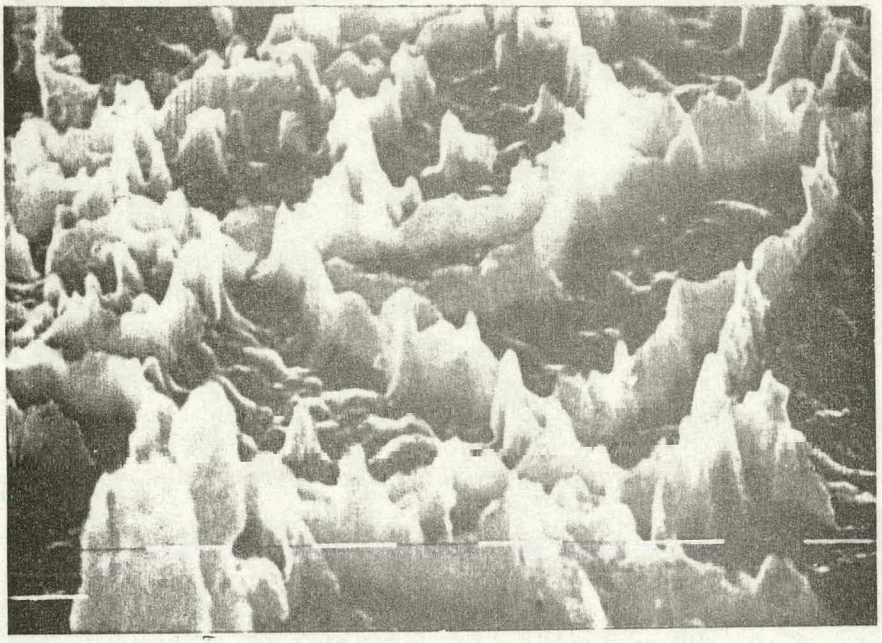

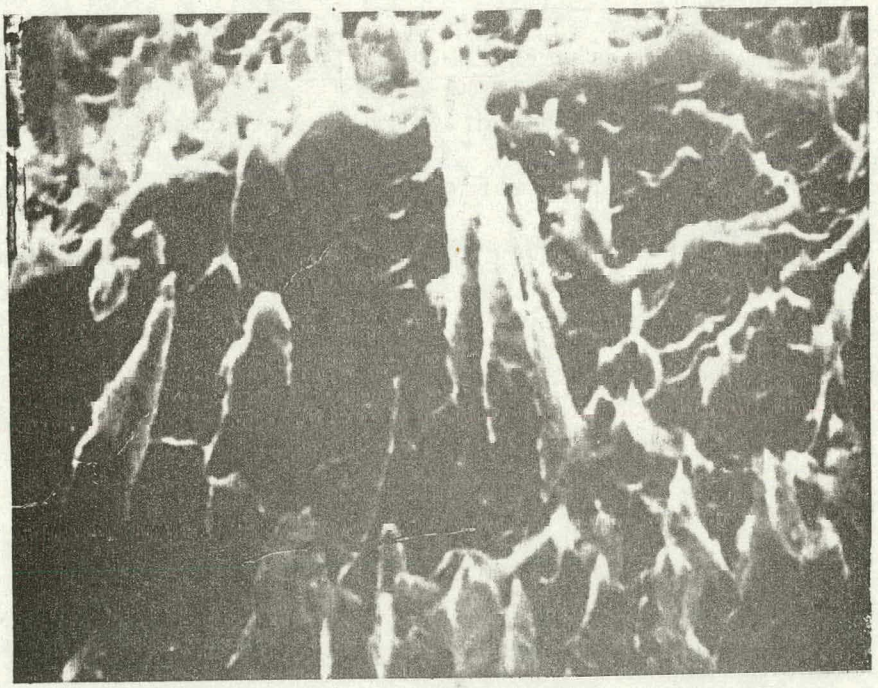

Fig. 21 Scanning Electron Micrographs of Cu_2S removed from CdS and (CdZn)S cells.

a) CdS cell 778.B14

b) (CdZn)S cell M154.B11 (19% Zn)

Both micrographs x 10,000

intrusions are also present at CdS/Cu_2S junction, however, they appear as "walls" around the CdS columnar boundaries, and typically extend only 1-2 μm into the CdS. Figure 21 shows representative views of these two types. These intrusions are expected to strongly influence the solar cell device characteristics, and the V_{oc} value of devices exhibiting long cone-like intrusions is found to decrease when the device is held in the open circuit condition. The formation of these intrusions is expected to depend on the (CdZn)S microstructure, and will also be influenced by the manner in which the Cu_2S is formed.

This new information about the (CdZn)S-Cu_2S morphology requires a modification to the earlier model[7] used to explain V_{oc} decay, and suggests an alternative mechanism. Initially, it was proposed that the decay occurs as a consequence of charging effects (i.e. traps, their distribution and density) in the depletion region of the (CdZn)S. It is this effect which is employed to interpret time dependent dark I-V characteristics for CdS/Cu_2S cells.[9] For the (CdZn)S/Cu_2S cells it was proposed[7] that even with light there were not the necessary population of hole traps, and/or the hole traps were not being charged in the critical junction region. The existence of cone-like Cu_2S intrusions suggests that tunneling becomes a factor in the junction operation. Since the appropriate wavelength light does not reach these deep cone intrusions, the reduction in the space charge region, and hence the higher collection fields, occurs only after sufficient time has passed to trap holes. As holes become trapped, the fields become larger as a consequence of the point geometry of the cones and tunneling is promoted in these regions. The time dependence is associated with the narrowing of the space charge region at points which are at different depths below the junction. As a consequence of these varying depths the amount of light reaching them and the speed at which the tunneling takes place will

vary. The decrease in V_{oc} is due to the fact that once tunneling is established, these regions carry a higher current than the planar regions of the junction and in effect have a lower barrier height.

An alternative model which relates these Cu_2S cone intrusions to the V_{oc} time decay involves the motion of copper. At V_{oc} in the light, a potential difference exists across the length of the cone intrusions which tends to promote the motion of copper in the Cu_2S toward the back electrode. At the cone points the copper can precipitate at grain boundaries leading to a junction shunt. The magnitude of the shunt, and hence the reduction in V_{oc} will depend on the amount of precipitated copper, which in turn depends on time. When the light is removed, the copper dissolves back into the Cu_2S cone intrusion, thus removing the shunt and allowing the observed V_{oc} recovery before the light is next applied.

4.2.3 Phase 3 Application of CdS Cell Fabrication Technology to (CdZn)S

During the past year full integration of (CdZn)S films into the CdS cell fabrication process has been accomplished. Several process variables had to be adjusted to ensure cell yield. For example, in order to avoid shorts since the (CdZn)S films were typically less than 20 μm thick, it was necessary to reduce the HCl etch time for film texturing. During the coming year alternative texturing etches will be investigated in order to exercise greater control on the cell texture.

The utilization of the standard CuCl solution[7] for the junction formation yielded Cu_2S of suitable thickness (equivalent thickness 300-400 nm) with stoichiometries that could be optimized by subsequent reducing heat treatments. Prior to this year the heat treatments resulted in a general degradation of all cell properties (i.e. V_{oc}, j_{sc} and FF). However with

the improvement of (CdZn)S film quality, (CdZn)S/Cu_2S cells are now responding to cell heat treatments in a similar manner to CdS/Cu_2S cells.

The technology for the evaporation of 32.5 line/cm gold grids and the application of double layer A-R coatings, which have been developed for the CdS/Cu_2S cell, have been successfully transferred to (CdZn)S/Cu_2S cells.

4.2.4 Phase 4 Statistical Sample

Figure 22 shows the distribution of the best conversion efficiency and the best current density at 100 mW/cm^2 illumination for nine cells which have a double A-R coating (TiO_2/SiO_2). The nine cells were selected from an initial set of sixteen cells from three different substrates. Prior to the selection of cells to receive the A-R layer and subsequent optimization of Cu_2S stoichiometry fourteen of the sixteen cells were over 6% efficiency; two were shorted. The best V_{oc} values, calculated from $V_{oc} = \frac{kT}{q} \ln \frac{j_L}{j_o}$ at j_L = 20 mA/cm^2, were in the range of 580-600 mV; the zinc concentration for the three substrates was approximately 10%.

Figure 23 shows the current voltage curve of the most efficient cell (8.19%) from the above sample set measured under an ELH simulator intensity of 92 mW/cm^2. The 68% fill factor is typical of this set of cells which generally had fill factors between 60 and 70%. The values of lumped series resistance and shunt conductance calculated from the I-V curve for the cell in Figure 23 are 2.9 ohm-cm^2 and 3.22 x 10^{-3} $ohm^{-1}cm^{-2}$. respectively. The shunt conductance is the major contributor to the fill factor loss, and is probably indicative of intrusive Cu_2S morphology. Although less of a factor,

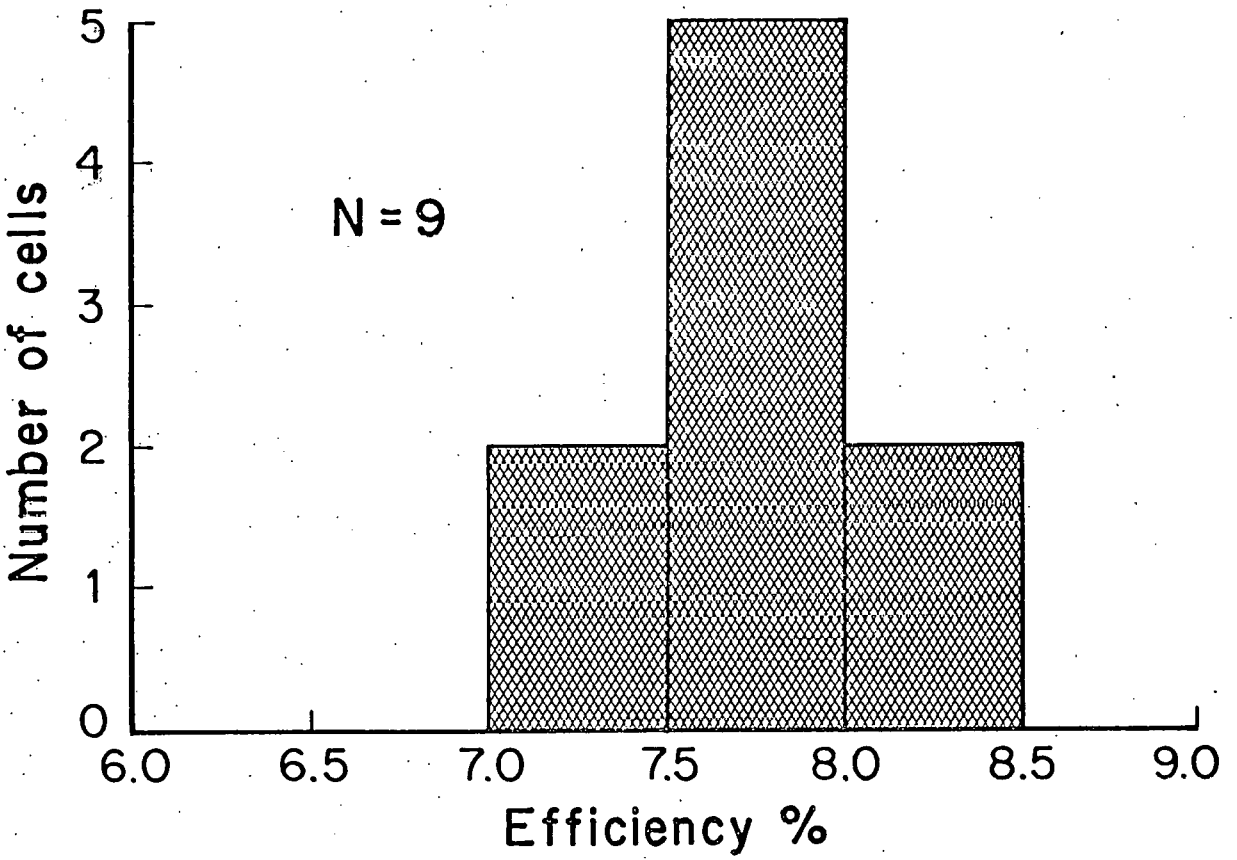

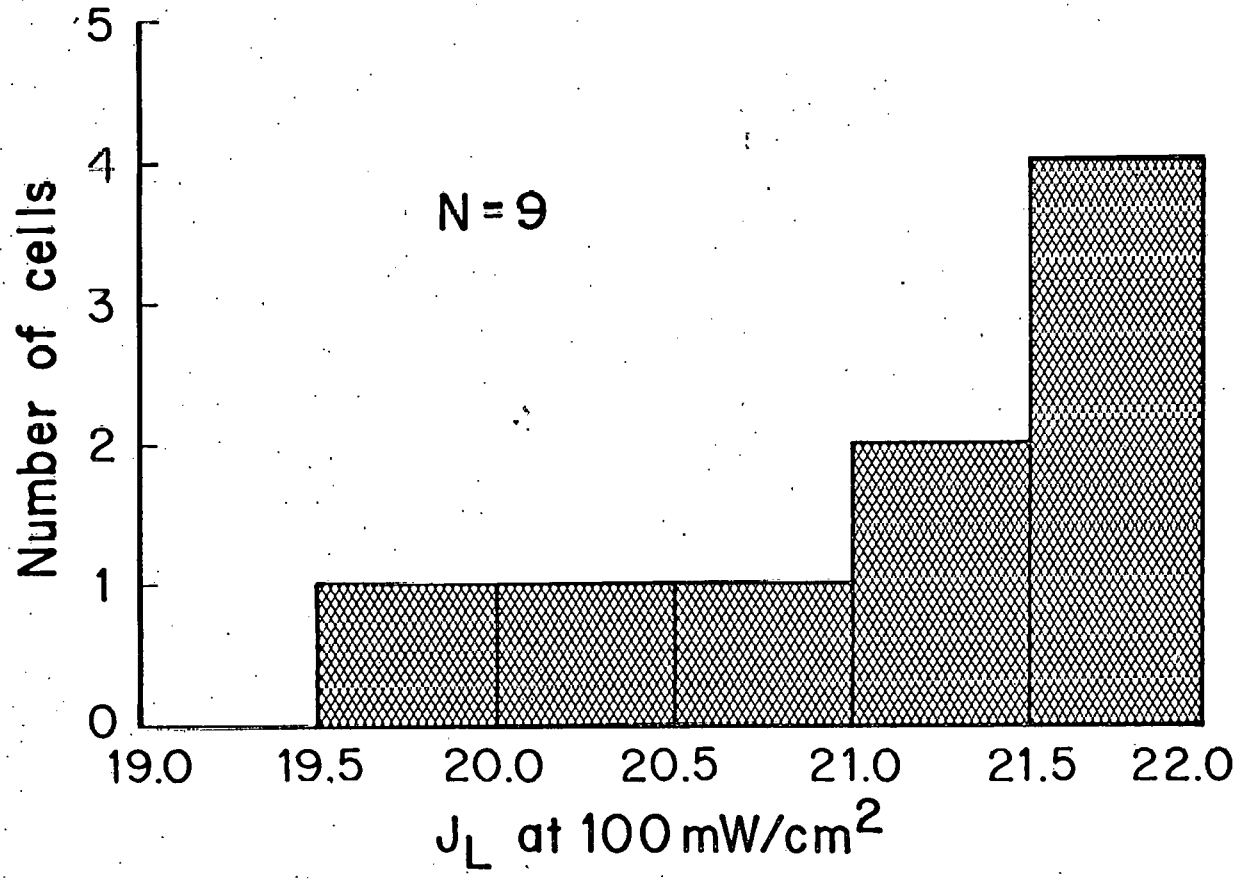

Figure 22 Distribution of Efficiency and Light Generated Current for a Sample of nine (CdZn)S/Cu_2S Cells.

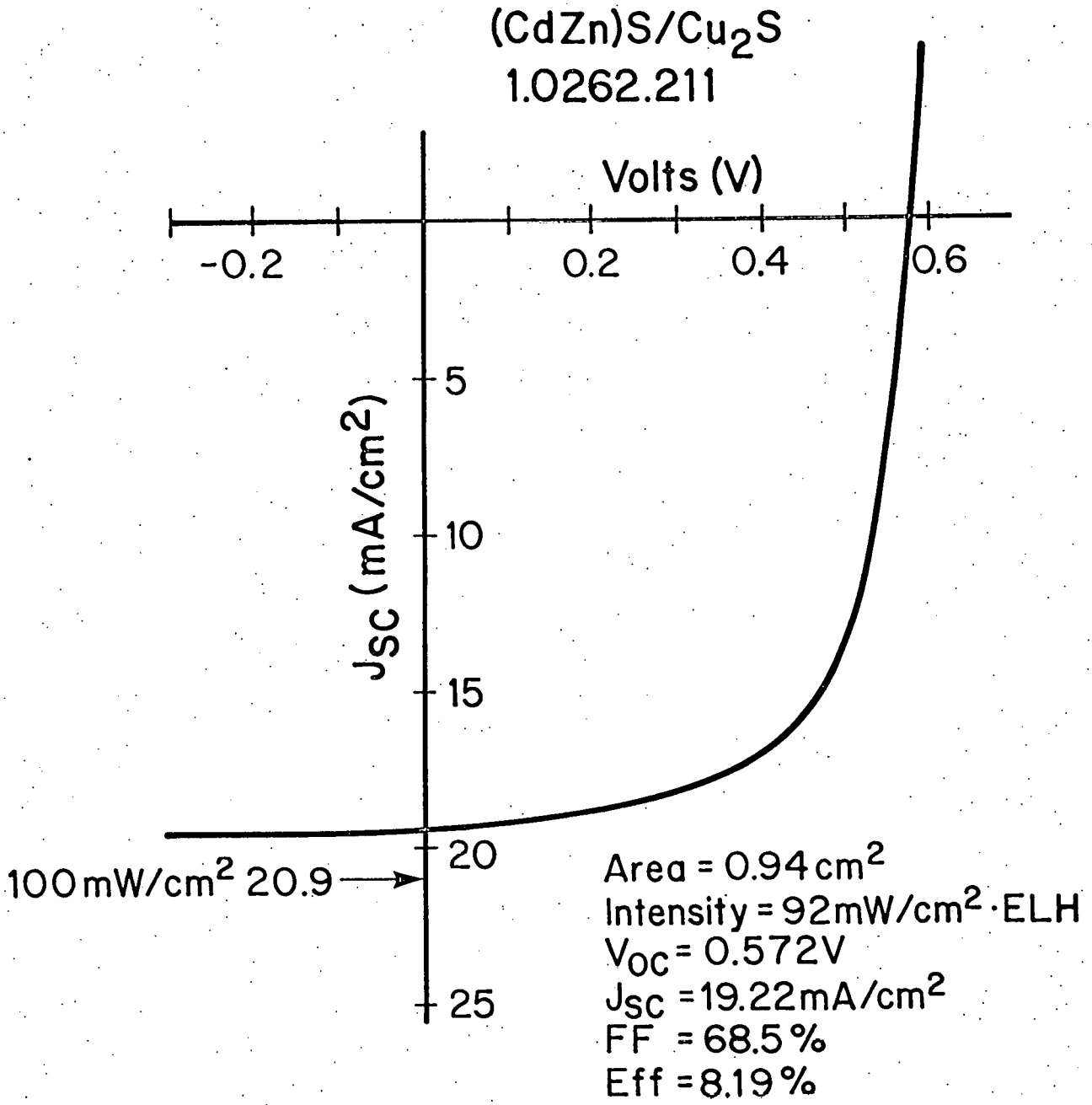

Figure 23 Current-Voltage Curve for (CdZn)S/Cu_2S Cell Containing 9% Zinc.

the series resistance is still somewhat high, and is probably a consequence of the relatively high resistivity (100 ohm-cm) of the (CdZn)S film. It is anticipated that the development of non-intrusive Cu_2S will reduce shunt losses in fill factor, and that the achievement of lower (CdZn)S film resistivities with continued development of post-deposition heat treatments will reduce the series losses.

4.3 Task 3 Electro-Optic Analysis and Modeling

The testing cells for basic current-voltage performance continues to provide the day to day direction for the cell development tasks. Longer term direction for programs is provided by the in-depth studies of various aspects of cell structure and operation. Particular attention has been given to the junction field in the CdS and (CdZn)S and to the identity and role of hole traps.

4.3.1 Phase I Feedback Analysis

The substrate evaluation process (SEP) was devised in order to allow a relatively fast method of qualifying material made by the standard process on a pass/fail basis. In general, one piece (4 cells) was taken from a substrate and sent through the evaluation process; the substrate was then passed or failed according to the performance of that piece. Immediately after manufacture and each heat treatment, the cells were tested. If a fill factor greater than 55% was achieved, the values for R, G, J_L and J_o were computed. A set of standardized criteria, based on the values of FF, J_L and J_o were then employed to determine the next heat treatment for each of the cells. The SEP continued until a piece had at least one cell with $J_L \geq 18$ mA/cm^2 and a $J_o \leq 5 \times 10^{-8}$ mA/cm^2 (not necessarily during the same test). A piece failed if J_L or J_o did not satisfy these requirements, and if the cells on that piece

did not respond to the appropriate heat treatments.

A statistical analysis of the data from the SEP was carried out to determine if we could discriminate between passed and failed material at an earlier stage, and to attempt to identify any parameters that might account for the poor performance of the failed material. The process conditions and the initial I-V parameters were treated as continuous random variables. For each parameter, the sample from the material that failed was compared to the sample from the material that passed (pieces that technically failed, but which came close to passing were classified as borderline and not included in the statistical tests). The comparisons were made using the Wilcoxon[10] two-sample test (IMSL subroutine-NRWRST) and the sample distributions were displayed using an available graphics program. A full description of the statistical analysis and the graphical displays are given in Appendix A.

The conclusions drawn from this analysis are as follows:

1. Several of the initial I-V parameters allowed discrimination between passed and failed material.

   a) The maximum initial fill factor discriminates strongly. The Wilcoxon test shows a highly significant difference between the passed and failed samples. (See page A-3). This result can be seen graphically (Fig. A-1). A horizontal line drawn through the 66% fail factor mark divides most of the passed from most of the failed material.

   b) Ability to discriminate was also observed in the variables R, G and J_o

2. J_L and the parameters measured after evaporation (CdS thickness-THCDS, Resistivity ρ, Photoluminescence P_L) showed no ability to discriminate. For example, P_L - the ration of the relative peak height of the green edge emission (520 nm) to the relative peak height of free exciton (488 nm) - was tested with the Wilcoxon and showed no significant difference between the

passed and failed populations. See pages A16 and A17. It must however be remembered that all the material submitted for SEP was grown under the conditions established for acceptable CdS. Previous use of photoluminescence to assess the quality of the CdS covered luminescent behavior well outside the range dealt with here.

3. About half of the material failed due to one parameter alone - J_o. In other words, about half the material met the J_L requirement of 18 mA/cm^2, but not the J_o requirement of 5×10^{-8} mA/cm^2. One possible explanation of this is a morphology problem, since J_o is related to the effective junction area.

4.3.2 Phase 2 Junction Field in CdS

In addition to measuring variations in junction field by means of the spectral response technique, the field can also be obtained from the capacitance of CdS/Cu_2S cells, measured on the set-up described in an earlier report.[11] Recent modifications to the method are described below under Phase 3.

As described in a recent paper[12] the junction field F_2 in the uniform-space-charge approximation is proportional to the capacitance C according to the equation

$$F_2 = \frac{2(V_D-V)}{w} = \frac{2(V_D-V)}{\varepsilon\varepsilon_o} \frac{C}{A}$$

where w is the width of the depletion layer, V_D the diffusion voltage, V the applied bias voltage, and A the area of the junction. Changes in V and in white-light intensity Φ strongly affect C.

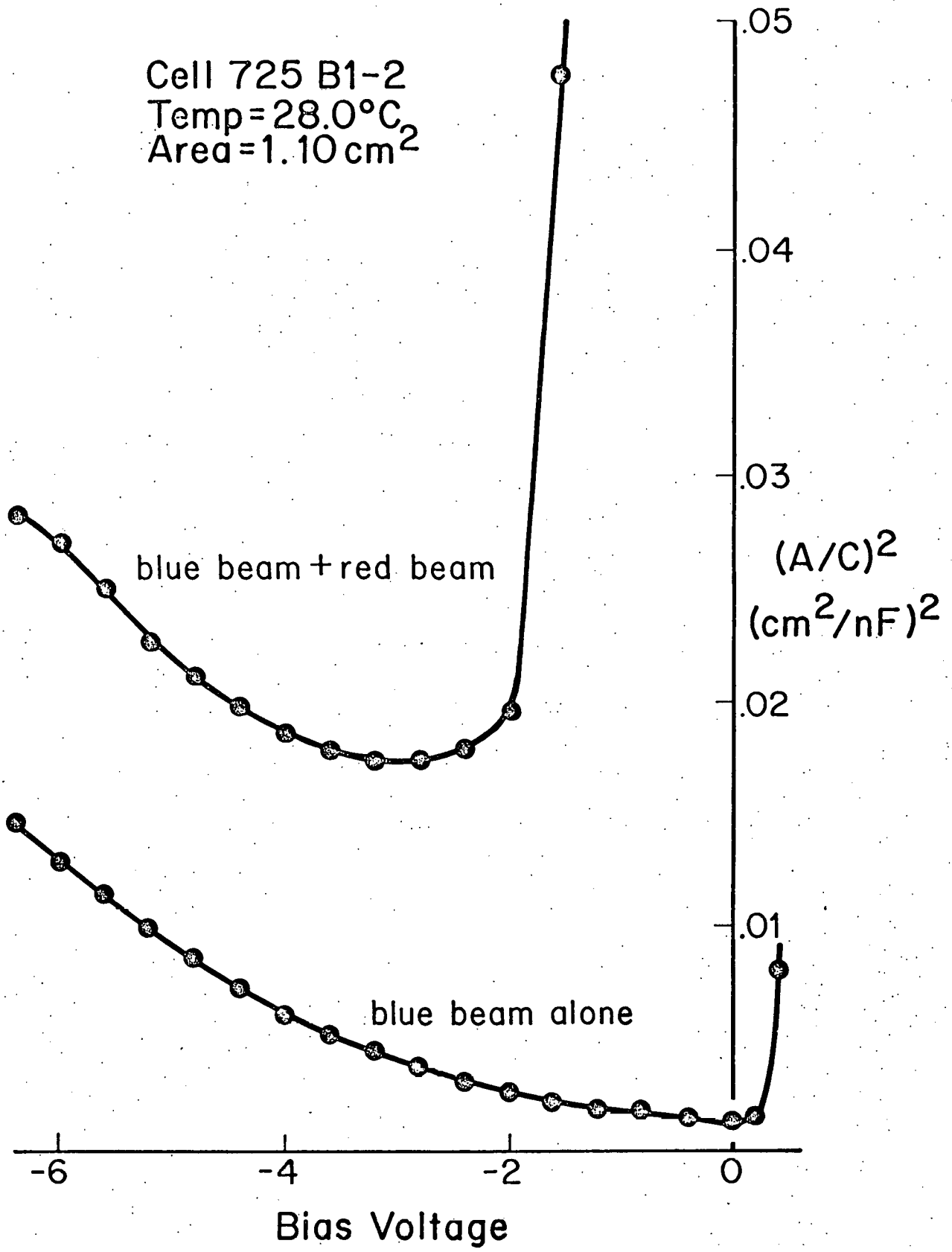

Figure 24 Variation of Inverse Capacitance with Bias Voltage and Illumination for a CdS/Cu_2S Cell.

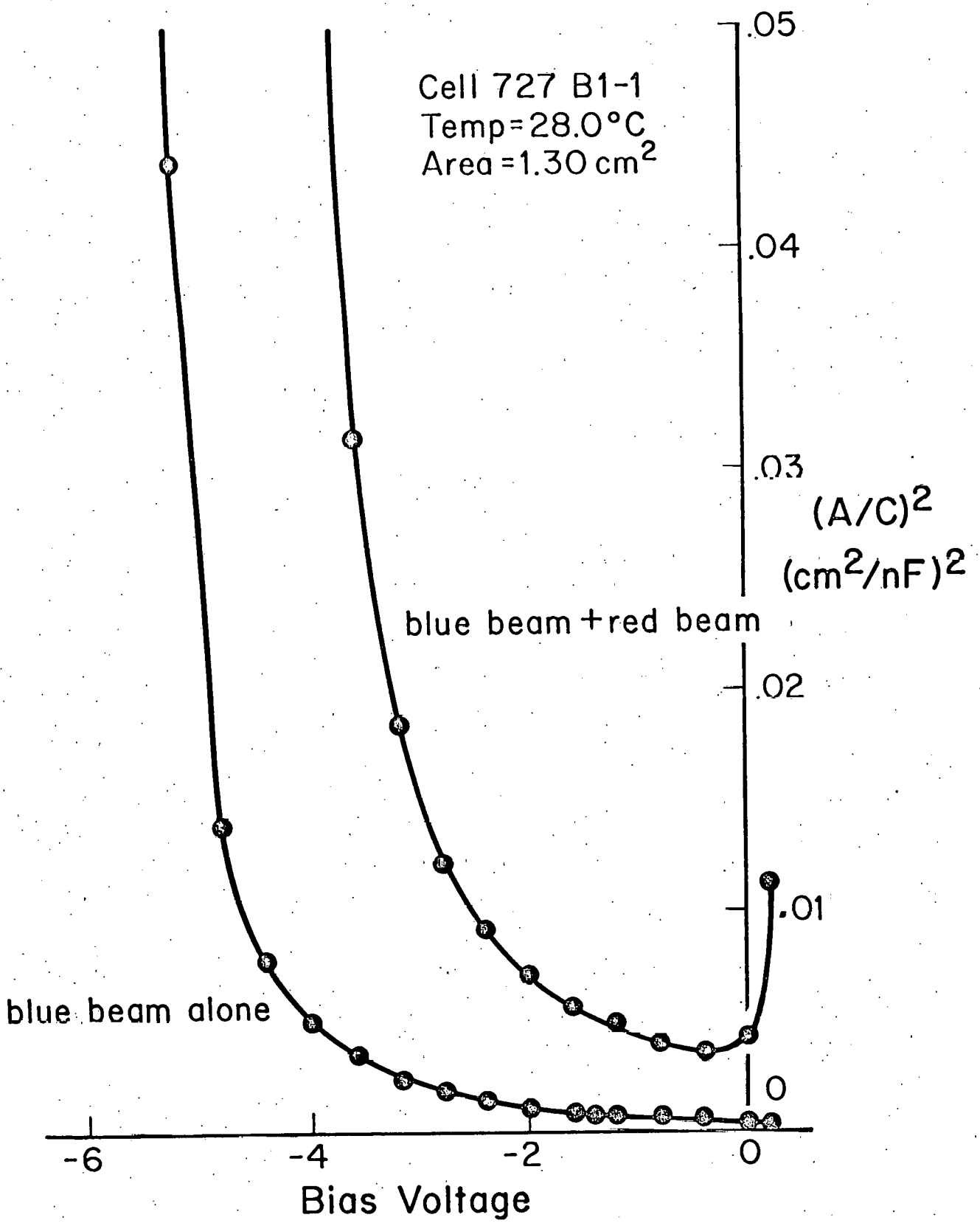

Figure 25 Variation of Inverse Capacitance with Bias Voltage and Illumination for a CdS/Cu_2S Cell.

The spectral content of the light striking the cell also has a strong effect on capacitance because of the loading and unloading of hole traps. Preliminary data on C versus V variation in two cells excited by either a blue beam alone or by blue and red beams simultaneously appear in Figures 24 and 25. The blue beam is produced by passing light from a 50-watt tungsten-iodine lamp thru color glass filters so that 350 nm < λ < 580 nm approximately. The red beam is produced by passing light from a 650 watt tungsten-iodine lamp thru a filter with short-wavelength cut off at about 660 nm. Intensities were adjusted repeatedly to maintain the current output of a monitor Si cell constant at its AM1 value.

The curves strongly depart from a linear increase of C^{-2} with reverse bias, except for limited ranges under blue light alone and near zero bias. Even under the blue beam alone, the slope gradually increases as the bias goes farther into reverse. The addition of red light strongly decreases C in cell #725 B1-2, which had good efficiency. The effect is to raise the general level of the curve while its slope changes to the opposite sign near zero bias. This effect probably reflects the introduction into the depletion region of a high density of free electrons from the Cu_2S.

In cell 727 B1-1, a lower efficiency cell, there is much less change in C at small bias upon turning on the red beam. At larger values of reverse bias, C^{-2} for either illumination diverges markedly from linear with V.

Because of such anomalous behavior and because of the large differences between two cells whose performance parameters are not strikingly different, it was decided to obtain further C-versus-V data for varying levels of white-light illumination for other cells. It was considered especially desirable to determine behavior at very low, but non-zero, values of Φ. These data, as $(A/C)^2$

versus V plots, appear in Figures 26 and 27. Table 5 gives Φ for the nine curves for both cells. Again a large difference between two cells was seen. It is believed that the results in Figure 26, for cell 20860.111, are more characteristic of cells of fairly high efficiency. We will discuss these results first.

Table 5

White Light Intensities for the Curves Shown in Figures 26 and 27

Curve	Φ/Φ_{AM1}
0	0(dark)
1	3.4×10^{-4}
2	9.1×10^{-4}
3	.0034
4	.011
5	.035
6	.10
7	.33
8	1.00

Dark capacitance is seen to be almost constant with V except at large reverse bias, $V \lesssim -7$ volt. This is consistent with the interpretation of capacitance resulting from an insulating layer composed of the charge-compensated region rather than from the depletion layer proper. Thus changes in the reverse bias which change depletion layer thickness w would have little effect on capacitance until w reached the limit of the compensated region. This may be seen at - 7 volt, where C begins to decrease. The possibility that this behavior at large reverse bias is associated with conduction effects is however not ruled out.

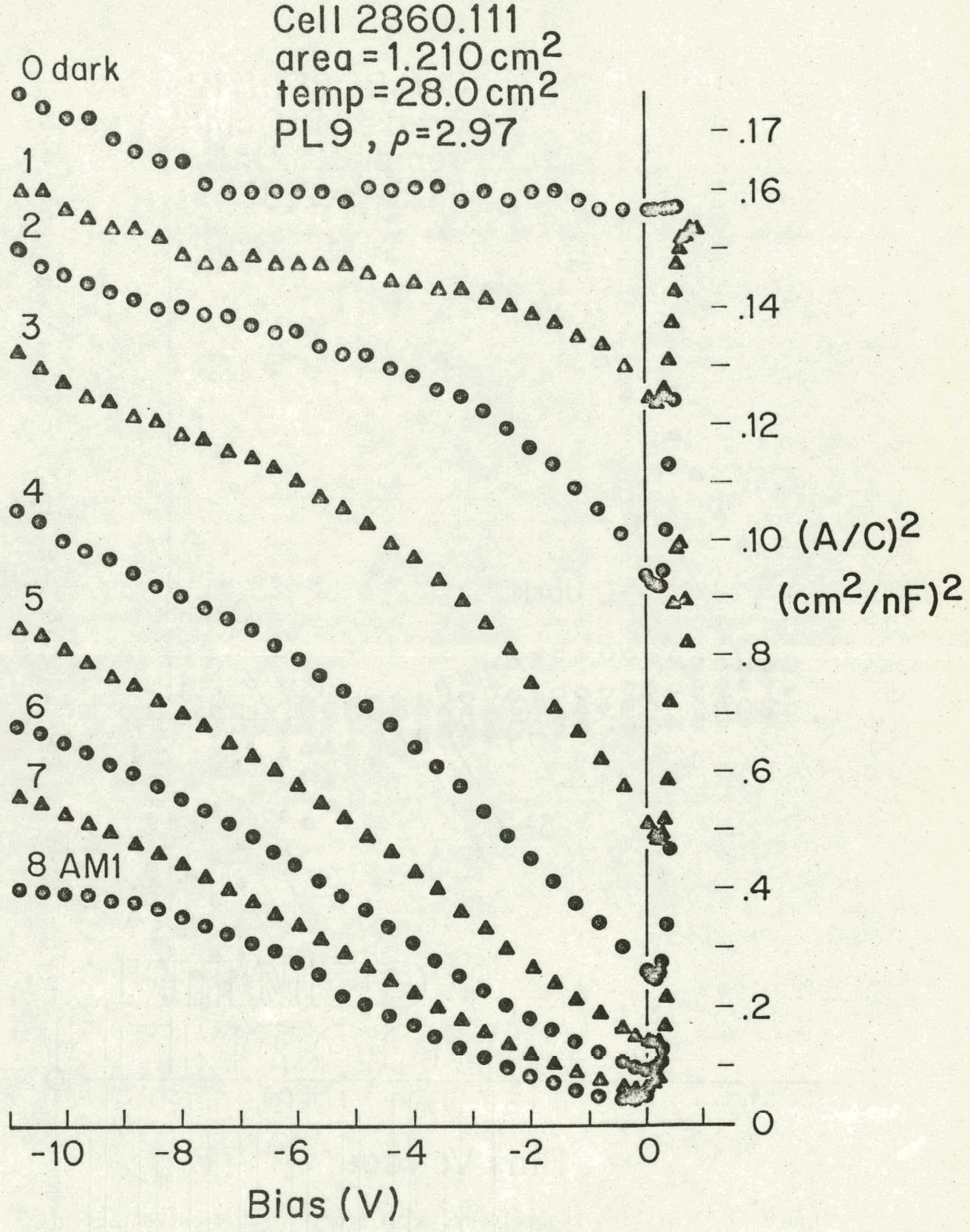

Figure 26 Reciprocal Capacitance as a Function of Bias Voltage for Light

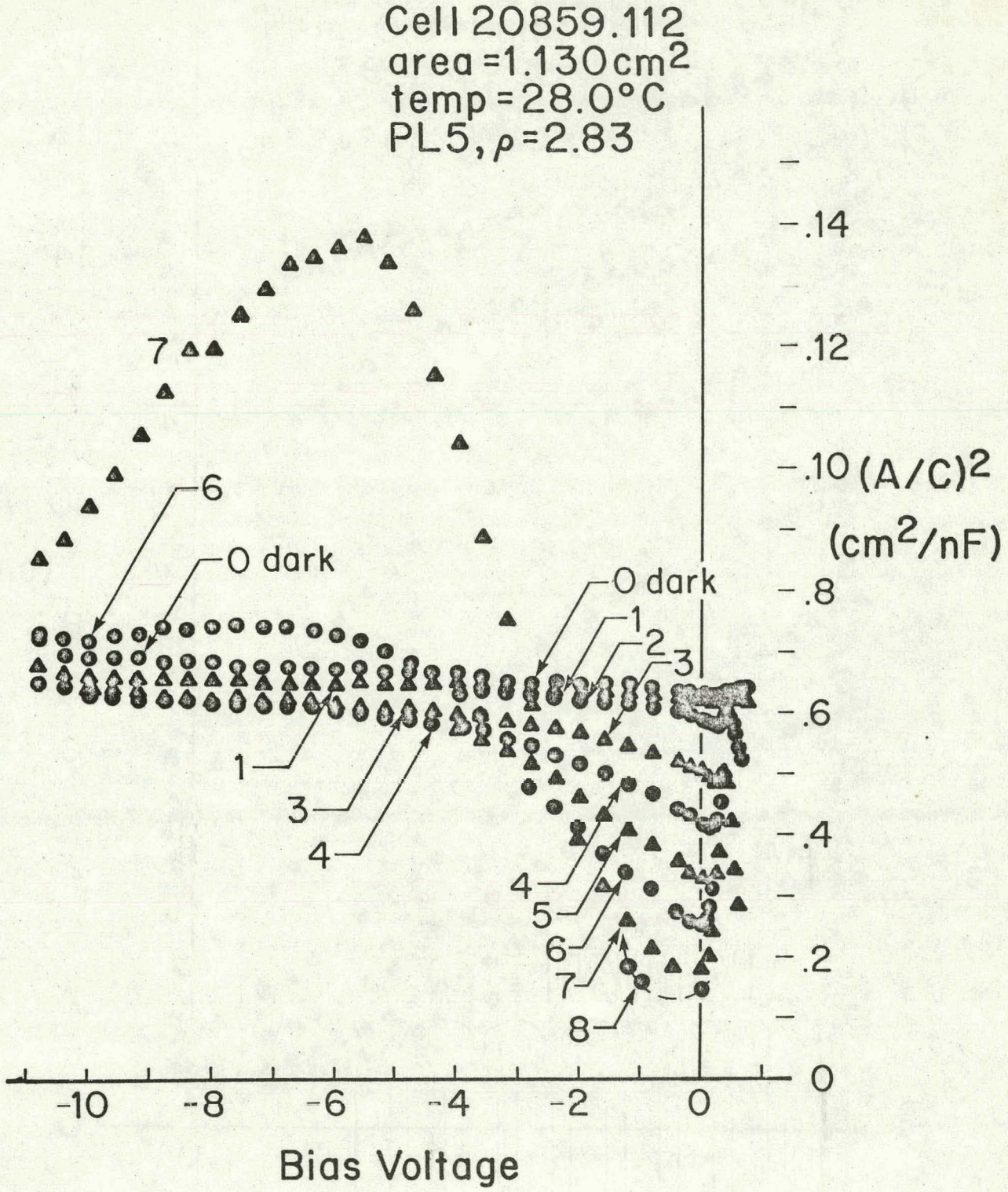

Figure 27 Reciprocal Capacitance as a Function of Bias Voltage of Light Intensities Given in Table 5. At AM1 the Capacitance is Approaching Zero.

Each curve has three or four apparently straight-line regions in reverse bias beyond about -0.5 volt. Even though boundaries between these regions are not in every case clear, a consistently linear region at small reverse bias can be seen in every curve, with a clear-cut variation of slope with Φ. Namely, the slope of these regions gradually increases from dark to about Φ = .0034 AM1, after which it gradually decreases to the highest intensity, Φ = AM1.

We can take this slope to be inversely proportional to effective donor density $N_D^* = N_D - N_T$ according to the equation

$$\left(\frac{A}{C}\right)^2 = \frac{2(V_D - V)}{q\varepsilon\varepsilon_o N_D^*}$$

where N_D is the donor density in CdS and N_T is the density of negatively ionized acceptors in the compensated region. Figure 28 shows how N_D^* varies with Φ.

The observation that N_D^* first decreases and then increases as the illumination of cell 20860.111 increases is unexpected, but may be the result of a competition between two processes such as the following: (1) Under more intense light, Φ > .0034 AM1, hole trapping predominates. The short-wavelength component of Φ produces electron-hole pairs, allowing the deep traps to capture holes in increasing numbers. (2) At lower intensities, $0 < \Phi \lesssim .0034$ AM1, electron trapping predominates. Free electrons produced in the Cu_2S by the long-wavelength component enter the CdS, where they increase N_T and thereby decrease N_D^*.

Cell 20859.112, which had a somewhat lower efficiency, showed significantly different variation of C with V, except that C again was almost

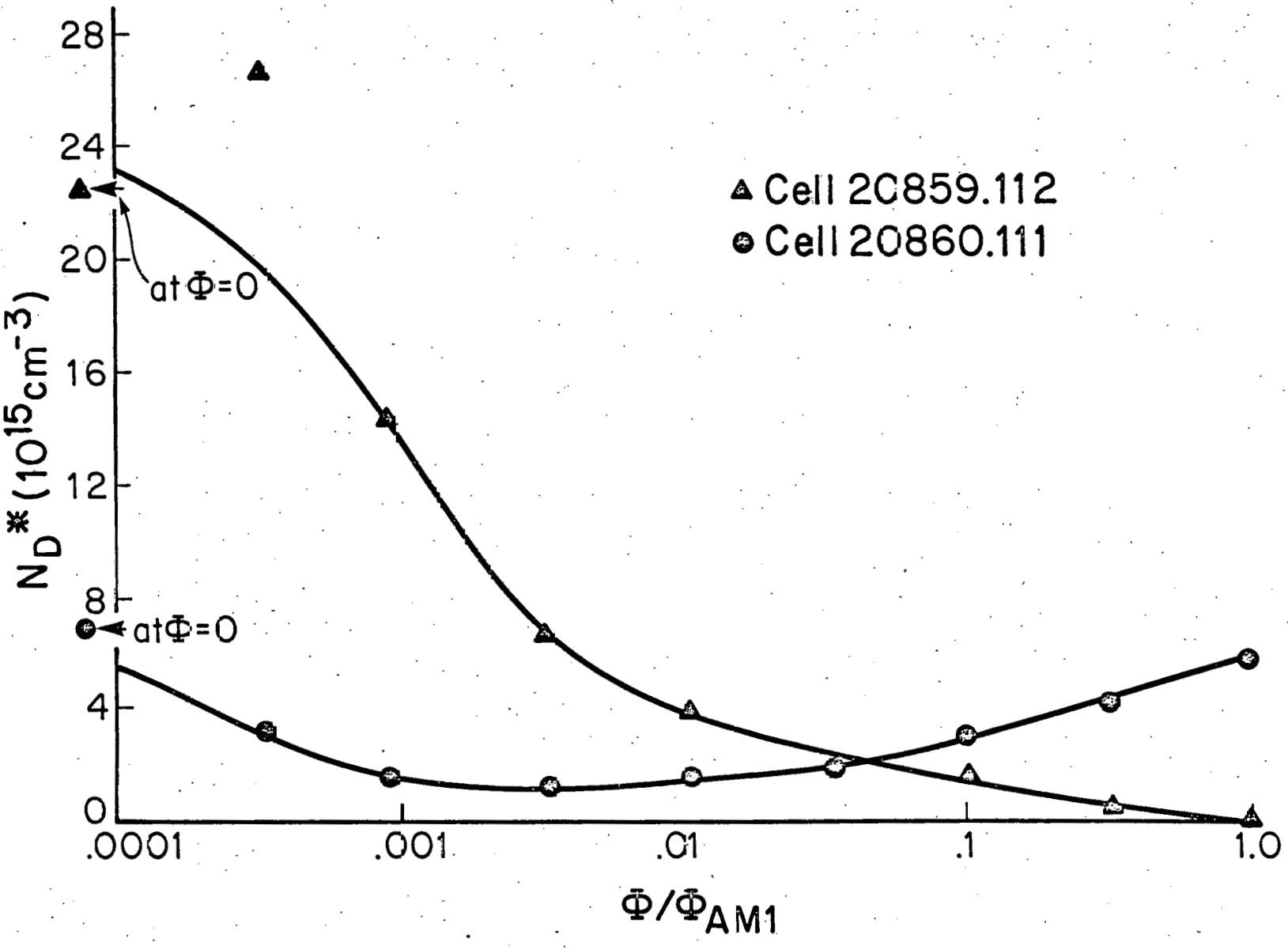

Figure 28 Effective Donor Density as a Function of Light Intensity.

constant in the dark. The difference between dark capacitance and capacitance at AM1 was much less in this cell, so that the curves for different intensities largely overlap. As in the more efficient cell, a linear region in the $1/C^2$ versus V curve at low reverse bias occurs fairly consistently. However, as Φ increases, the slope for this cell continues to increase, until, near or at AM1, a region with $V < -1.26$ volt occurs where C goes to zero, allowing the slope to become unbounded. The derived variation in N_D^* is shown in Figure 28.

Further measurements and theoretical analysis is needed in this area and experiments will be done on a series of cells to determine why two such divergent sets of curves can be obtained. Also, variations in response with changes in intensity of red and blue light over a wide range may be instructive. This method may separate the two competing mechanisms mentioned above.

4.3.3 Phase 3 Junction Field in (CdZn)S

Spectral response measurements and photocapacitance measurements have begun on mixed sulfide samples, comparing results to those obtained with CdS cells as a baseline. This has been accompanied by improvements in the set-up of both types of experiments, affording greater accuracy and flexibility in the techniques. A full description of the spectral response equipment is given in Appendix B.

The general behavior of the (CdZn)S cells is similar to CdS cells with the anticipated shift in the band edge peak. Figures 29 and 30 show this shift most clearly in the collection efficiency curves without bias light.

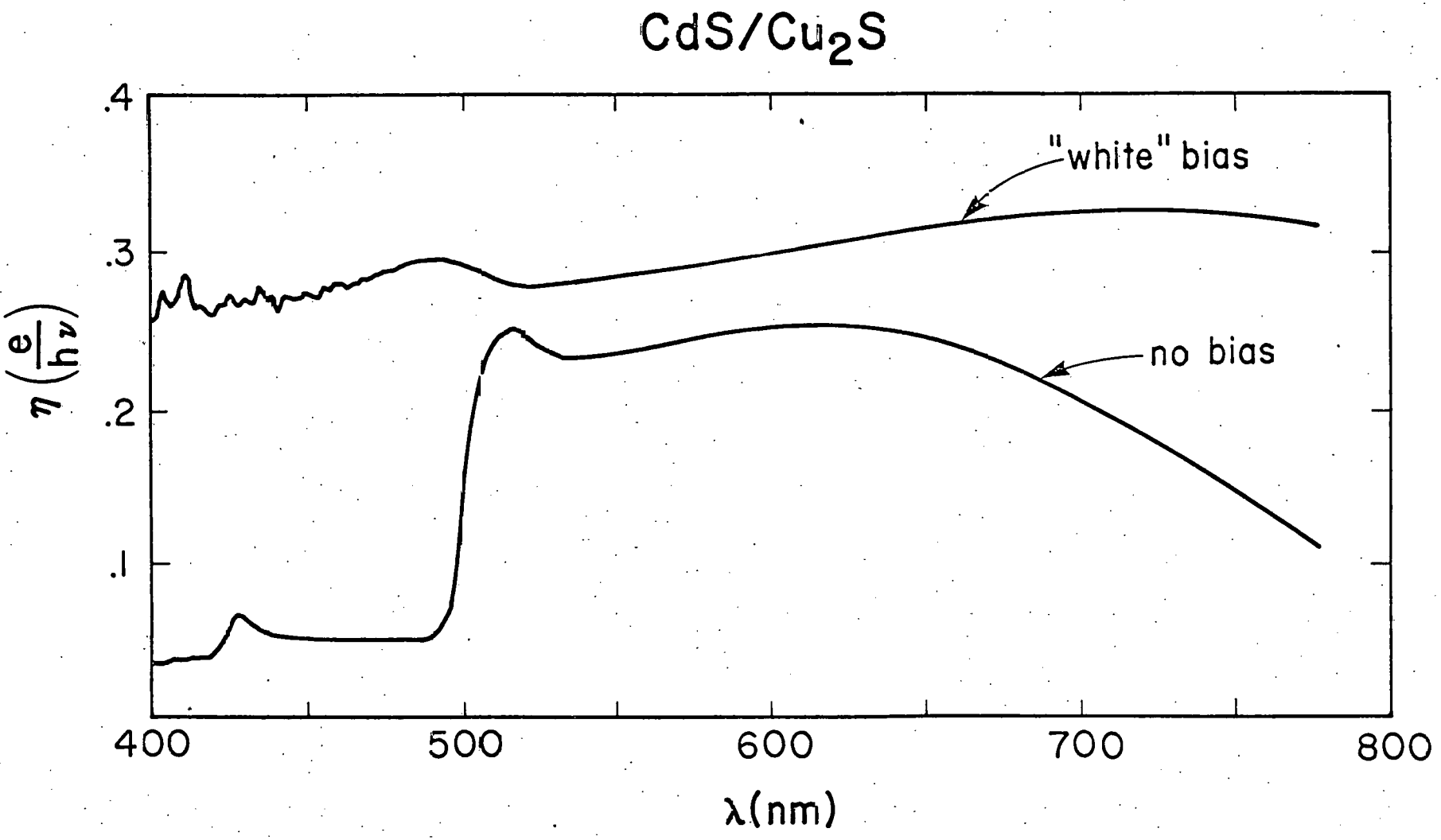

Figure 29 Spectral Response of CdS/Cu_2S Cell #M112 B1.2.

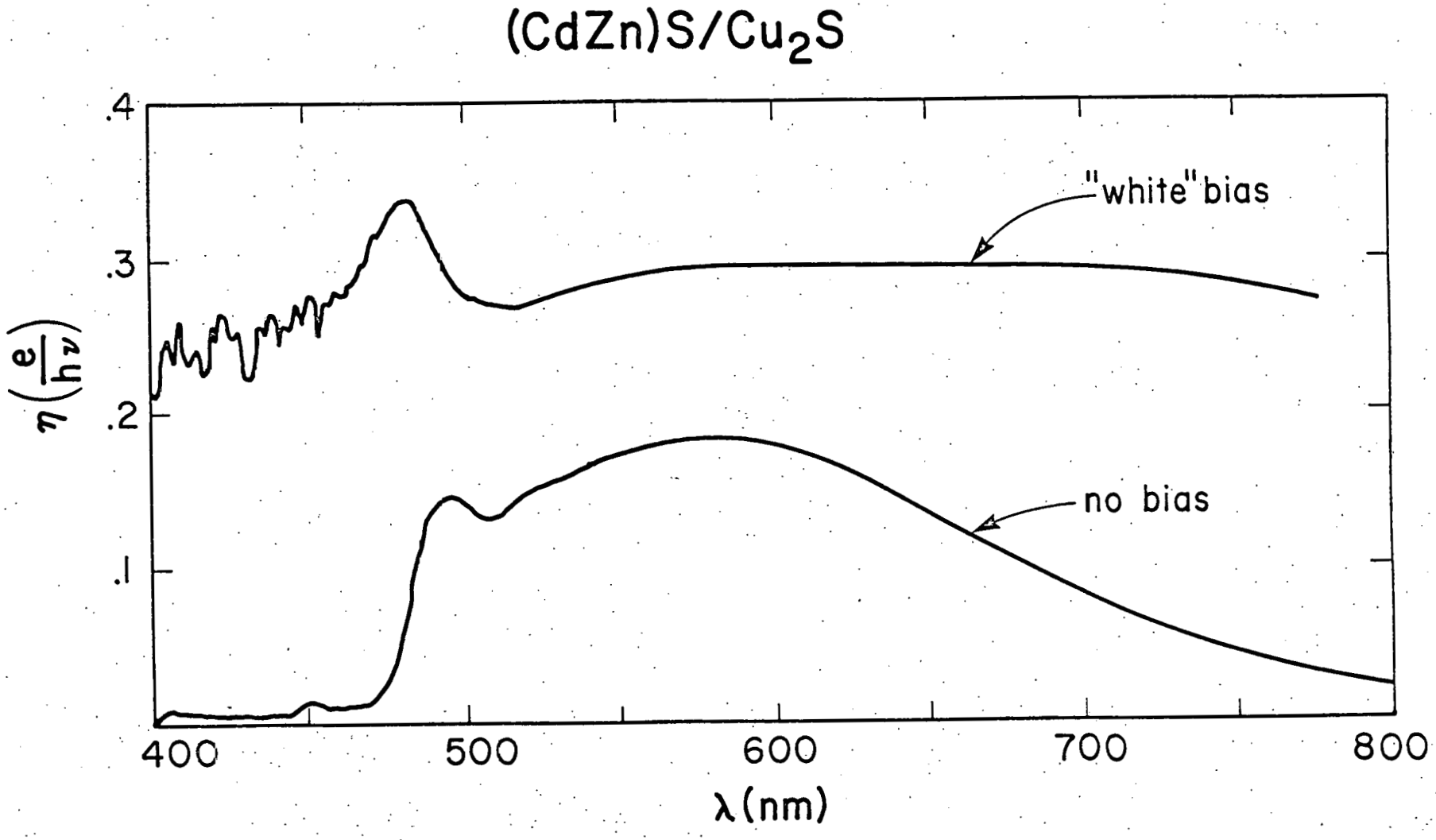

Figure 30 Spectral Response of (CdZn)S/Cu2S Cell #M111 B1.4

In the photocapacitance set-up, sample mounting has been improved, so that cells are presently mounted on a temperature controlled block in a light-tight box with a window on which filters are mounted. Errors resulting from variation of Φ across the cell and in the process of setting Φ have been identified and eliminated by adding a diffuser, so that there is no imaging of the source on the sample. Components recently added to the system include a controllable cryostat able to maintain temperature anywhere from 77 to 300 K, a high-speed shutter for transient capacitance measurements, and a chart recorder.

4.3.4 Phase 4 Quantify Junction Recombination

Losses resulting from electron-hole recombination at the junction limit the available current and voltage. These losses have been measured both by means of the photocapacitance and spectral response of functioning devices. Results of an experiment on the effects of successive heat treatments are described below.

Photocapacitance measurements of junction recombination, as described in earlier reports, involve measuring the capacitance C and current I of a cell under white-light intensity Φ from dark to AM1 or slightly brighter. The light intensity is monitored by the current I_{si} of a monitor silicon cell. The collection efficiency is obtained from these readings as follows

$$\eta_c(\Phi) = \frac{I(\Phi)\ I_{si}\ (AM1)}{35 \times I_{si}(\Phi) \times A}$$

where 35 mA/cm^2 corresponds to the maximum current expected at AM1, i.e. 100% efficiency. A is the cell area.

The junction field, F_2, is related to the capacitance at zero bias by

$$F_2 = \frac{2V_D}{\varepsilon\varepsilon_o} \frac{C}{A}$$

where the diffusion voltage, V_D, can be taken to equal .75 V. A plot of ε^{-1} against η_c^{-1} should be linear for all but very low values of . (12)

$$F_2^{-1} = \frac{\eta_Q \eta_c^{-1} - 1}{S_1/\mu_2}$$

Figure 31 gives an example of such a plot, with quantum efficiency $\eta_Q = 0.49$ from the η_c^{-1} intercept and $S_1/\mu_2 = 13{,}700$ V/cm from the F_2^{-1} intercept. S_1 is the interface recombination velocity and μ_2 is the electron mobility in the CdS. In single crystal CdS, $\mu_2 \simeq 300$ cm^2/V-sec, has been reported giving a value of $S_1 \simeq 4\times10^6$ cm/sec.

Four $Cd_{1-x}Zn_xS/Cu_2S$ cells were selected as having fairly well optimized properties from earlier heat treatments. These properties, particularly efficiency, had, however, deteriorated somewhat during storage. Table 6 gives the parameters obtained from their I-V curves and from photocapacitance measurements. They were then submitted to a series of four heat treatments consisting usually of 16 hours at 150°C in a H_2-Ar atmosphere, and the parameters were remeasured after each heat treatment. Two CdS/Cu_2S cells underwent similar measurements for comparison with the above, before and after a single heat treatment of the same nature. The results for these cells are given in Table 7.

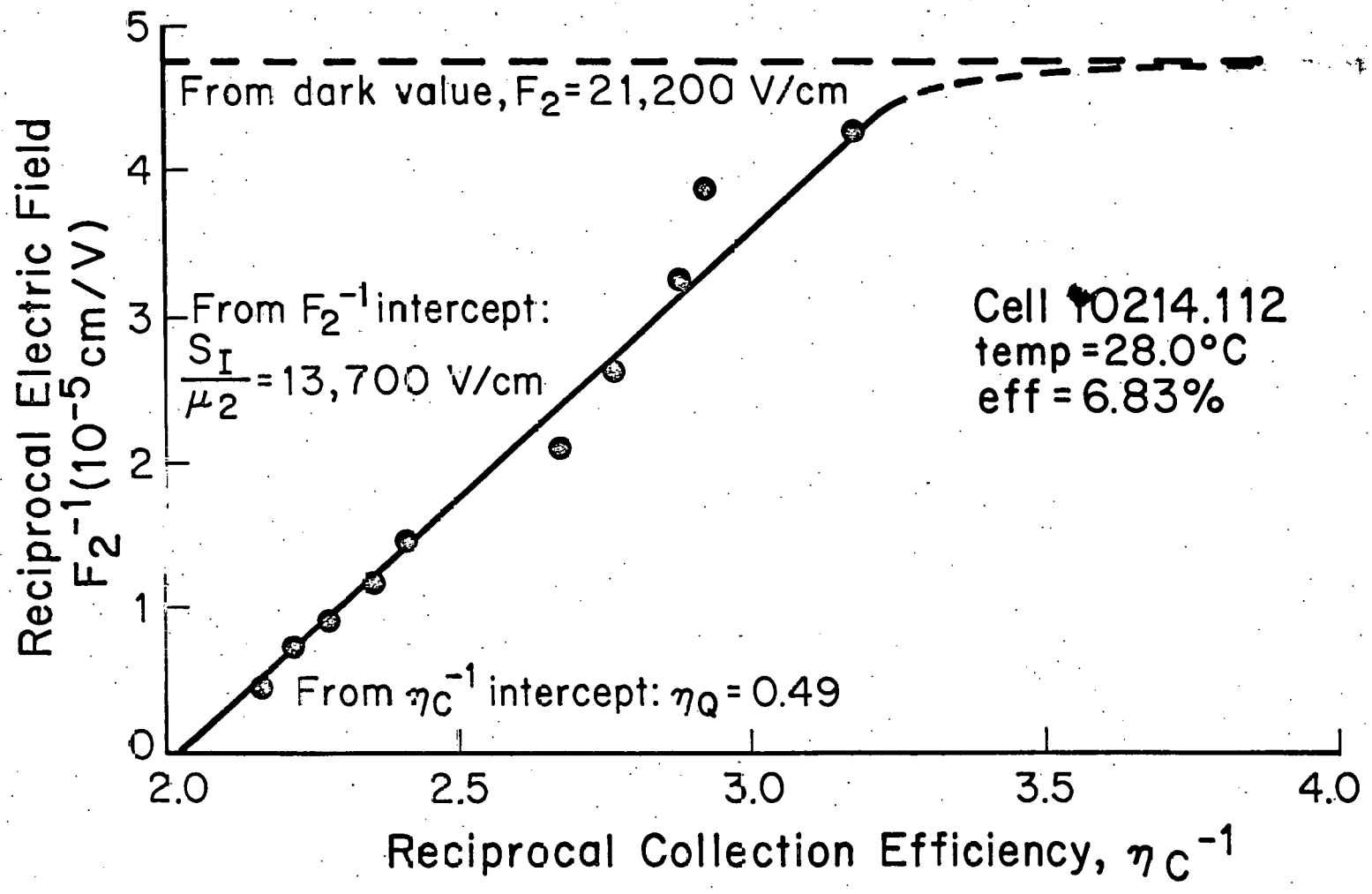

Figure 31 Reciprocal Electric Field versus Reciprocal Collection Efficiency for a (CdZn)S/Cu_2S Cell Containing 13% Zinc.

Table 6

Parameters of $Cd_{1-x}Zn_xS/Cu_2S$ Cells Following Heat Treatments (HT's)

	Cell M214 A1-1 x = .17					Cell M214 A1-2 x = .17				
No. of HT's	0	1	2	3	4	0	1	2	3	4
V_{oc}(V)	.576	.5740	.5847	.5952	.5984	.569	-	-	-	.5704
J_{sc}(mA/cm^2)	11.93	14.61	15.54	15.40	14.63	14.04	-	-	-	15.90
Fill Factor (%)	71.4	69.3	68.4	68.4	71.2	69.6	-	-	-	62.5
Efficiency (%)	5.91	7.00	7.45	7.76	7.51	6.69	-	-	-	6.83
ηQ	.30	.40	.45	-	.40	.37	.42	.48	.48	.49
S_1/μ_2(10^3 V/cm)	32.1	16.3	12.6	-	5.8	27.5	11.8	16.0	19.2	13.7
C_{dark}/A (mF/cm^2)	30.4	20.7	14.9	-	3.97	18.2	16.4	15.3	13.2	12.5
C_{AM1}/A	113.0	115.0	118.0	114.0	105.0	115.0	124.0	126.0	121.0	123.0

Table 6, continued

	Cell M216 Al-4 x = .072					Cell M250 Al-2 x = .18				
No. of HT's	0	1	2	3	4	0	1	2	3	4
V_{oc}	.552	.567	.569	.567	.570	.598	.589	.585	.592	.580
J_{sc}	10.29	14.06	16.07	17.02	15.89	12.58	15.44	16.18	15.05	16.47
Fill Factor	68.0	67.8	65.0	63.5	65.3	69.7	57.9	62.8	60.7	59.5
Efficiency	4.66	6.50	7.17	7.39	7.13	6.32	6.34	7.16	6.51	6.85
η_Q	.35	.43	.49	.51	.48	.30	.44	.47	.39	.46
S_1/μ_2 (10^3V/cm)	26.6	21.3	19.8	16.4	18.2	6.8	3.5	2.9	3.3	3.3
C_{dark}/A	17.4	17.0	16.2	15.3	15.4	2.57	2.55	2.36	2.40	2.33
C_{AM1}/A	167.0	176.0	184.0	186.0	180.0	119.0	135.0	133.0	128.0	139.0

Table 7

Parameters of CdS/Cu_2S Cells Before and After Heat Treatment

	Cell 949 A2-2		Cell 949 A2-3	
	Before	After	Before	After
V_{oc} (V)	.523	.521	.516	.511
J_{sc} (mA/cm^2)	9.01	20.48	15.05	16.53
Fill Factor (%)	26.4	46.3	66.9	67.8
Efficiency (%)	1.50	5.95	6.26	6.90
η_Q	-	.58	.45	.48
S_1/μ_2 (10^3 V/cm)	41.3	1.3	3.6	1.9
C_{dark}/A (nF/cm^2)	1.16	1.19	2.28	2.53
C_{AM1}/A (nF/cm^2)	4.95	53	46.3	54.5

The variations in measured parameters for the (CdZn)S cells exhibit the following features: 1) C_{dark} decreases, in some cases by a large amount. This behavior was expected because of diffusion of compensating Cu ions into the CdS. 2) C_{AM1} increases slightly for some of the first heat treatments and then levels off. This seems to parallel the variation in efficiency. 3) η_Q increases strongly at first, followed by a leveling off or a more gradual increase. 4) S_1/μ_2 shows almost the reverse behavior, decreasing strongly at first, after which it levels off or slightly increases. Thus the optimizing quality of heat treatment is seen to accompany a decrease in interface recombination.

The more limited data on the CdS cells show similar behavior, insofar as comparison is possible. In cell 949 A2-2, which had a very low efficiency before heat treatment, the linearity the F_2^{-1} plot was insufficient to allow η_Q to be determined; the value of S_1/μ_2 in Table 7 is highly uncertain. After heat treatment, both of these parameters assumed reasonable values, as did the efficiency. Note that values of S_1/μ_2 in these cells is generally much smaller than in the $Cd_{1-x}Zn_xS/Cu_2S$ cells.

Further measurements of the effects of heat treatment are needed, along with theoretical interpretation in greater depth. It will be particularly valuable to start such a series of measurements with cells having minimal heat treatment.

4.3.5 Identify Degradation Mechanisms

The reversibility of degradation induced by exposure to air has been established and is discussed in section 4.4. Some insight into the effects

of thermal exposure on cell properties can be deduced from the various heat treatment studies used to optimize initial cell performance. In particular it has been found that long term exposure to a temperature of $\sim 200^{o}C$ produces irreversible losses in fill factor. Treatment up to 100 hours at $150^{o}C$ causes only a 1-2% loss in fill suggesting that whatever mechanism is operative (Excessive CdS compensation) will not be a significant limiting factor in actual cell deployment.

4.3.6 Phase 6 Identify Trap Levels

Impurities in the region of CdS adjoining the junction in CdS/Cu_2S cells, most probably substitutional Cu ions diffused across the junction, constitute hole traps. The large variations in collection efficiency described above under "Junction Field" and "Junction Recombination" result from changes in the density and ionization of these traps.

In order to determine the energy levels of these impurities and the cross sections of transitions involving them, experiments have been started to investigate variation in photocapacitance and photocurrent with illumination. Quenching of capacitance and current as affected by the spectral content of the light exciting cells will be described here.

Figure 32 gives the results of an experiment using a single beam of light with wavelength from the infra-red region ($\sim$2.8 μm) to a variable cutoff λ_{cut} between 810 nm and 390 nm. In order to compensate for the varying number of photons, the illumination intensity was adjusted at each λ_{cut} so as to keep I_{si}, the monitor current, constant at approximately its AM1 value. Although the current rises steadily with λ_{cut} between 680 and 480 nm, the capacitance shows a strong quenching around 600 nm.

A better measure of quenching comes from the use of two beams: Beam 1 is "blue" and constantly on, Beam 2 is "red" and switched on and off ("chopped") to produce changes in capacitance and current. Thus -

$$\Delta C = C(\text{red off}) - C(\text{red on})$$

$$\Delta I_{CdS} = I_{CdS}(\text{red off}) - I_{CdS}(\text{red on})$$

$$\Delta I_{Si} = I_{Si}(\text{red off}) - I_{Si}(\text{red on})$$

The light sources were high-intensity tungsten-iodine lamps, followed, for beam 1, by color glass filters passing 560 nm > λ > 320 nm and, for Beam 2 by one of a series of color glass filters passing 2.8 μm > λ > λ_{cut}. Fig. 33 shows fractional changes of C and I_{CdS}, normalized by dividing by fractional change in I_{Si} so as to compensate for effects of varying intensity at different wavelengths.

The plots are consistent with a model in which blue light decreases N_T, the density of electrons contained in hole traps, so that C and I_{CdS} both increase. Red light introduces electrons into the depletion region, causing an increase in N_T by electron capture. We find a decrease in capacitance under red light in spite of a simultaneous increase in I_{CdS}.

We conclude that more information can be gained on hole trap properties by monitoring capacitance rather than the cell current. This is particularly important in transient measurements. Experiments on transient capacitance have accordingly been initiated. Some results have been obtained at room temperature, but no conclusions on trap levels can be drawn until low temperature measurements have been completed.

The photoluminescence of as grown CdS films has been measured at 77°K and the dominant peaks in the spectrum tentatively identified. A

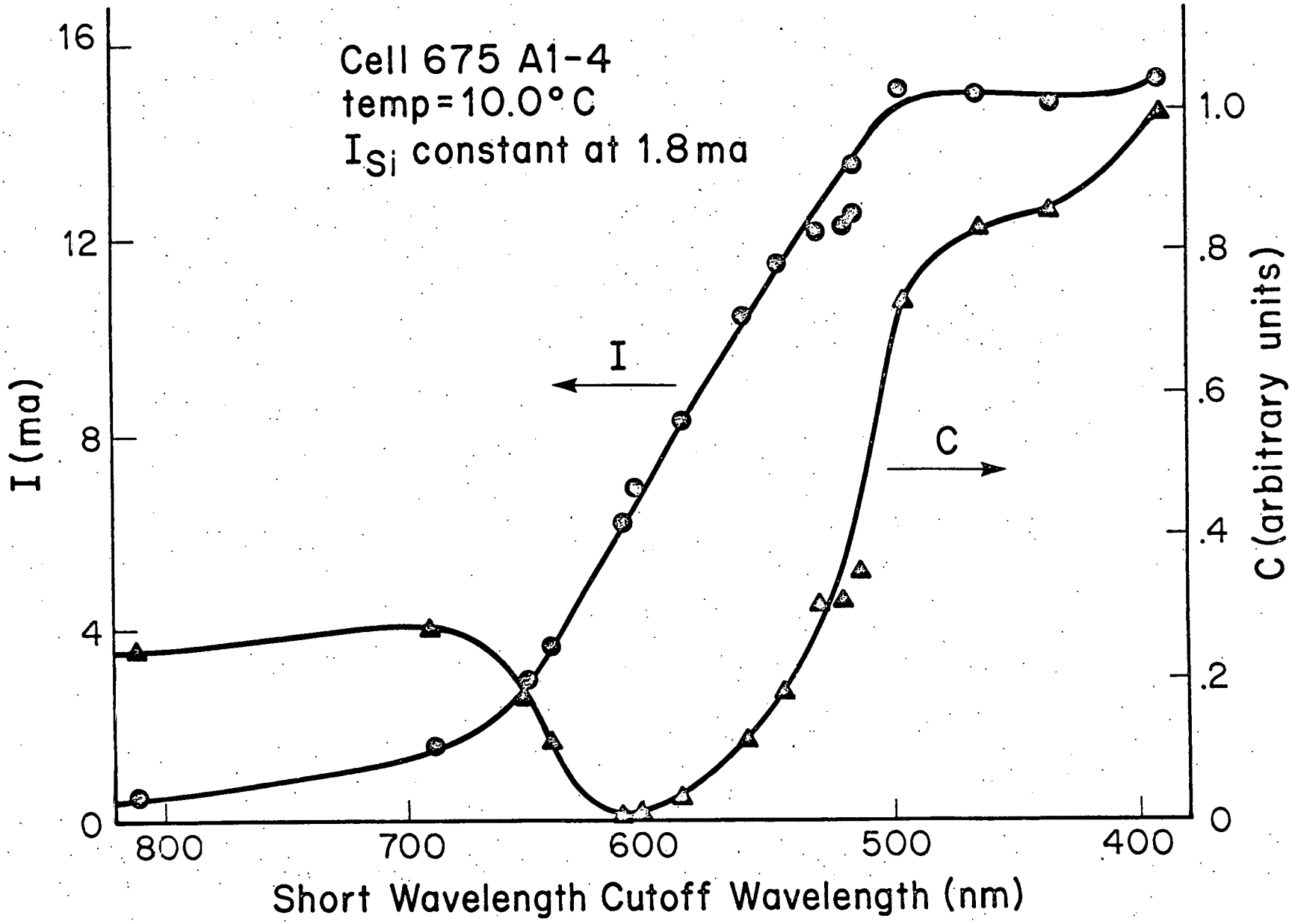

Figure 32 Capacitance and Short Circuit Current as a Function of the Short Wavelength Cutoff.

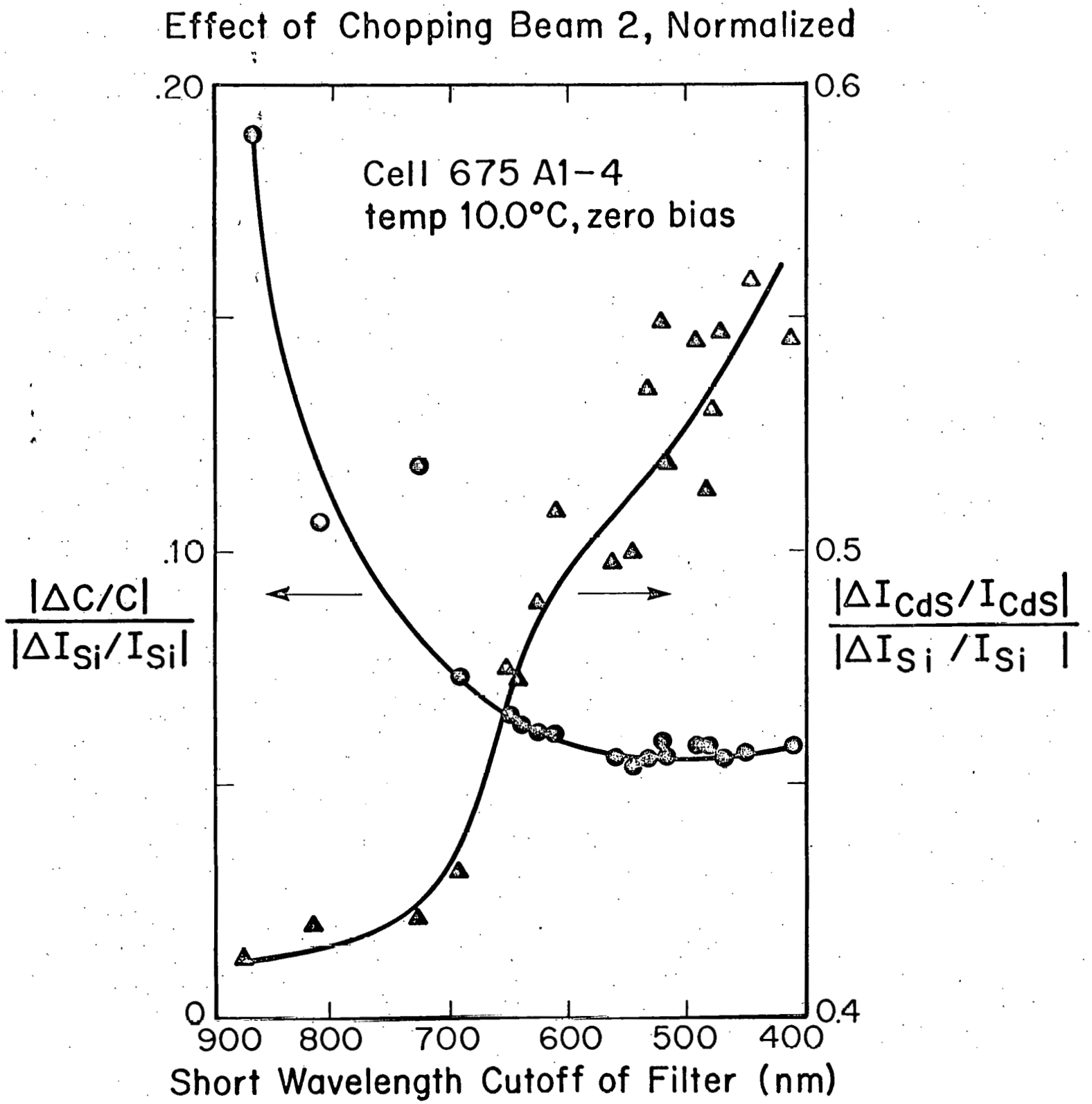

Figure 33 Fractional Change in Current and Capacitance as a Function of The Short Wavelength Cutoff.

typical emission spectrum for CdS used to manufacture high efficiency cells is shown in Fig. 34 for an excitation of 400 nm. The peak at 488 nm is a free exciton transition and the complex peak at ∿520 nm is the CdS green edge emission which is due to a transition between a free electron and hole trapped at an acceptor level accompanied by 0, 1, 2, ... LO phonons.[13] The third peak at ∿780 nm is believed to be associated with an impurity or complex defect state. Efforts to identify this peak are currently being pursued.

Photoluminescence spectra are being routinely recorded for all CdS substrates grown and the ratio of the relative peak heights of edge emission to the exciton peak is calculated. The relationship between this ratio and cell performance is being investigated. Preliminary results indicate that the ratio is not a sensitive predictor of cell performance. High efficiency cells ($\eta \geq 8\%$) have been produced on CdS films with peak ratios from 0.5-5.0. However, the photoluminescence characteristic are valuable as a predictor of cell performance in a broader sense. The CdS used for high efficiency cells ($\eta > 8\%$) should exhibit primarily the exciton and green edge emission. In some films a broad luminescence band is observed between 600 and 700 nm which is believed to be due to multiple impurities. If this band is present, the CdS is not suitable for the production of high efficiency cells. (Virtually all films currently produced at IEC do not have this broad band.)

A detailed study of the relationship of photoluminescence characteristics to growth conditions and CdS grain size is nearly completed and a detailed report will be written in the next quarter. Also, preliminary experiments will be performed to evaluate the usefulness of photoluminescence techniques as a tool for investigating the CdS/Cu_2S junction.

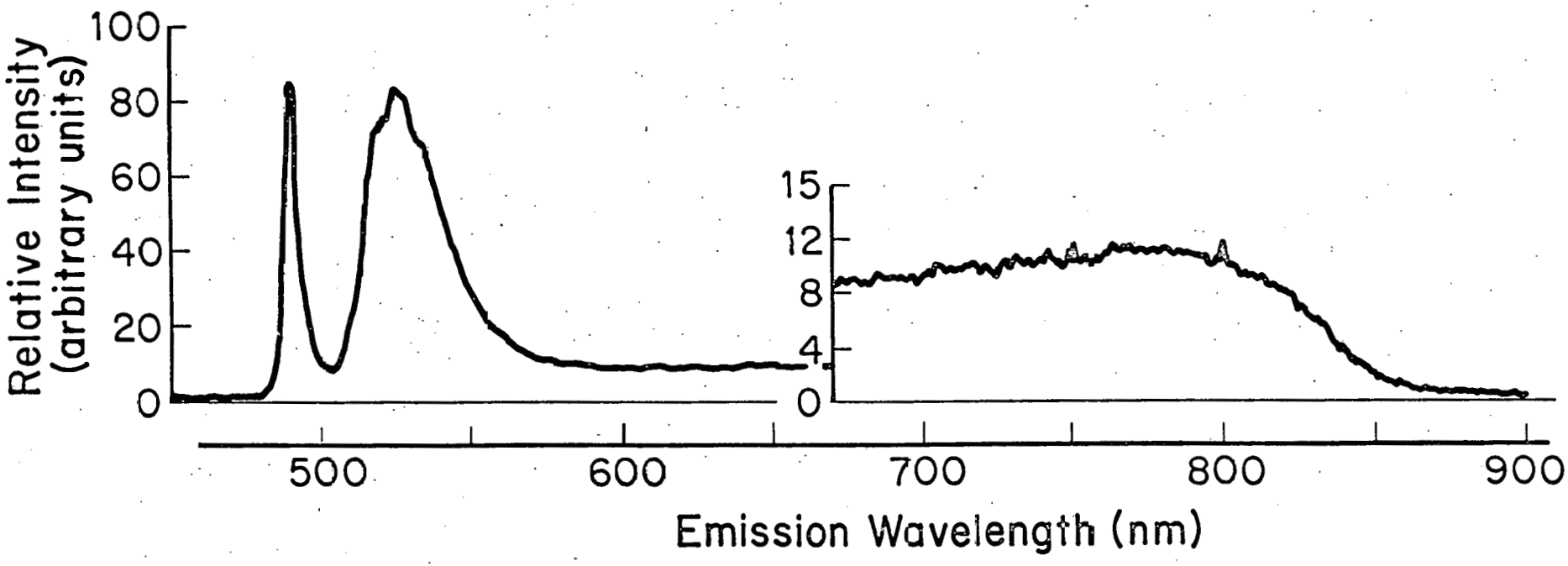

Figure 34 Photoluminescence Spectrum at 77°K for CdS Substrate #21031.

4.3.7 Theoretical Modeling

Optimal Material Properties

As the conversion efficiency of the cells approach the limits set by the optimal material properties, the major performance parameters, V_{oc}, J_{sc} and FF, begin to interact significantly. An analysis of the optimal properties for the CdS and Cu_2S layers has been completed and published.[14] It is shown that the donor density in the CdS must be in the range of 10^{16} - $10^{17}/cm^3$ with the Cu_2S acceptor density about two orders of magnitude larger, 10^{18} - $10^{19}/cm^3$. The CdS donor density is largely controlled by the growth conditions and the Cu_2S acceptor density by reducing heat treatments.

Optical Behavior of Planar Junction Cells

An analysis of reflectance of thin-film CdS/Cu_2S cells leads to the following conclusions:

1) Light trapping in the Cu_2S layer is responsible for the high photon efficiency of the textured Cu_2S cell. It arises from the diffuse reflection of light at the CdS/Brass interface, followed by total internal reflection of the reflected rays at the outer Cu_2S boundary. A quantitative analysis[2] shows that this effect accounts for the low observed reflectance at $\lambda>550$ nm for CdS/Cu_2S cells. From this calculation, it is seen that little is gained by modifying the angular distribution of reflectance beyond a minimum diffuseness (e.g. from $\cos\theta$ to $\sin\theta\cos\theta$) Figure 35.

2) A further decrease in reflectance is due to the front surface texture of the Cu_2S caused by the HCl etch of the CdS. In the approximation in which $\lambda <<$ (typical size of texture features) a model of multiple reflection of geometrical rays can be used. The results are shown in the figures 35 and

and 36. As the texture sharpness increases, more reflections occur and the total reflectance decreases. This suggests that an optimum texture may exist for the product $V_{oc} \times J_L$, since obviously after a certain sharpness has been reached, a further increase would not reduce the reflectance but would increase $A_J/A_\perp$.

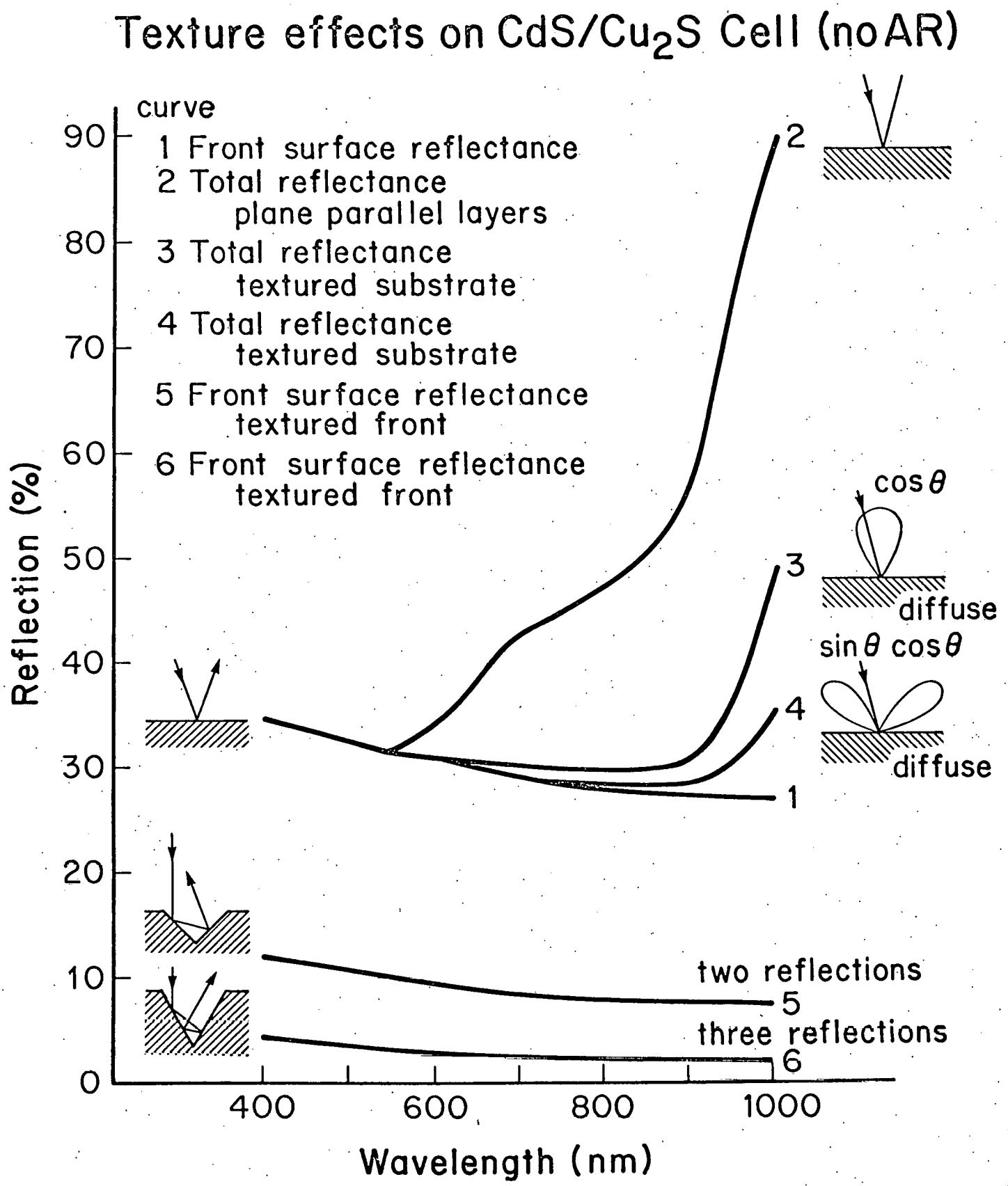

Figure 35 Effects of Texture on Total Reflectance from a CdS/Cu_2S Cell Without an A-R Coating.

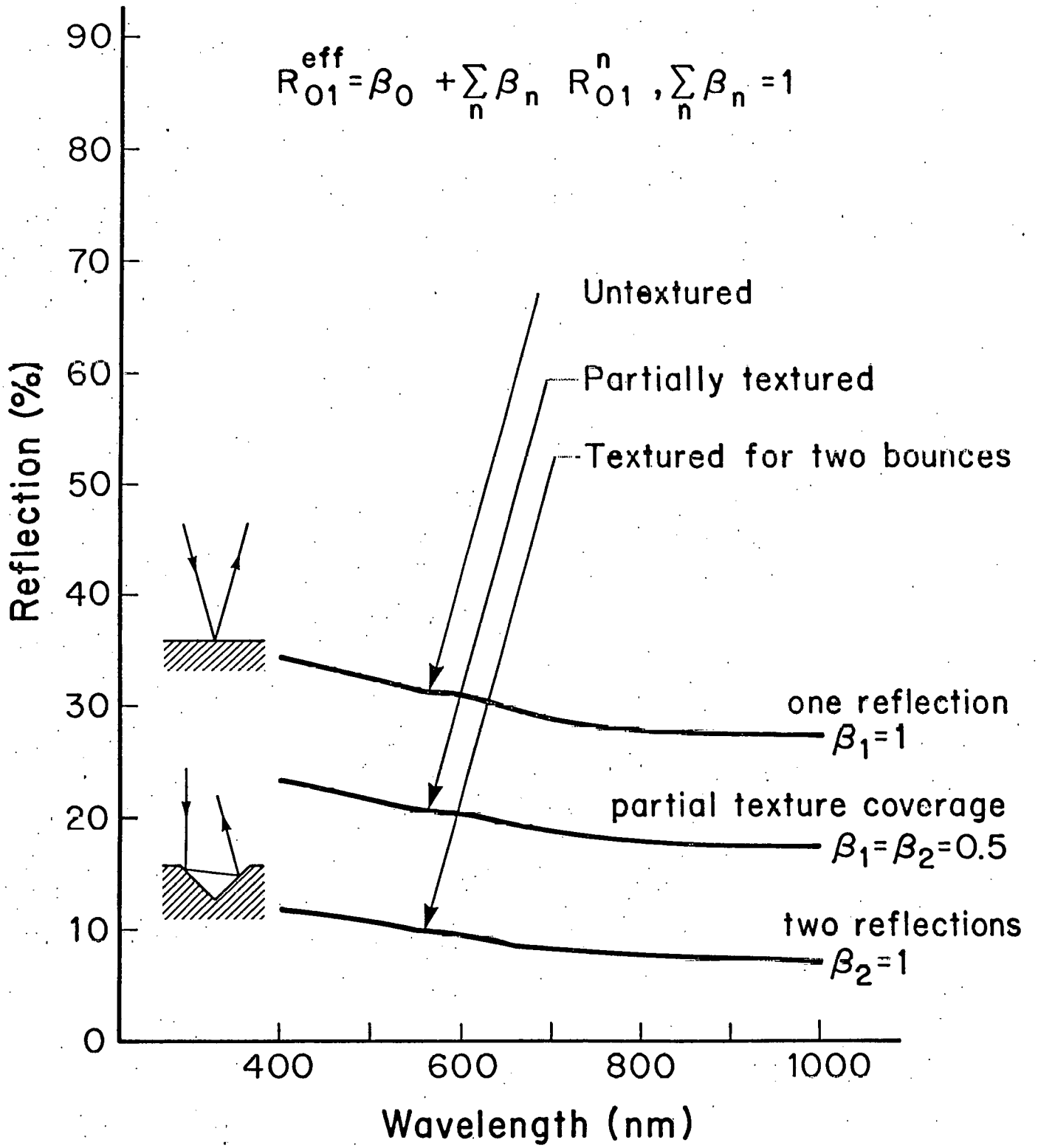

Figure 36 Calculated Front Surface Reflection from Planar and Textured Cu_2S Surfaces.

4.4 Task 4 Encapsulation for Improved Stability

A first order series of experiments have been made with the goal of developing an integral encapsulant. In addition a limited number of cells were exposed to sunlight while protected by a non-integral encapsulation system. The latter proved in fact to be inadequate to protect the cells from the atmosphere.

4.4.1 Phase 1 Review LSSA Experience

The review of the reports from the LSSA project have concluded that only an inorganic glass will combine total hermetic sealing, high transmissivity and resistance to long term weathering and degradation. Accordingly the development of a glass based integral encapsulation was initiated. Electron beam evaporation was found to be a promising technique for depositing the encapsulant directly onto the surface of the cell.

4.4.2 Phase 2 Optical Quality Encapsulant

Several glasses were deposited by e-beam evaporation up to a thickness of several microns. Deposition rates of 50 to 70 Å/sec. were readily achieved. Optical quality of these glass films were evaluated by measuring the reflectance plus transmittance using an integrating sphere. Optimum results were obtained for a Barium Alumino-Borosilicate film deposited from a specially prepared source material (IEC 9658) of the following composition:

SiO_2 49%, B_2O_3 14.5%, Al_2O_3 10.5%, BaO 24.8% and Pb 1.2%. The R+T spectra of a 2 μm thick 9658 glass deposited on a 7059 glass plate and of the substrate alone are shown in Figure 37. The refractive index and the thermal expansion coefficient of such a film were found to be 1.49 and $5 \times 10^{-6}\ ^{o}C^{-1}$.

4.4.3 Phase 3 Electronic Compatibility

IEC 7658 type glass of 5 μm thick were deposited by e-beam evaporation onto six CdS/Cu_2S cells. The behavior of the cells before and after encapsulation (Table 8) showed that the glass is electronically compatible and has good optical transmission as expected.

Table 8

The performance of two typical CdS/Cu_2S cells coated with 5 μm of e-beam evaporated glass

Cell #	Date	V_{oc}(V)	J_{sc}(mA/cm^2)	FF(%)	η%	Condition
799 A13	1/9/79	.488	16.0	66.5	6.26	bare
	1/19/79	.489	13.3	69.8	5.48	glass coated
800 A13	1/19/79	.474	15.5	66.9	5.93	bare
	1/19/79	.473	13.0	66.8	4.93	glass coated

However, in its present form the glass film did not provide complete hermetic sealing. The data in Figure 38 shows the variation of efficiency, open circuit voltage and short circuit current of a typical integrally encapsulated cell as a function of aging time in laboratory air at 25°C. The poor permeability is due to the loss of adhesion at the edges of the glass film. This loss of adhesion

was revealed by painting the edges of the film with black ink which spread over the surface of the cell by capillary action. The micrograph of figure 39 shows ink under the glass film.

Life Testing not Specified in Work Statement

Life testing was performed on three non-integrally encapsulated cells. The test consisted of monitoring the cell parameters during prolonged roof top exposure under short circuit conditons.

The start of the exposure was 11/20/78 for cells 695.B13 and 688.A11 and 5/9/79 for cell 695.A14. The first two were encapsulated between a glass plate and a copper block using an elastomeric silicon semi-gel manufactured by Transene Corp. as the potting compound. Cell 695.A14 was encapsulated between a glass plate and a Kovar block with Dow Corning QL 2577 as the potting compound. The exposure test of cells 695.B13 and 688.A11 has been completed and the results will be discussed in the present report. Since cell 695.A14 has not been under exposure for sufficiently long period of time test results of this cell will not be presented here.

The glass plate used in all three cases was Corning 757. Tests were made to determine possible degradation of the glass and the potting compound under the influence of temperature and UV exposure. The transmittance of the glass/potting compound/glass sandwich structure was measured before and after heating in air at 170°C for 72 hours. No change in transmission was observed. The transmittance was also unchanged after 6 hours of exposure to UV (43 mW/cm^2).

The two cells, 695.B13 and 688.A11, were processed in June 1978 and were stored in H_2/Ar atmosphere, in the dark, until they were encapsulated in

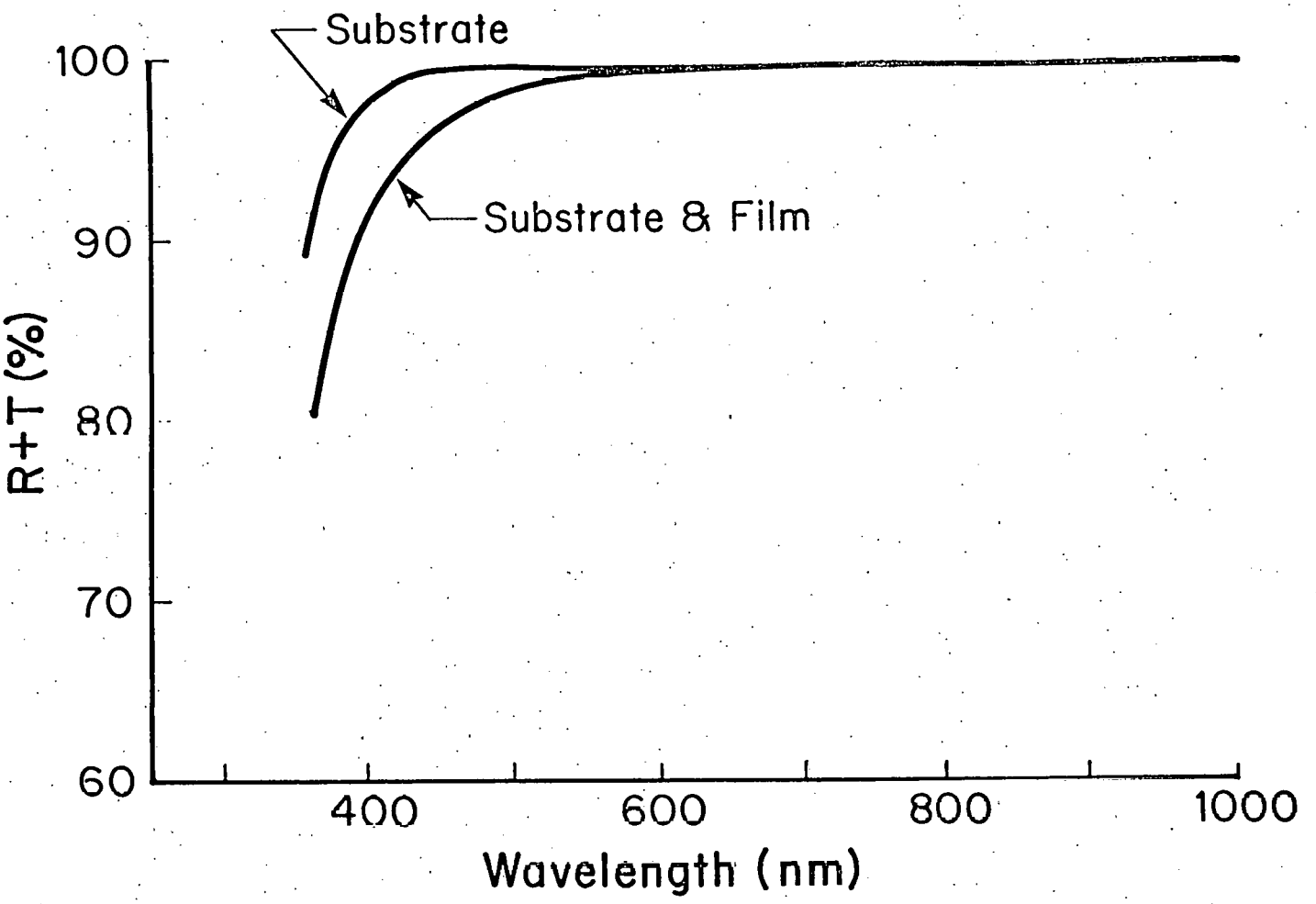

Figure 37 Reflectance Plus Transmittance of an Electron Beam Deposited 2 um Film of IFC 9658 Glass on a 7059 Glass Plate.

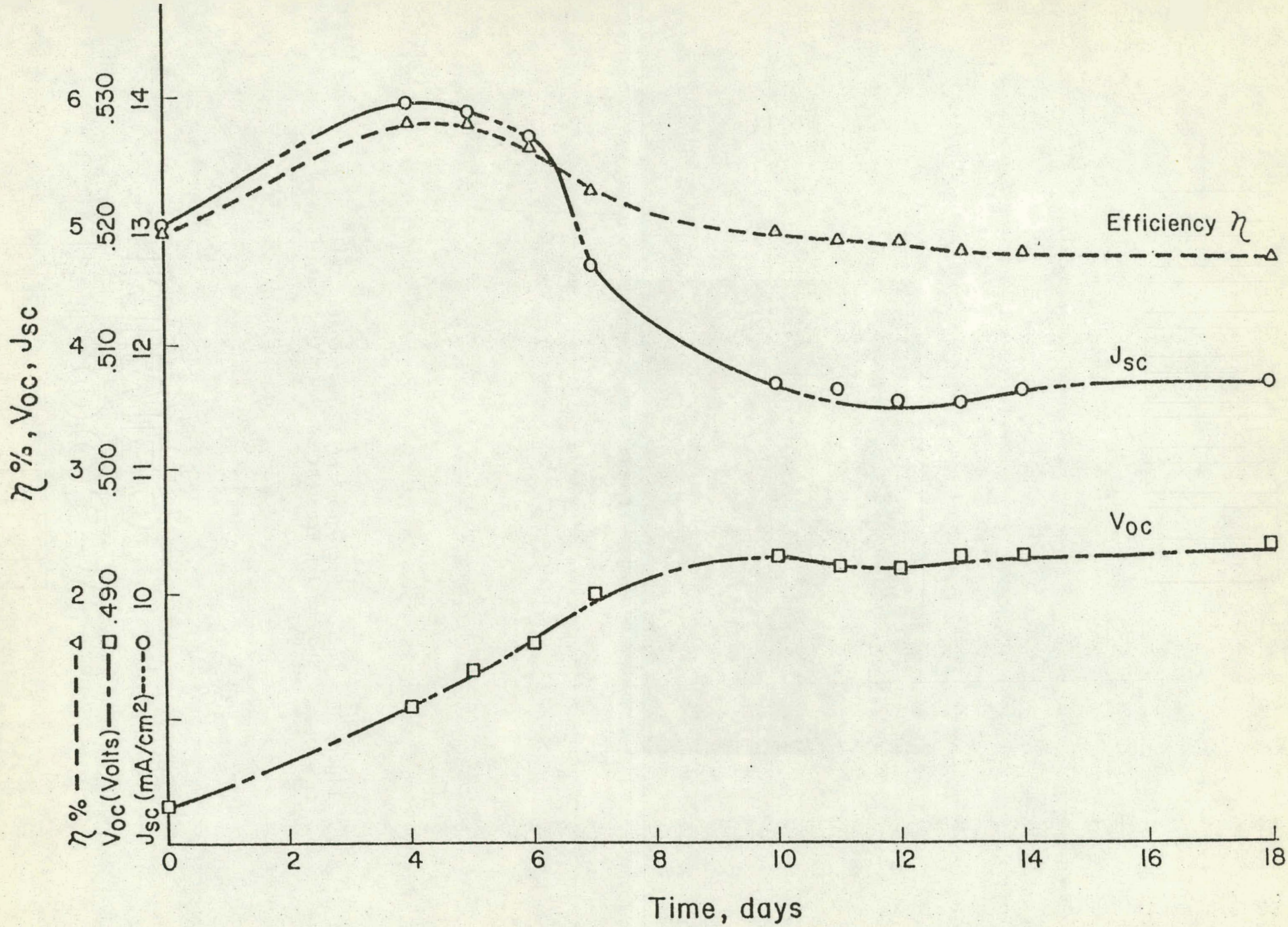

Figure 38 Aging of an Integrally Encapsulated CdS/Cu_2S Cell #800A13 in Air at 25°C.

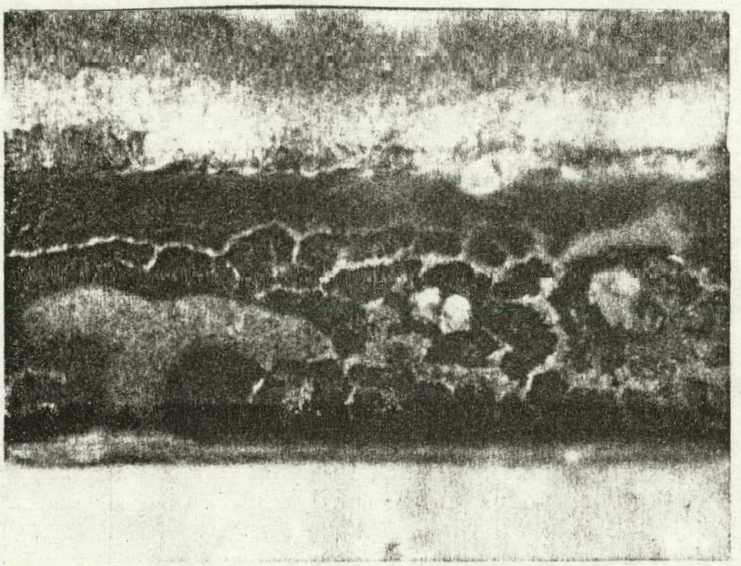

Figure 39 Optical Micrograph of a Glass Coated Cell Showing Ink Penetration under the Glass Film x 800.

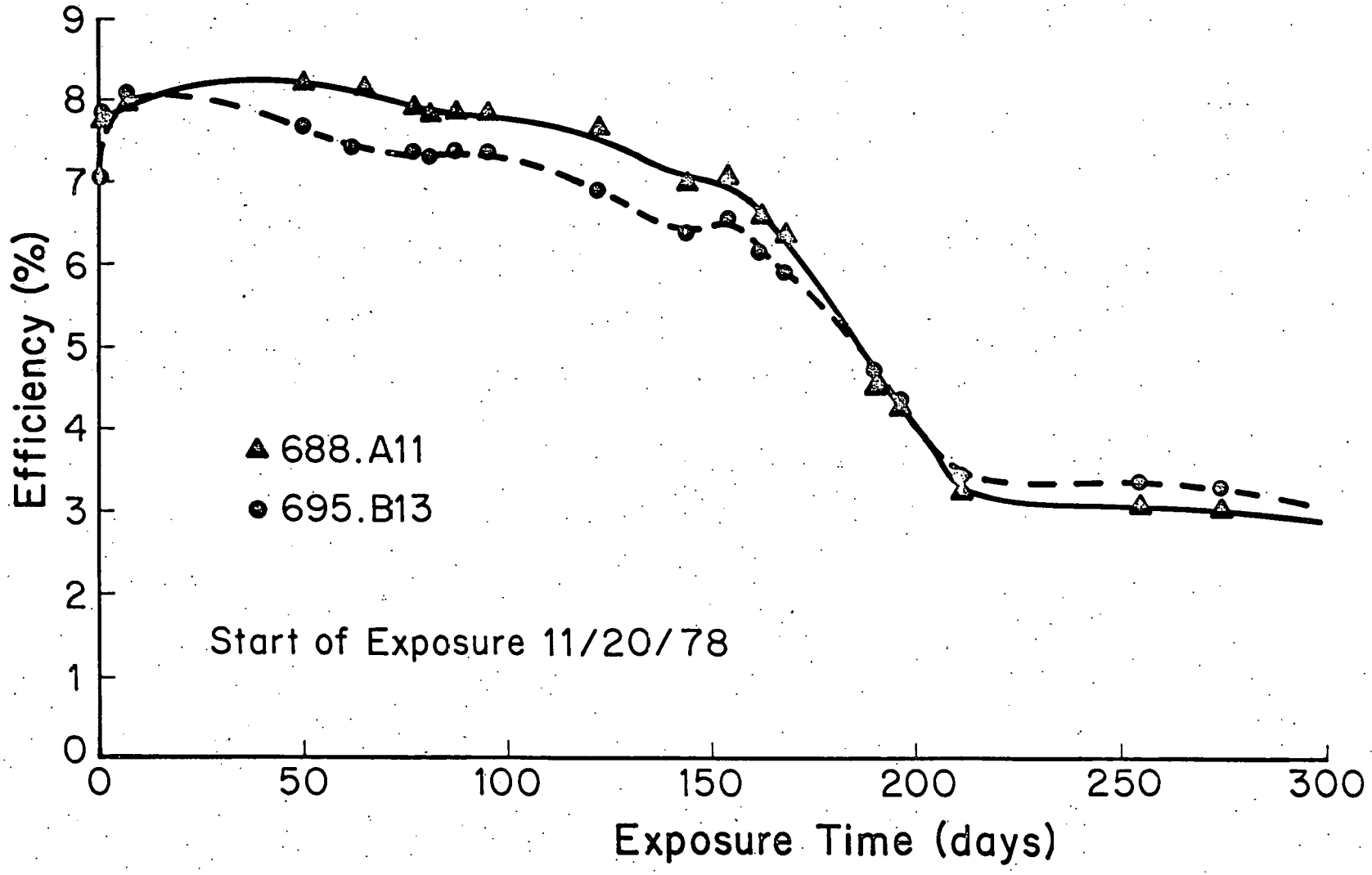

Figure 40 Efficiency as a Function of Exposure Time for 2 CdS/Cu_2S Cells. Subsequent Heat Treatment Restored the Cells to the Pre-Exposure Efficiency Indicating Inadequate Encapsulation.

November 1978. Table 9 gives the performance of the cells at the beginning and at the end of this storage period. The data shows that some degradation had occurred during this period.

Table 9

Performance of Cells 695.B13 and 688.A11 Before and After Storage

Cell #	Date	V_{oc}(V)	J_{sc}(mA/cm^2)	FF(%)	η(%)
695.B13	6/23/78	.492	20.8	70.4	8.69
	11/18/78	.486	18.65	63.8	6.96
688.A11	6/16/78	.523	19.8	69.9	8.71
	11/18/78	.530	18.11	67.1	7.76

Over a period of 9 months of exposure these cells showed approximately 60% decrease in efficiency as can be seen in Figure 40. It is clear that hermetic sealing is not achieved by this type of packaging and that a rapid loss of performance at the onset of warm humid weather (after 120 days of exposure corresponding to the end of March 1979) is observed.

Cell 688.A11 was subjected to vacuum and reducing heat treatments after the roof top exposure. As a consequence the efficiency was restored to 7.72%, virtually identical to the efficiency before roof top exposure. Cell 695.B13 showed a similar recovery as a result of the post-exposure heat treatment.

There is a tendency for encapsulated or sealed cells to show an initial rise in V_{oc}. This is believed to be related to the sensitive interplay between Cu_2S stoichiometry and V_{oc} and J_{sc}.[14] Further investigations will be carried out.

REFERENCES

1. IEC Progress Report XR-9-8063-1-01, June 1979.

2. J. A. Bragagnolo, 2nd European Community Photovoltaic Solar Conference, Berlin pp. 882.889, D. Reidel, Boston 1979.

3. IEC Progress Report XR-9-8063-1-02, August 1979.

4. E. Eser, Quarterly Report "Critical Studies in Materials and Durability" Subcontract XS-9-8310-1 (Prime Contract EG-77-C-01-4042, September 1979.

5. R. E. Halsted, Physics and Chemistry of II-VI Compounds, M. Aven and J. S. Prener (Eds.) John Wiley & Sons, Inc., New York, Chapter 8, 1967.

6. L. C. Burton and T. L. Hench, Appl. Phys. Lett., 29, 612 (1976).

7. IEC Final Report "CdS/Cu_2S Heterojunction Cell Research" Contract EG-77-C-03-1576, May 1979.

8. F. A. Shirland, J. Appl. Phys. 50, 4714 (1979).

9. IEC Progress Report, E(49-18)-2538 PR76/1, January 1977.

10. F. Wilcoxon, Biometrics Bulletin 1, 80-3, 1945.

11. IEC Progress Report XR-9-8063-1-03, August 1979.

12. A. Rothwarf, J. E. Phillips and N. C. Wyeth, 13th IEEE Photovoltaic Specialists Conference, p. 399, 1978.

13. R. E. Halsted, Physics and Chemistry of II-VI Compounds, North Holland, Amsterdam, 1967, p. 385.

14. A. Rothwarf, 2nd European Community Photovoltaic Solar Conference, Berlin pp. 370-378, D. Reidel, Boston 1979. See also Appendix C, Reference 11.

Appendix A

Statistical Analysis of SEP Data

Statistical Analysis of SEP Data

K. V. Jarva 10/79

INTRODUCTION:

Forty pieces (4 cells each) were made by the standard process. Following manufacture and then after each heat treatment, the cells were tested, and, if possible, the values for FF, R, G, J_L and J0 were computed. (Because of approximations used to simplify calculations, R, G, J_L and J0 are only valid for cells having fill factors of 55% or higher.) A set of standardized criteria based on the values of FF, J_L and J0 were then employed to determine the next heat treatment for each of the cells. This process - the substrate evaluation process (SEP) - was continued until a piece passed or failed. In order to pass, a piece had to have at least one cell that had a $J_L \geq 18$ mA/cm^2 and a J0 $\leq 5 \times 10^{-8}$ mA/cm^2 (not necessarily during the same test). A piece failed if J_L or J0 did not satisfy these requirements, and if the cells on that piece did not respond to the appropriate heat treatments. Actually the pieces were grouped into three categories: those that obviously failed, those that passed and border line cases. This last class was comprised of pieces that had at least one cell satisfy either the J_L or J0 requirement and came within one unit of satisfying the other; i.e. cells having $J_L \geq 18$ mA/cm^2 and 5×10^{-8} mA/cm^2 < J0 < 6×10^{-8} mA/cm^2 or, J0 $\leq 5 \times 10^{-8}$ mA/cm^2 and 17 mA/cm^2 < J_L < 18 mA/cm^2 were considered border line cases. (See pg. 2).

GOALS:

1) Descriminate between good and bad material as early as possible in the standard process by examining initial IV data (FF,R,G,J_L,J0) and the parameters measured after evaporation (THCDS, RHO (p), PL) - CdS thickness, resistivity and photoluminescence grade.

2) Attempt to identify parameters that descriminate and that may be related to the physical condition of the material.

METHODS:

1) The pieces that went through the process were divided into three groups: those that passed the SEP criteria, those that obviously failed, and the border line cases. The SEP criteria was devised empirically, and thus the demands on J_L and J0 are somewhat arbitrary; also a few of the pieces that were originally classed as bad material may have actually passed with more heat treatment; hence the third catogory.

2) The process parameters and the initial IV parameters were treated as continuous random variables. For each parameter, the sample from the material that obviously failed was compared to the sample from the material that passed. The comparisons were made graphically using MINITAB, and via the Wilcoxon two-sample test (IMSL subroutine - NRWRST).

3) All IV test data available on the material that obviously failed was examined in an attempt to identify parameters that related to the poor performance of this material.

CONCLUSIONS:

1) Several of the initial IV parameters show the ability to descriminate

Fill Factor: Samples containing the highest initial fill factor (i.e. the one measured after manufacture) were compared using the Wilcoxon two-sample test. All 12 pieces were used from the failed sample (sample 1) and all 23 pieces from the passed sample (sample 2). Border line cases were not considered. H0 was taken to be that the means of the two populations were identical (i.e. H0: U1 = U2), vs. H1: U1 < U2. H0 was rejected at alpha greater than 0.24×10^{-5}. See page 5.

The three samples (failed, passed, and border line) were ordered, numbered and then plotted against their number in the respective sample. For scaling purposes, only cells having fills greater than 48% were considered. (See graph #1, page 6). Note that a horizontal

line drawn at the 66 or 67% fill factor mark discriminates nicely between the passed and the failed material, 19/23 of the passed material falling above the line, and virtually all of the failed material falling below it.

Ln(J0): Analysis of the minimum ln(J0) was similar to that for fill factor. The samples were somewhat smaller (8 pieces in the failed sample and 22 in the passed) because J0 calculations are not accurate for fill factors less than 55%. The hypothesis tested was H0: U1 = U2 against H1: U1 > U2. Again H0 was rejected; this time, for alpha greater than 0.37×10^{-3}. See page 8.

The graphical analysis also is similar to that done for fill factor, with a horizontal line between 2.0 and 2.2 offering good discrimination. [Note J0 is reported on units of 10^{-8} mA/cm^2, and the vertical axis is ln $(J0 \times 10^{+8})$]. See graph #2, page 9.

R and G: Both the minimum initial series resistance, R (Ω-cm^2), and the minimum initial shunt conductance, G(mmho/cm^2), parameters were tested with the Wilcoxon. Again, the hypothesis that the failed and passed populations were identical would be rejected. See pages 11 & 12

2) The process parameters and maximum initial J_L showed no ability to discriminate.

J_L: The Wilcoxon test was used on samples consisting of the maximum initial J_L (mA/cm^2). The pieces in the samples were the same as for lnJ0, R, and G. In this case H0: U1 = U2 could not be rejected at a significant level of alpha. See page 13.

This result was displayed graphically. See graph #3, page 14 and note that piece 999.11 from the passed group was eliminated for scaling purposes.

PL: Photoluminescence was analyzed with the Wilcoxon. The samples consisted of all pieces from the failed and the passed groups. Again H0: U1 = U2 could not be rejected. See page 16 and graph #4, page 17.

THCDS and RHO: The thickness of the CdS, THCDS (μm) and the resistivity, R(Ω-cm), were analyzed in the same manner as PL, and produced a similar

result - H0: U1 = U2 could not be rejected. See page 19 and 20.

3) Problems with J0 accounted for much of the failed material.

Of the obviously failed material:

i) 6/12 failed due to j0 alone. That is, at least one cell on the piece had a $J_L \geq 18$ mA/cm^2, but that (those) cell(s) never showed a J0 < 6 mA/cm^2. See table #5, page .

ii) Only 2/12 of the pieces failed due to J_L alone. That is, the best J_L on the piece was less than 17 mA/cm^2 while the best J0 on the corresponding cell was less than 5×10^{-8} mA/cm^2. See table #5, page .

iii) The remaining 4 pieces failed in both categories. It should be noted however that at least two of these had large J0 values and that the other two had fill factors so bad that J0 was rarely if ever computable.

WILCOXON 2-SAMPLE TEST ON FF

SAMPLE #1 HAS 12 ELEMENTS.
SAMPLE #2 HAS 23 ELEMENTS.

REJECT H0:U1=U2 IN FAVOR OF H1:U1=U2-DELTA,DELTA>0

PROBABILITY THAT STATISTIC IS <= MIN(W,2*E(W)-W) GIVEN H0
IS IN THE INTERVAL (-0.2196E-05,-0.2196E-05)
(UNCERTAINTY DUE TO TIES.)

PIECE	SAMPLE 1	PIECE	SAMPLE 2
931.11	64.900	930.11	73.600
943.11	64.300	932.11	71.300
947.11	66.100	934.11	70.800
947.12	59.600	935.21	68.800
949.11	67.000	935.22	68.900
957.11	50.800	939.11	71.500
963.11	48.600	940.11	71.500
985.11	53.600	941.11	68.300
988.11	59.100	944.11	70.700
990.11	57.800	945.11	67.100
993.11	64.400	948.11	69.500
1010.11	34.100	949.12	68.000
		952.11	63.800
		959.11	54.200
		960.11	67.300
		962.11	71.600
		986.11	62.500
		989.11	61.200
		992.11	67.500
		999.11	71.200
		1007.11	73.300
		1009.11	74.200
		1011.11	73.300

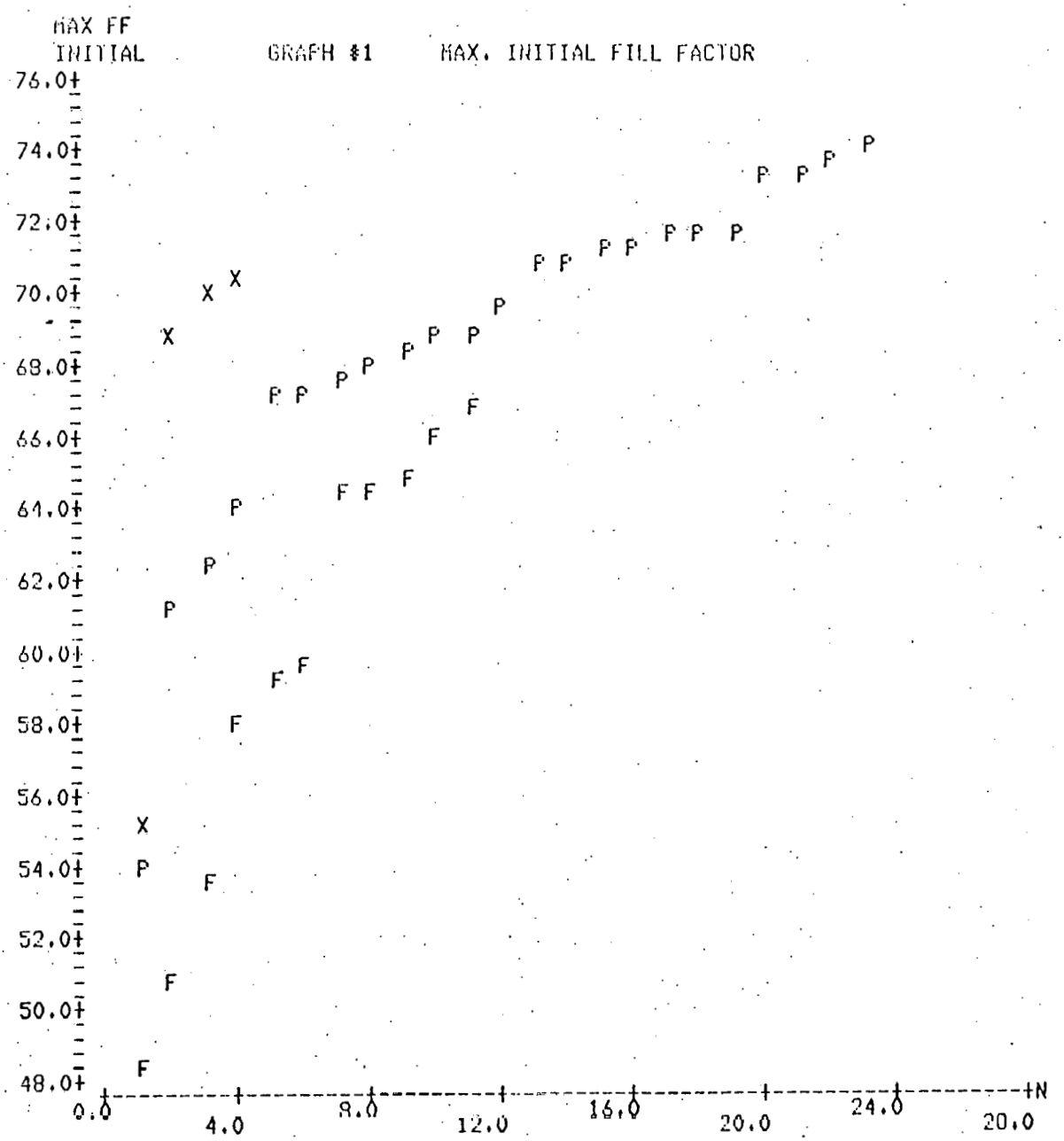

USED ALL PIECES WITH MEASURABLE FILL FACTOR >= 48%.
P REPRESENTS PIECES THAT SATISFIED THE THE SEP CRITERIA.
F REPRESENTS PIECES THAT DIDN'T QUALIFY.
X REPRESENTS BORDER LINE CASES.
***** SEE TABLE #1.

TABLE #1 (DATA FOR GRAPH #1)

N	FAILED PIECES	FILL FACTOR MAX INITIAL	PASSED PIECES	FILL FACTOR MAX INITIAL
1	963-11	48.6000	959-11	54.2000
2	957-11	50.8000	989-11	61.2000
3	985-11	53.6000	986-11	62.5000
4	990-11	57.8000	952-11	63.8000
5	988-11	59.1000	945-11	67.1000
6	947-12	59.6000	960-11	67.3000
7	943-11	64.3000	992-11	67.5000
8	993-11	64.4000	949-12	68.0000
9	931-11	64.9000	941-11	68.3000
10	947-11	66.1000	935-21	68.8000
11	949-11	67.0000	935-22	68.9000
12			948-11	69.5000
13			944-11	70.7000
14			934-11	70.8000
15			999-11	71.2000
16			932-11	71.3000
17			939-11	71.5000
18			940-11	71.5000
19			962-11	71.6000
20			1011-11	73.3000
21			1007-11	73.3000
22			930-11	73.6000
23			1009-11	74.2000

N	BORDER LINE PIECES	FILL FACTOR MAX INITIAL
1	950-11	55.3000
2	942-11	68.7000
3	994-11	70.2000
4	953-11	70.5000

WILCOXON 2-SAMPLE TEST ON LNJO

SAMPLE #1 HAS 8 ELEMENTS.
SAMPLE #2 HAS 22 ELEMENTS.

REJECT H0:U1=U2 IN FAVOR OF H1:U1=U2+DELTA,DELTA>0

PROBABILITY THAT STATISTIC IS <= MIN(W,2*E(W)-W) GIVEN H0 IS 0.3653E-03

PIECE	SAMPLE 1
931.11	2.957
943.11	2.810
947.11	2.072
947.12	2.657
949.11	2.087
988.11	3.763
990.11	2.385
993.11	2.305

PIECE	SAMPLE 2
930.11	1.575
932.11	1.625
934.11	1.807
935.21	1.973
935.22	2.117
939.11	1.714
940.11	2.042
941.11	2.263
944.11	1.966
945.11	2.076
948.11	1.904
949.12	1.947
952.11	2.387
960.11	1.942
962.11	1.914
986.11	1.581
989.11	3.292
992.11	1.094
999.11	2.515
1007.11	1.634
1009.11	1.746
1011.11	1.762

LNEMIN JOI
INITIAL GRAPH #2 LNEMIN, INITIAL JOI

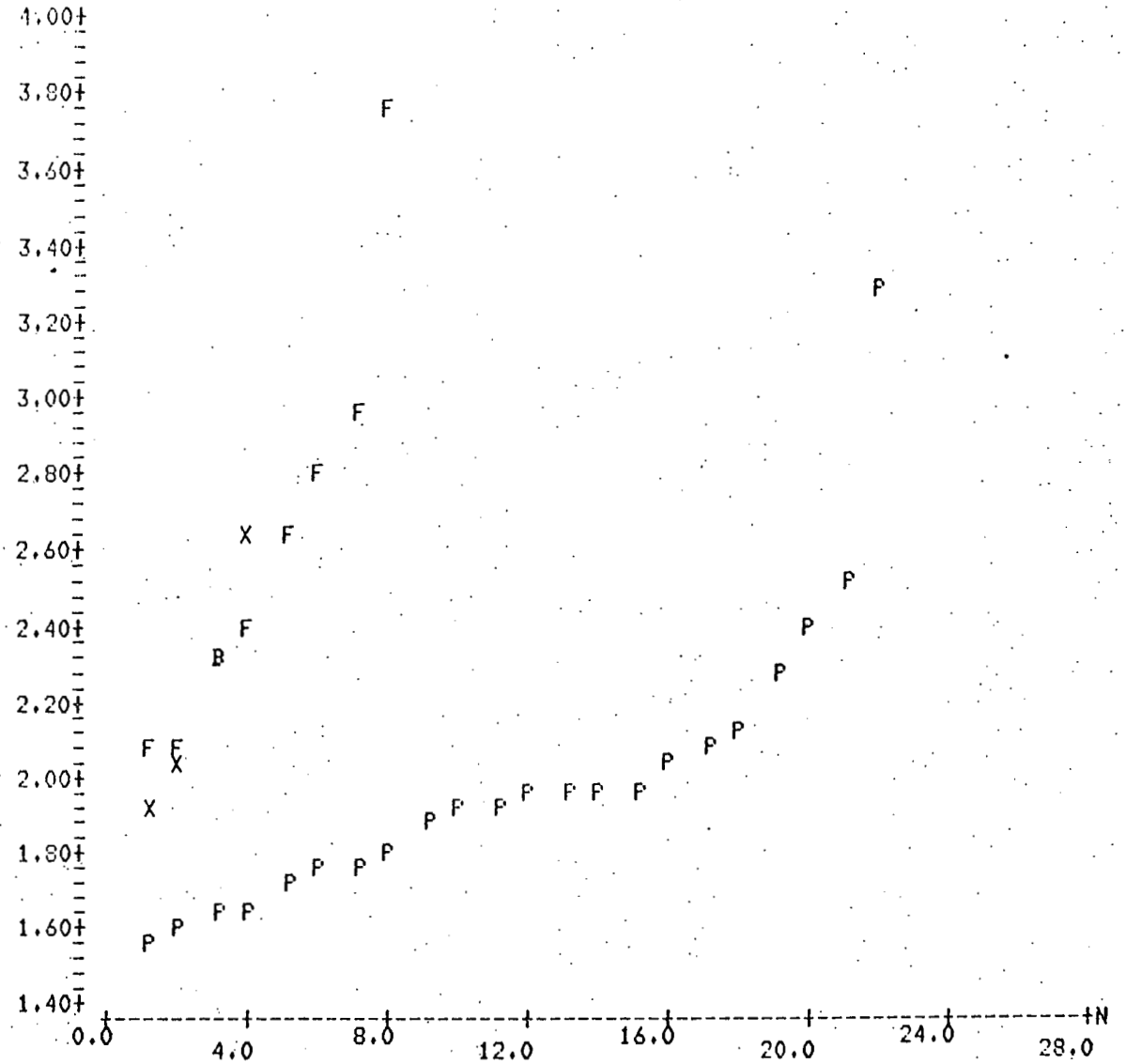

USED ALL PIECES HAVING MAX. INITIAL FILL FACTORS >= 55%.
P REPRESENTS PIECES THAT SATISFIED THE THE SEP CRITERIA.
F REPRESENTS PIECES THAT DIDN'T QUALIFY.
X REPRESENTS BORDER LINE CASES.
B REPRESENTS TWO POINTS, ONE BORDER LINE AND ONE FAILED.
***** SEE TABLE #2.

TABLE #2 (DATA FOR GRAPH #2)

N	FAILED PIECES	LN[JO] MIN INITIAL	PASSED PIECES	LN[JO] MIN INITIAL
1	947-11	2.07191	930-11	1.57464
2	949-11	2.08667	986-11	1.58063
3	993-11	2.30508	932-11	1.62472
4	990-11	2.38499	1007-11	1.63413
5	947.12	2.65676	939-11	1.71362
6	943-11	2.80958	1009-11	1.74606
7	931-11	2.95652	1011-11	1.76164
8	988-11	3.76259	934-11	1.80665
9			992-11	1.89371
10			948-11	1.90405
11			962-11	1.91398
12			960-11	1.94248
13			949.12	1.94748
14			944-11	1.96613
15			935.21	1.97297
16			940-11	2.04213
17			945-11	2.07594
18			935.22	2.11722
19			941-11	2.26291
20			952-11	2.38739
21			999-11	2.51511
22			989-11	3.29205

N	BORDERLINE PIECES	LN[JO] MIN INITIAL
1	942-11	1.90672
2	994-11	2.02512
3	953-11	2.30098
4	950-11	2.65211

WILCOXON 2-SAMPLE TEST ON R

SAMPLE #1 HAS 8 ELEMENTS.
SAMPLE #2 HAS 22 ELEMENTS.

REJECT H0:U1=U2 IN FAVOR OF H1:U1=U2+DELTA,DELTA>0

PROBABILITY THAT STATISTIC IS <= MIN(W,2*E(W)-W) GIVEN H0 IS 0.8791E-03

PIECE	SAMPLE 1
931.11	3.970
943.11	3.940
947.11	2.678
947.12	6.244
949.11	2.340
988.11	4.040
990.11	2.690
993.11	3.780

PIECE	SAMPLE 2
930.11	1.438
932.11	2.283
934.11	1.880
935.21	2.626
935.22	2.539
939.11	1.513
940.11	1.588
941.11	2.389
944.11	1.900
945.11	2.445
948.11	1.949
949.12	1.906
952.11	3.150
960.11	2.417
962.11	1.770
986.11	3.130
989.11	4.300
992.11	2.270
999.11	4.000
1007.11	1.360
1009.11	1.730
1011.11	1.300

WILCOXON 2-SAMPLE TEST ON G

SAMPLE #1 HAS 8 ELEMENTS.
SAMPLE #2 HAS 22 ELEMENTS.

REJECT H0:U1=U2 IN FAVOR OF H1:U1=U2+DELTA,DELTA>0

PROBABILITY THAT STATISTIC IS <= MIN(W,2*E(W)-W) GIVEN H0 IS 0.4615E-03

PIECE	SAMPLE 1	PIECE	SAMPLE 2
931.11	2.978	930.11	1.232
943.11	3.011	932.11	1.448
947.11	3.843	934.11	2.215
947.12	4.113	935.21	2.377
949.11	3.800	935.22	2.438
988.11	6.600	939.11	2.136
990.11	9.320	940.11	2.152
993.11	3.640	941.11	2.964
		944.11	2.213
		945.11	3.334
		948.11	2.538
		949.12	2.891
		952.11	4.799
		960.11	3.761
		962.11	1.640
		986.11	3.020
		989.11	4.720
		992.11	3.360
		999.11	0.520
		1007.11	1.310
		1009.11	0.940
		1011.11	1.260

WILCOXON 2-SAMPLE TEST ON JL

SAMPLE #1 HAS 8 ELEMENTS.
SAMPLE #2 HAS 22 ELEMENTS.

ACCEPT H0:U1=U2

PROBABILITY THAT STATISTIC IS <= MIN(W,2*E(W)-W) GIVEN H0
IS IN THE INTERVAL (0.3651E+00, 0.3651E+00)
(UNCERTAINTY DUE TO TIES.)

PIECE	SAMPLE 1	PIECE	SAMPLE 2
931.11	10.850	930.11	13.800
943.11	15.710	932.11	13.590
947.11	13.330	934.11	12.160
947.12	9.450	935.21	13.850
949.11	14.720	935.22	11.460
988.11	17.420	939.11	15.790
990.11	16.130	940.11	16.740
993.11	14.320	941.11	14.370
		944.11	13.000
		945.11	14.530
		948.11	13.200
		949.12	15.490
		952.11	15.580
		960.11	16.100
		962.11	16.520
		986.11	10.230
		989.11	14.940
		992.11	15.880
		999.11	3.200
		1007.11	11.870
		1009.11	13.280
		1011.11	13.800

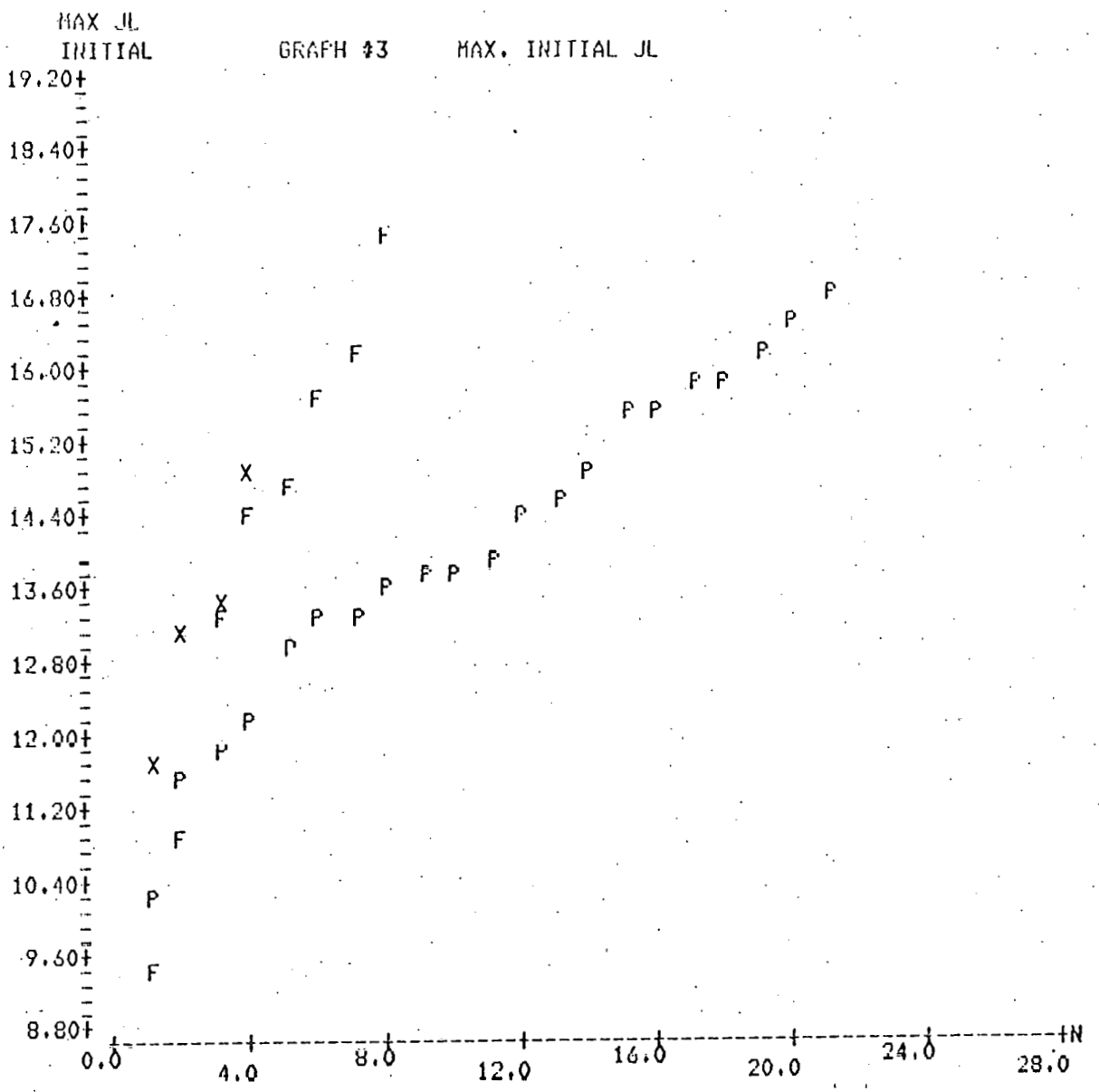

USED ALL PIECES HAVING MAX. INITIAL FILL FACTOR >= 55% EXCEPT 999.11 (SCALING)

P REPRESENTS PIECES THAT SATISFIED THE THE SEP CRITERIA.
F REPRESENTS PIECES THAT DIDN'T QUALIFY.
X REPRESENTS BORDER LINE CASES.
***** SEE TABLE #3.

TABLE #3 (DATA FOR GRAPH #3)

N	FAILED PIECES	JL MAX INITIAL	PASSED PIECES	JL MAX INITIAL
1	947-12	9.4500	986-11	10.2300
2	931-11	10.6500	935-22	11.4600
3	947-11	13.3300	1007-11	11.8700
4	993-11	14.3200	934-11	12.1600
5	949-11	14.7200	944-11	13.0000
6	943-11	15.7100	948-11	13.2000
7	990-11	16.1300	1009-11	13.2800
8	988-11	17.4200	932-11	13.5900
9			930-11	13.8000
10			1011-11	13.8000
11			935-21	13.8500
12			941-11	14.3700
13			945-11	14.5300
14			989-11	14.9400
15			949-12	15.4900
16			952-11	15.5800
17			939-11	15.7900
18			992-11	15.8800
19			960-11	16.1000
20			962-11	16.5200
21			940-11	16.7400

N	BORDER LINE PIECES	JL MAX INITIAL
1	953-11	11.6200
2	942-11	13-1200
3	950-11	13.4200
4	994-11	14.0100

WILCOXON 2-SAMPLE TEST ON PL

SAMPLE #1 HAS 12 ELEMENTS.
SAMPLE #2 HAS 23 ELEMENTS.

ACCEPT H0:U1=U2

PROBABILITY THAT STATISTIC IS <= MIN(W,2*E(W)-W) GIVEN H0
IS IN THE INTERVAL (0.2408E+00, 0.3724E+00)
(UNCERTAINTY DUE TO TIES.)

PIECE	SAMPLE 1	PIECE	SAMPLE 2
931.11	1.100	930.11	1.000
943.11	1.300	932.11	0.500
947.11	3.800	934.11	1.600
947.12	3.800	935.21	0.800
949.11	2.800	935.22	0.800
957.11	2.100	939.11	1.300
963.11	0.900	940.11	1.300
985.11	0.500	941.11	1.300
988.11	1.200	944.11	7.500
990.11	0.700	945.11	3.300
993.11	1.200	948.11	2.500
1010.11	1.000	949.12	2.000
		952.11	4.300
		959.11	1.000
		960.11	1.400
		962.11	0.400
		986.11	0.900
		989.11	0.800
		992.11	0.700
		999.11	0.300
		1007.11	1.600
		1009.11	0.700
		1011.11	1.100

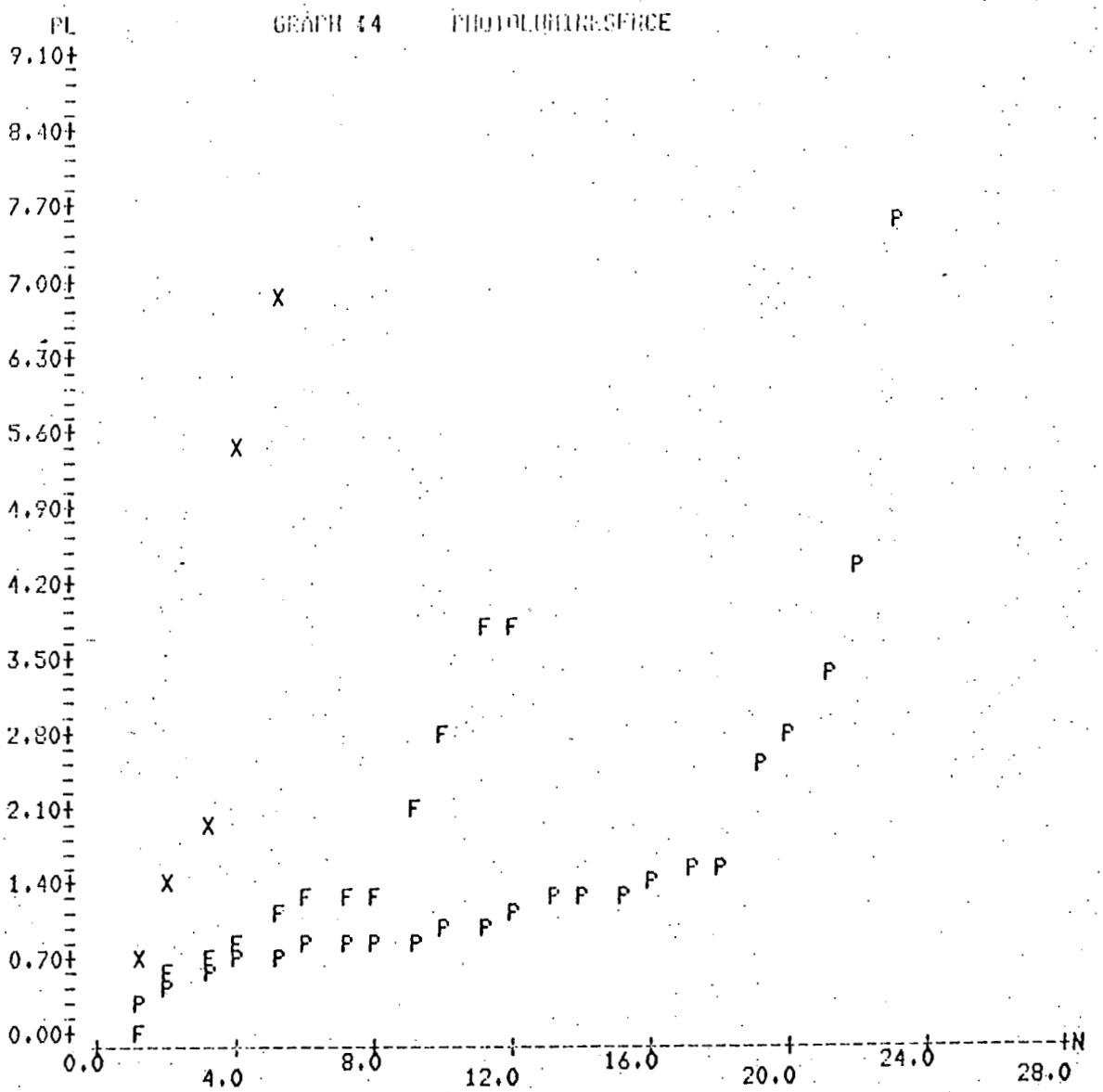

USED ALL AVAILABLE PIECES.
P REPRESENTS PIECES THAT SATISFIED THE THE SEP CRITERIA.
F REPRESENTS PIECES THAT DIDN'T QUALIFY.
X REPRESENTS BORDER LINE CASES.
***** SEE TABLE #4.

TABLE #4 (DATA FOR GRAPH #4)

N	FAILED PIECES	PL	PASSED PIECES	PL
1	1010-11	0.00000	999-11	0.30000
2	985-11	0.50000	982-11	0.40000
3	990-11	0.70000	932-11	0.50000
4	963-11	0.90000	992-11	0.70000
5	931-11	1.10000	1009-11	0.70000
6	988-11	1.20000	935-22	0.80000
7	993-11	1.20000	935-21	0.80000
8	943-11	1.30000	989-11	0.80000
9	957-11	2.10000	986-11	0.90000
10	949-11	2.80000	930-11	1.00000
11	947-12	3.80000	959-11	1.00000
12	947-11	3.80000	1011-11	1.10000
13			939-11	1.30000
14			941-11	1.30000
15			940-11	1.30000
16			960-11	1.40000
17			1007-11	1.60000
18			934-11	1.60000
19			948-11	2.50000
20			949-12	2.80000
21			945-11	3.30000
22			952-11	4.30000
23			944-11	7.50000

N	BORDER LINE PIECES	PL
1	994-110	0.70000
2	942-110	1.40000
3	946-110	2.00000
4	953-110	5.50000
5	950-110	6.00000

WILCOXON 2-SAMPLE TEST ON THODS

SAMPLE #1 HAS 12 ELEMENTS.
SAMPLE #2 HAS 23 ELEMENTS.

ACCEPT H0:U1=U2

PROBABILITY THAT STATISTIC IS <= MIN(W,2*E(W)-W) GIVEN H0
 IS IN THE INTERVAL (0.1314E+00, 0.1390E+00)
(UNCERTAINTY DUE TO TIES.)

PIECE	SAMPLE 1	PIECE	SAMPLE 2
931.11	37.900	930.11	34.800
943.11	33.300	932.11	28.900
947.11	29.900	934.11	27.900
947.12	29.900	935.21	32.200
949.11	32.400	935.22	32.200
957.11	27.500	939.11	27.300
963.11	30.700	940.11	34.300
985.11	45.100	941.11	33.600
988.11	30.900	944.11	23.200
990.11	29.100	945.11	30.000
993.11	24.600	948.11	27.800
1010.11	33.500	949.12	32.400
		952.11	20.900
		959.11	26.400
		960.11	28.800
		962.11	30.000
		986.11	30.600
		989.11	36.300
		992.11	34.900
		999.11	26.800
		1007.11	21.800
		1009.11	31.000
		1011.11	25.200

WILCOXON 2-SAMPLE TEST ON RHO

SAMPLE #1 HAS 12 ELEMENTS.
SAMPLE #2 HAS 23 ELEMENTS.

ACCEPT H0:U1=U2

PROBABILITY THAT STATISTIC IS <= MIN(W,2*E(W)-W) GIVEN H0
 IS IN THE INTERVAL (0.3595E+00, 0.4659E+00)
(UNCERTAINTY DUE TO TIES.)

PIECE	SAMPLE 1	PIECE	SAMPLE 2
931.11	2.700	930.11	0.500
943.11	0.700	932.11	2.000
947.11	1.700	934.11	0.600
947.12	1.700	935.21	0.600
949.11	1.300	935.22	0.600
957.11	1.000	939.11	1.200
963.11	5.300	940.11	0.900
985.11	0.600	941.11	0.600
988.11	1.200	944.11	2.600
990.11	0.700	945.11	2.200
993.11	2.000	948.11	1.500
1010.11	0.300	949.12	1.300
		952.11	3.000
		959.11	3.000
		960.11	2.000
		962.11	0.500
		986.11	1.900
		989.11	1.300
		992.11	0.400
		999.11	1.600
		1007.11	2.900
		1009.11	1.400
		1011.11	1.900

Table #5

Pieces that failed due to J0 alone

Piece	Cell	J_L (mA/cm^2)	Best J0 ($\times 10^{-8}$ mA/cm^2)
943-11	1	18.08	7.76
957-11	2	18.95	9.54
985-11	1	19.80	44.13
988-11	2	19.79	6.25
990-11	2	21.93	7.15
993-11	4	18.16	6.08

Pieces that failed due to J_L alone

Piece	Cell	Best J_L (mA/cm^2)	J0 ($\times 10^{-8}$ mA/cm^2)
931-11	1	16.34	4.12
947-11	1	12.51	4.80

Appendix B

THE DESIGN AND UTILIZATION OF A MICROPROCESSOR-CONTROLLED ABSOLUTE SPECTRAL RESPONSE SYSTEM

L.M. Kilgren, N.C. Wyeth, and W.E. Devaney

Presented at

Commission of the European Communities 1979
Photovoltaic Solar Energy Conference

April 25, 1979 Berlin (West)

THE DESIGN AND UTILIZATION OF A MICROPROCESSOR-CONTROLLED ABSOLUTE SPECTRAL RESPONSE SYSTEM

L.M. Kilgren, N.C. Wyeth, and W.E. Devaney*
Institute of Energy Conversion
University of Delaware
Newark, DE 19711

1. Introduction

A fully automated system has been assembled which permits the direct monitoring of solar cell output under varying conditions of illumination and bias voltage. The primary system components are a chopped monochromatic light source of continuously variable wavelength, a lock-in amplifier, and a microprocessor. Analogue-to-digital and digital-to-analogue conversion allows the microprocessor to be used to control data acquisition and to perform data conditioning and output.

2. System Description

The system is shown schematically in Figure 1. A grating monochromator is driven by a stepping motor under control of the microprocessor. The monochromatic beam is focused on the surface of a silvered light-chopping blade placed at 45° to the path of the incoming light beam. The transmitted beam illuminates the cell under test through an appropriate lens system. The beam reflected from the chopper is monitored to give a continuous measurement of the primary beam intensity. The light-chopper control provides the reference signal for a lock-in amplifier which is used to measure the AC output of the cell. An ELH tungsten-iodide lamp driven by a stabilized DC supply provides the bias light. The cell under test is mounted on a thermoelectric temperature-controlled block with electrical connections for application of a bias voltage and measurement of cell output. A flat pyro-

* Present address: SES, Inc. Newark, DE 19711

electric detector can be substituted for the cell block and the intensity-wavelength curve of the monochromatic beam stored in the microprocessor as the monochromator is stepped through the wavelength range of 400 nm to 1600 nm (a grating change is made at 800 nm). The microprocessor uses the stored reference intensity curve to compute the collection versus wavelength performance of the cell under test and then either prints out the digital data or displays the analogue information on a video terminal or provides hard copy on an x-y plotter.

3. Applications

A major advantage of the present system is the ability to measure the spectral response of the cell while under normal operating conditions of both illumination and voltage bias. This feature is essential for cells such as CdS/Cu_2S in which the total illumination strongly influences the collection efficiency (1).

3.1 Spectral response under normal operating conditions

The quantum efficiency of a cell or the number of current carriers collected per incident photon is measured as a function of wavelength with the cell at zero bias (short circuit current). The system can be used with the chopped monochromatic beam only, or alternatively, the spectral response can be measured while the cell is illuminated with either a broad band white light or with a second continuous (DC) monochromatic bias beam. Figure 2 shows collection efficiency as a function of wavelength for a CdS/Cu_2S cell both with and without bias light.

3.2 Internal photoelectric emission

When the photon energy of the incident beam is reduced below the smallest bandgap in a junction device, the current due to internal photoelectric emission of carriers over junction barriers less than the band

gap can be detected. The microprocessor is programmed to generate a plot of the square root of the normalized response versus photon energy, which by linear extrapolation to the energy axis gives the barrier height (2). Figure 3 shows a typical curve of the square root of collection efficiency vs. photon energy for a CdS/Cu_2S cell.

3.3 Minority carrier diffusion length

For certain ranges of absorber/generator layer thickness and minority carrier diffusion length the spectral response of a photovoltaic cell can be analyzed to set a slower limit to the diffusion length without needing a detailed knowledge of the absorption behavior of the active semiconductors (3). Figure 4 shows a clearly definable peak in collection efficiency vs. wavelength for a cell of appropriate Cu_2S thickness. The diffusion length in turn can then be used to determine the wavelength dependence of the absorption coefficient from the spectral response curve. Figure 5 is a comparison with published data of the calculated dependence of the absorption constant on wavelength (4).

3.4 Interface recombination and junction field studies

The use of phase-sensitive detection to measure the cell response to a modulated light source superposed on a DC bias light also makes it possible to measure the light-generated current as a function of the cell bias voltage (5). Measurements on CdS/Cu_2S cells show that the light-generated current can vary with applied voltage. Figure 6 shows the variation of light-generated current as a function of bias voltage for two cells of widely differing performance characteristics. The sensitivity to bias voltage is found to be strongly influenced by the intensity and spectral content of the applied bias light and the structure and history of the cell

under test. Figure 7 shows the light-generated current for a CdS/Cu_2S cell under three different conditions of spectral content of the bias illumination. Figure 8 shows the same data, but at reduced bias light intensity. This technique which reveals cell current collection performance at the maximum power point has major advantages over more traditional procedures which are confined to the vicinity of the short-circuit current.

References

(1) A. Rothwarf, J. Phillips, N.C. Wyeth, Thirteenth IEEE Photovoltaic Specialists Conference - 1978 (IEEE, New York, 1978) p. 399.

(2) J.I. Pankove, "Optical Processes in Semiconductors" (Dover, New York, 1975) pp. 314-319.

(3) N.C. Wyeth and A. Catalano, J. Appl. Phys. 50, 1304 (1979).

(4) B.J. Mulder, Physica Status Solidi (a) 13, 79 (1972).

(5) L.M. Kilgren, Proceedings of the 1979 Photovoltaic Solar Energy Conference (Comission of the European Communities and IEEE), to be published.

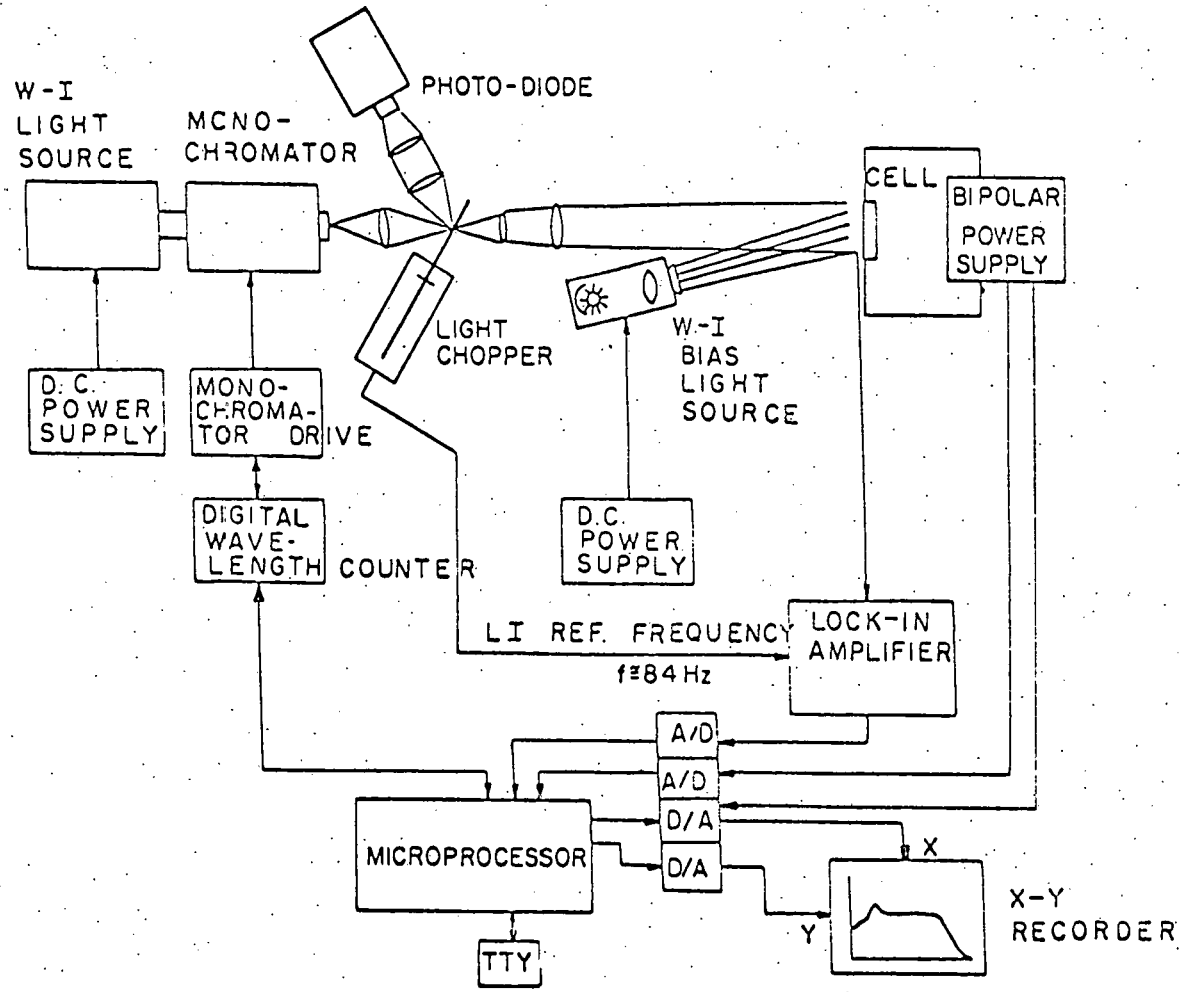

Figure 1 Experimental System.

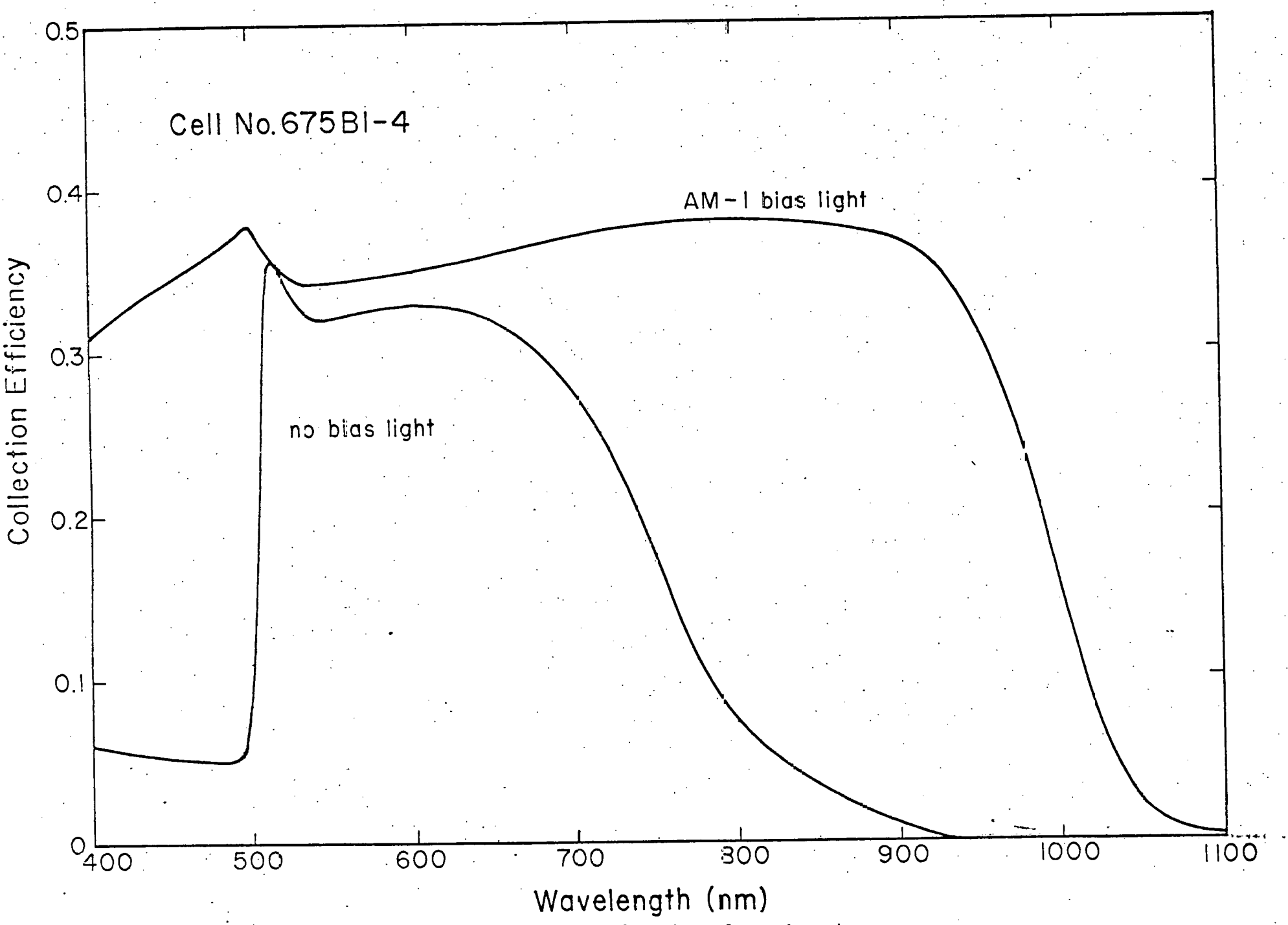

Figure 2 Collection efficiency as a function of wavelength.

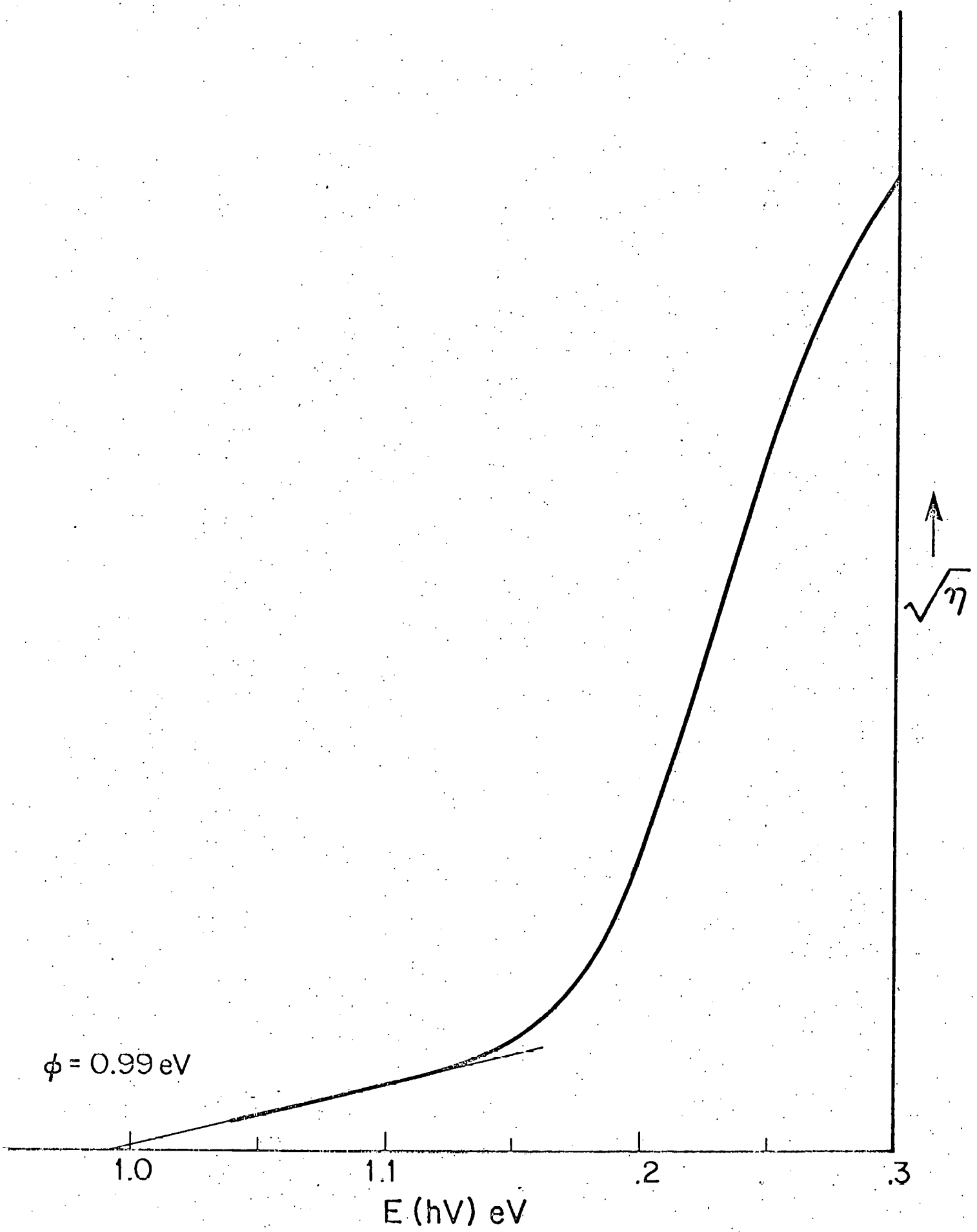

Figure 3 Square root of collection Efficiency as a Function of Photon Energy.

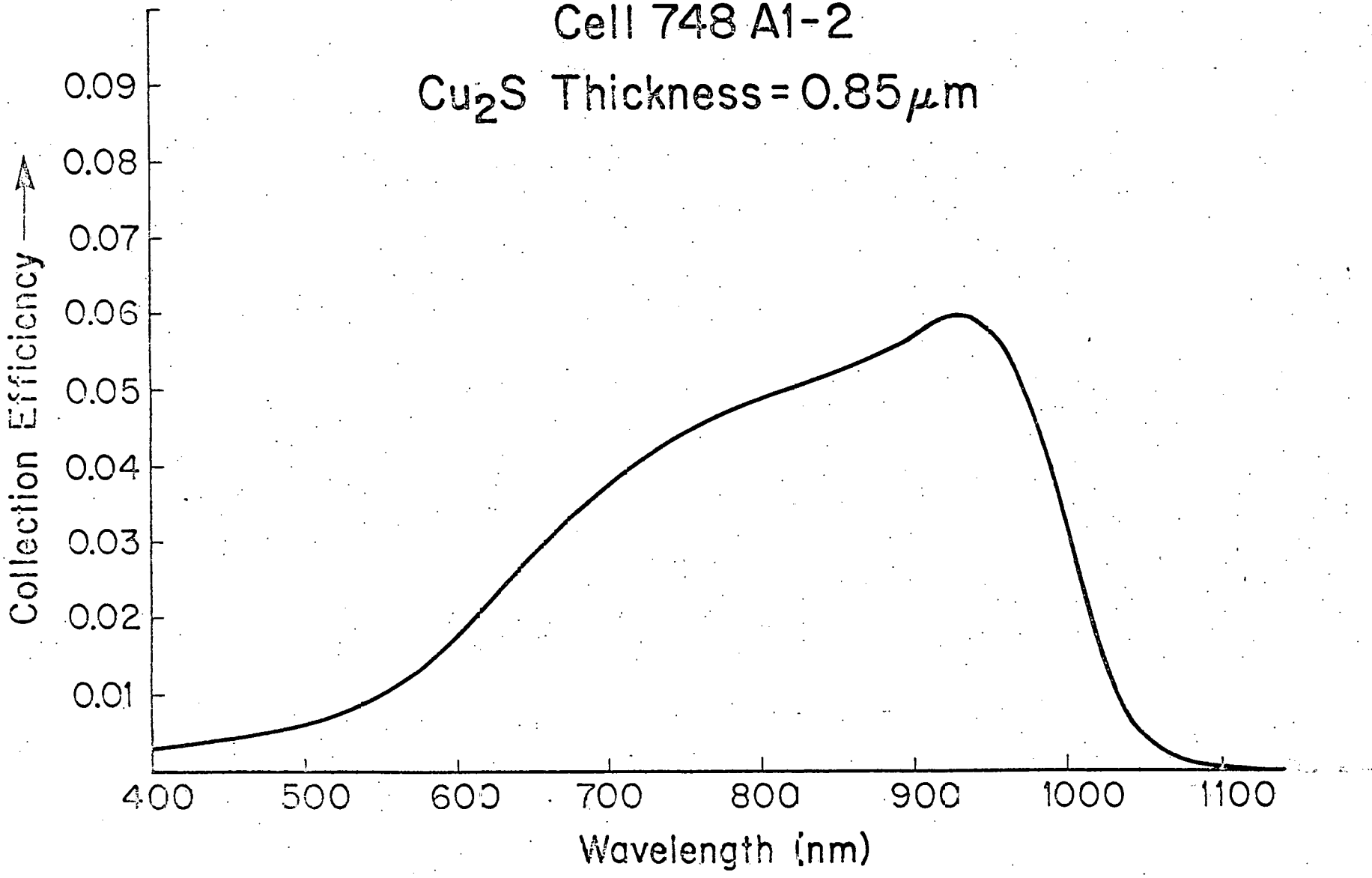

Figure 4 Collectior Efficiency as a Function of Wavelength for a Cell of Appropriate Cu_2S Thick s.

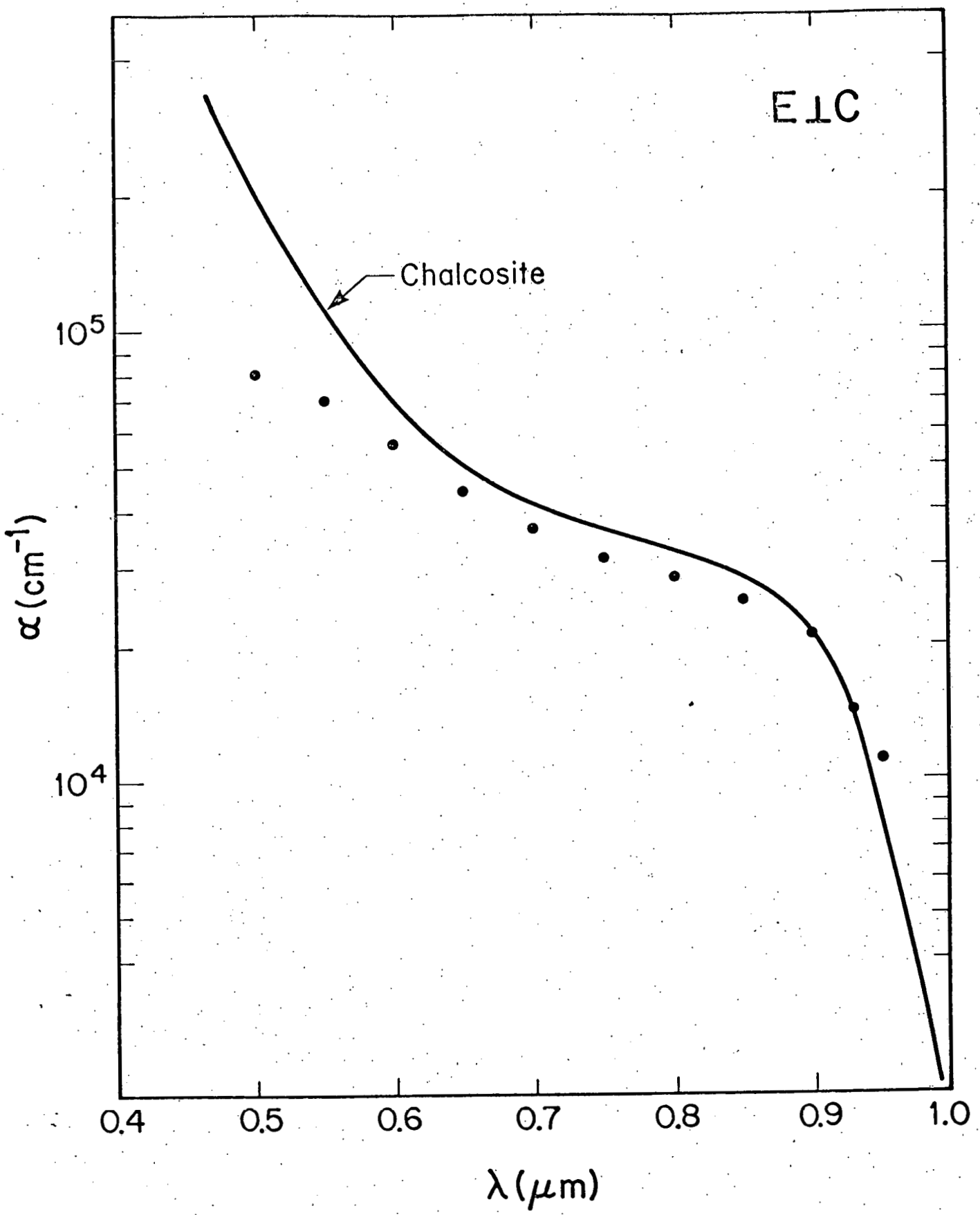

Figure 5 Absorption Coefficient as a Function of Wavelength.

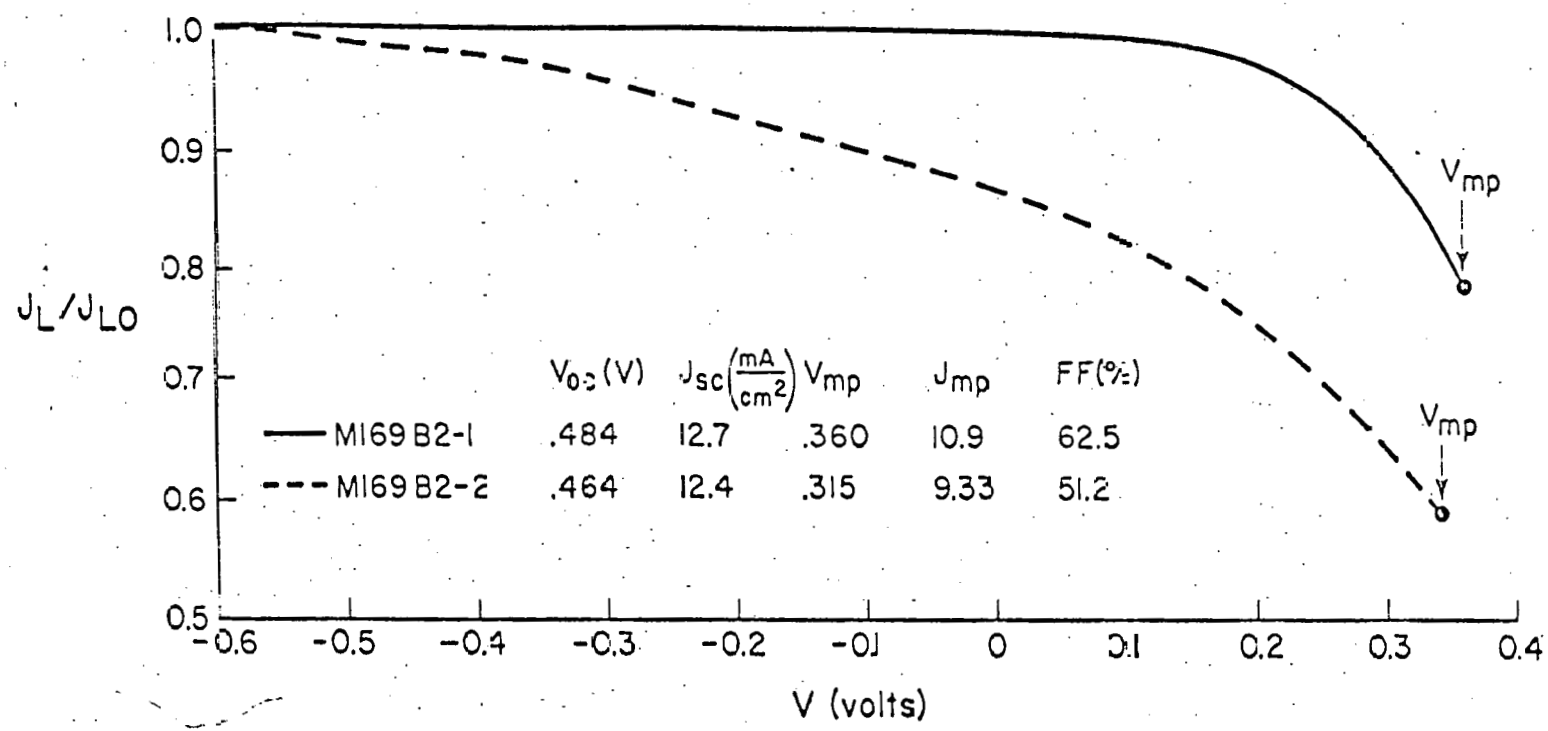

Figure 6 Relative light-generated current as a function of applied voltage for two cells at AM1 intensity.

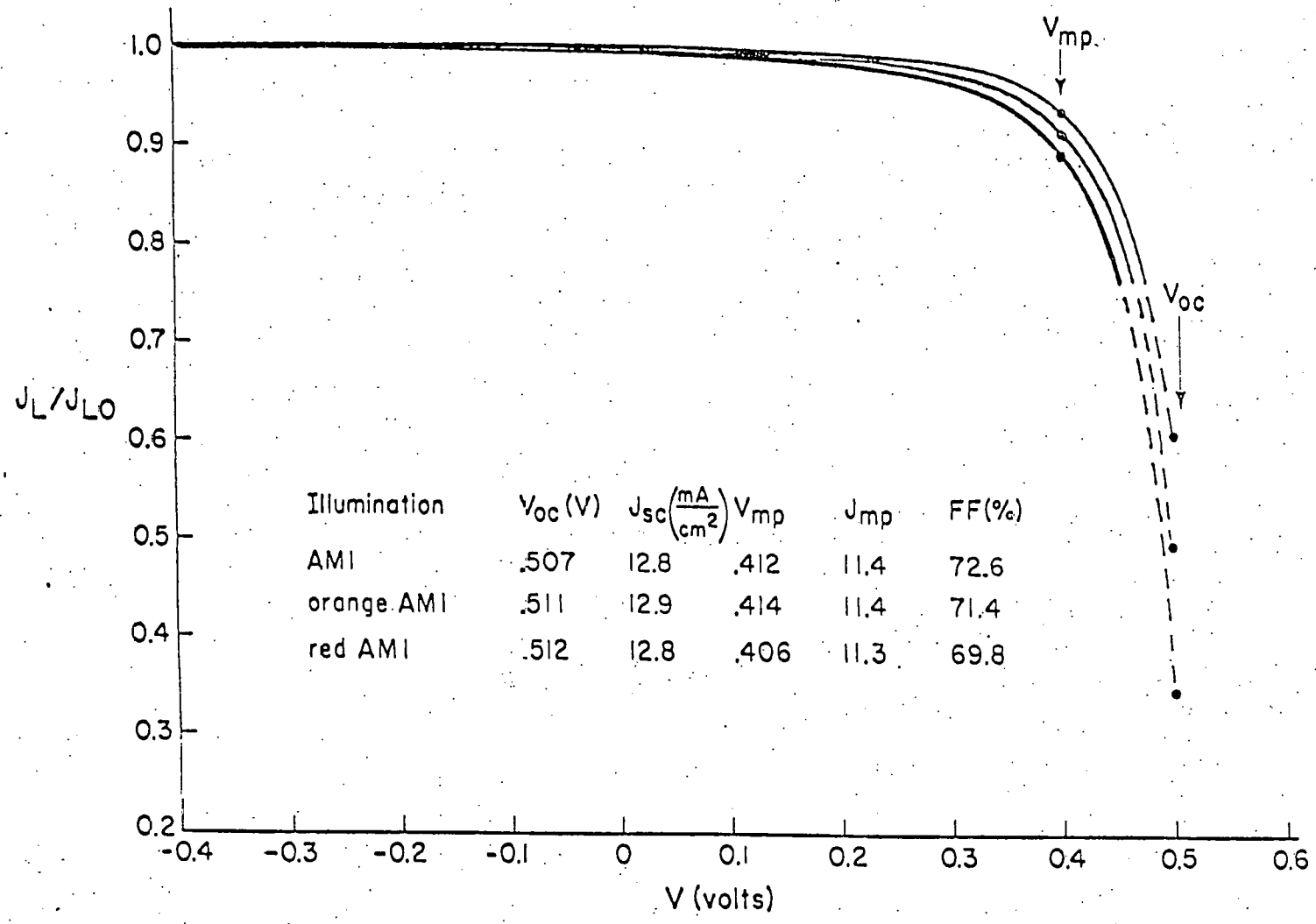

Figure 7 Relative light - generated current as a function of applied voltage for a cell at three different bias illuminations of AM1 equivalent intensity.

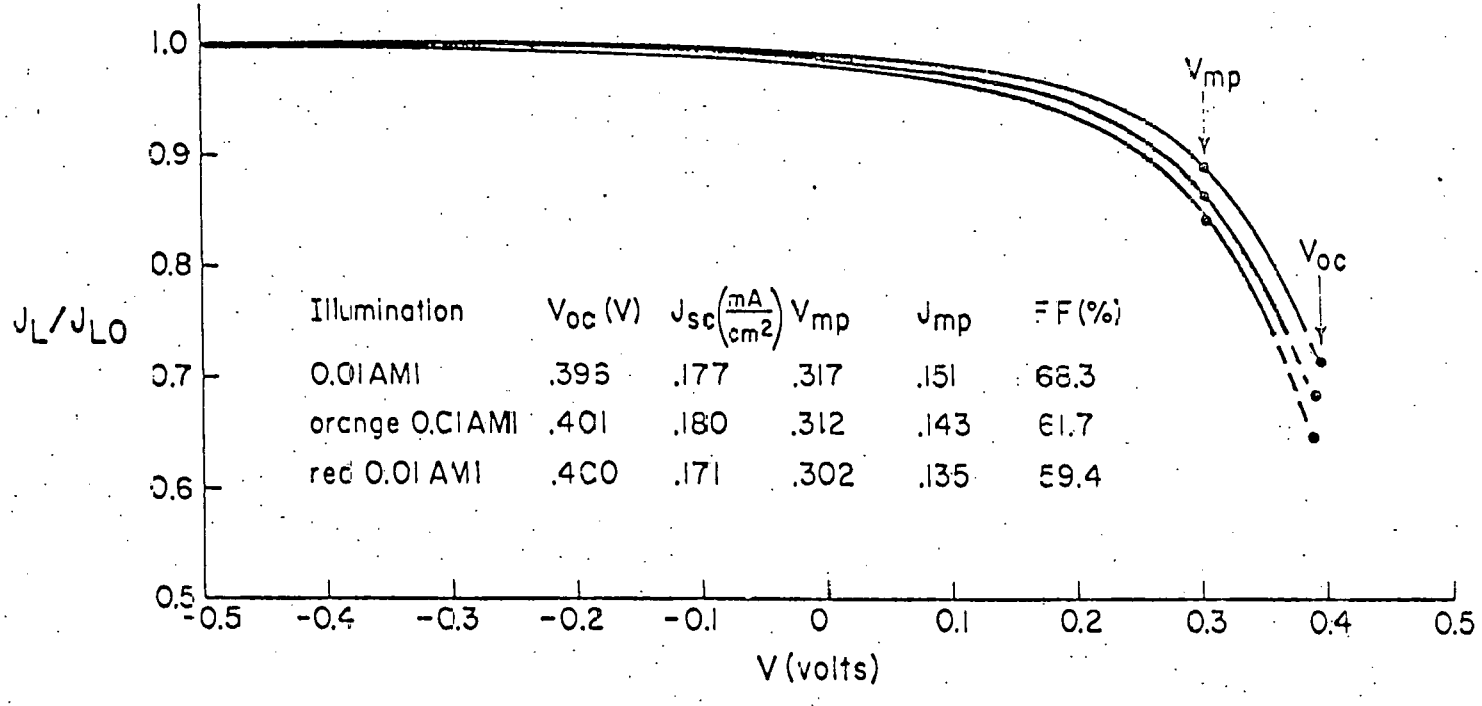

Figure 8 Relative light - generated current as a function of applied voltage for a cell at three different bias illuminations of 0.01 AMI equivalent intensity.

Appendix C

LIST OF RESEARCH CONTRIBUTORS

Dr. John D. Meakin, Director, Solar Cell Development, Principal Investigator

Mr. Edgar Ashmead, Research Technician

Dr. Allen M, Barnett, Director

Dr. Bill N. Baron, Associate Scientist

Mr. Steven L. Beard, Machinist

Mr. Usamah Besmar, Research Associate

Dr. Charles E. Birchenall, Distinguished Professor of Metallurgy

Dr. Robert W. Birkmire, Research Associate

Dr. Julio A. Bragagnolo, Research Associate

Mr. David M. Breeden, Research Technician

Mr. Jake Brown, Senior Design Machinist

Mr. Wayne A. Buchanan, Research Technician

Mr. John A. Cambridge, Research Associate

Ms. Vicky M. Dalton, Research Technician

Mr. James J. Desmond, Draftsperson

Mr. Louis C. DiNetta, Research Associate

Dr. Jeff W. Edington, Professor Material Science

Dr. Erten Eser, Research Associate

Dr. Robert B. Hall, Manager, Materials Processing

Mr. Thomas L. Hench, Research Associate

Mr. Kenneth V. Jarva, Research Associate

Ms. Leslie M. Kilgren, Research Associate

Ms. Gwendolyn A. Kyle, Senior Research Technician

Mr. Patrick G. Lasswell, Senior Research Technician

Dr. William J. Manthey, Research Associate

List of Contributors, cont'd

Mr. James V. Masi, Program Development Manager, Photovoltaics

Dr. Karl H. Norian, Research Associate

Dr. James E. Phillips, Research Associate

Mr. Brian C. Plunkett, Research Associate

Dr. Allen Rothwarf, Senior Scientist

Mr. Stephen Shea, Graduate Student

Ms. Maryanne Powers-Sneed, Senior Research Technician

Ms. Claudia J. Stone, Senior Secretary

Mr. Robert F. Wieland, Research Technician

Dr. N. C. Wyeth, Research Associate

Appendix D

REPORTS & PUBLICATIONS

Reports

Quarterly Progress Report	September - December 1978	XR-9-8063-1-01
	January - March 1979	XR-9-8063-1-02
	March - June 1979	XR-9-8063-1-03

Publications

1) "Measurement of Interface Recombination Velocity by Capacitance/Collection Efficiency Variation in Cu_2S/CdS Heterojunctions" by N. Convers Wyeth and A. Rothwarf, 6th Annual Conference on Physics of Compound Semiconductor Interfaces. To be published in Journal of Vacuum Science and Technology, November/December 1979.

2) "Appraisal of Thin Film Solar Cells" by Allen M. Barnett, 2nd European Community Photovoltaic Solar Energy Conference, D. Riedel Boston, MA 1979, pp. 328-343.

3) " Optimal Material Properties for CdS/Cu_2S Solar Cells" by A. Rothwarf, Ibid, pp. 370-378.

4) "Photon Loss Analysis and Design of Thin-Film Planar Junction Cu_2S/CdS Devices" by Julio A. Bragagnolo, Ibid, pp. 882-889.

5) "Thin Film (CdZn)S for Solar Cells" by T. L. Hench and R. B. Hall, Ibid, pp. 379-386.

6) "Interface Recombination and Junction Field Studies in the Cu_2S-CdS Solar Cell" by Leslie M. Kilgren, Ibid, pp. 344-351.

7) "The Design and Fabrication of High Efficiency Thin Film CdS/Cu_2S Solar Cells" by R. B. Hall and J. D. Meakin, Thin Solid Films, 63, pp. 203-211, 1979.

8) "Utilization of Cadmium in Solar Cells" by John D. Meakin, 2nd International Cadmium Conference, Cannes 1979. To be published by Metal Bulletin, London.

9) "The Design and Utilization of a Microprocessor-Controlled Absolute Spectral Response System" by L. M. Kilgren, N. C. Wyeth and W. E. Devaney, Photovoltaic Materials and Device Workshop, June 1979. SERI/TP-49-185, pp. 81-83. To be published in Solar Cells, Vol. 1, 1980.

10) "Experimental Determination of the Photon Economy in Polycrystalline Thin Film Photovoltaic Materials and Devices" by J. A. Bragagnolo and E.A. Fagen, Ibid, pp. 163-166. To be published in Solar Cells, Vol. 1, 1980.

11) "Perspective on Photovoltaic Material and Device Measurements" by A. Rothwarf, Ibid, pp. 5-9.

Reports & Publications, cont'd

12) "Structural and Chemical Characterization of Photovoltaic Materials and Devices" by John D. Meakin, Ibid, pp. 11-14.

13) "Capacitance as a Tool for Investigating Thin Film CdS/Cu_2S Heterojunctions" by W. J. Manthey and N. Convers Wyeth, Ibid, pp. 11-14.

14) "Low Cost Thin-Film CdS-Based Solar Cells: Progress and Promise" by A. M. Barnett and J. D. Meakin, A.S.M.E. 79-SOL-15, 1979.

15) "Advances in the Development of Low Cost, High Performance Cadmium Sulfide Based Thin-Film Solar Cells" by Allen M. Barnett, John D. Meakin and A. Rothwarf, ISES International Congress, Atlanta, 1979. To be published.

16) "Single Thermal Source Formation of $Zn_xCd_{1-x}S$ Thin Films" by L. C. Burton, T. L. Hench and J. D. Meakin, J. Appl. Phys. 50, pp. 6014 - 6015, 1979.

17) "The Design and Fabrication of CdS/Cu_2S Cells of 8.5% Conversion Efficiency" by Walter E. Devaney, Allen M. Barnett, George M. Storti and J. D. Meakin, IEEE Trans. Electron Devices, ED-26, pp. 205-210, 1979.

18) "Improvements in the Performance of a Low Cost Thin Film Solar Cell" by J. D. Meakin, Energy Technology VI, pp. 1088-1096, Government Institutes Inc., 1979.